THE UNIVERSITY OF MICHIGAN

COLLEGE OF ENGINEERING
Department of Aerospace Engineering
Aerodynamics Laboratory

Technical Report

AN EXPERIMENTAL STUDY OF THE STRUCTURE OF TURBULENCE NEAR THE WALL THROUGH CORRELATION MEASUREMENTS IN A THICK TURBULENT BOUNDARY LAYER

Bo-Jang Tu
William W. Willmarth

ORA Project 02920

under contract with:

DEPARTMENT OF THE NAVY
OFFICE OF NAVAL RESEARCH
CONTRACT NO. Nonr-1224(30), NR-062-234
WASHINGTON, D.C.

administered through:

OFFICE OF RESEARCH ADMINISTRATION ANN ARBOR

March 1966

This report was also a dissertation submitted by the first author in partial fulfillment of the requirements for the degree of Doctor of Philosophy in The University of Michigan, 1966.

ABSTRACT

An experimental investigation is described in which emphasis is given to revealing the structure of turbulence near the wall in a boundary layer. Measurements made include space-time correlations between the fluctuating wall pressure and the span-wise velocity component w, and between the various velocity components. The velocity correlations include measurements of the space-time correlation of the streamwise component of the fluctuating wall shear stress. Experiments have been conducted in a thick (5 in.) turbulent boundary layer with zero pressure gradient which is produced by natural transition on a smooth surface.

Sufficient data have been obtained to allow us to propose a qualitative model for the structure of turbulence near the wall. The proposed model outlines the sequence of events that result in the production of intense pressure and velocity fluctuations by stretching of the vorticity after it is produced by viscous stresses within and near the edge of the viscous sublayer. The measurements are in qualitative agreement with the model. Here, qualitative agreement means that the size and shape of the contours of constant correlation and the sign of the measured correlations are in agreement with the proposed model for the turbulent structure.

The proposed model as well as the result of measurements of the correlation between the fluctuating streamwise wall shear stress and the streamwise velocity component were found in favor of the concept that the turbulence is generated in the wall region distending into the central parts of the boundary layer. Since it is well-known from measurements that eddies of small size dominate near the wall, this implies that small eddies near the wall may become larger when they distend into the more central region. However, the physical mechanism of development from small to large eddies is not yet completely understood.

TABLE OF CONTENTS

TABLE OF CONTENTS (Concluded)

LIST OF ILLUSTRATIONS

LIST OF ILLUSTRATIONS (Continued)

NOMENCLATURE

a_w	hot-wire overheating ratio
e	fluctuating voltage across hot-wire; $e = Ir_w$
f	frequency
$\bar{f}_w$	mean wall shear stress
I	current through hot-wire
k	coefficient of thermal conductivity
Nu	Nusselt number; $Nu = \frac{Q}{\pi \ell k(T_w - T_e)}$
p	fluctuating wall pressure
Q	rate of heat loss from hot-wire; $Q = I^2 R_w$
R	Reynolds number based on distance from virtual origin of turbulent boundary layer
R_θ	Reynolds number based on momentum thickness
$(Rey)_w$	Reynolds number based on hot-wire diameter d; $(Rey)_w = \frac{Ud}{\nu}$
R_{pu_j}	normalized wall pressure-velocity correlations; see, e.g., Eqn. (VI-1)
$R_{u_i u_j}$	normalized velocity-velocity correlations; see Eqn. (V-1)
$R_{\tau_w \tau_w}$	normalized wall shear-wall shear correlations; see Eqn. (V-2)
$R_{\tau_w u_j}$	normalized wall shear-velocity correlations; see Eqn. (V-3)
R_e	resistance of hot-wire at ambient temperature, T_e
R_o	resistance of hot-wire at 0°C
R_w	resistance of heated wire at temperature, T_w
r_w	fluctuating resistance of heated wire

T_e or θ_e	ambient temperature of hot-wire
T_w or θ_w	temperature of heated wire
t	time
U	velocity in boundary layer in stream direction
U_∞	free stream velocity
U_τ	wall friction velocity
U_c	convection speed of fluctuating velocity field which is correlated with fluctuating wall pressure or fluctuating velocity at a fixed point; U_c is determined by $\partial R_{pw}(x_1,\tau)/\partial\tau = 0$ or $\partial R_{u_iu_j}(x_i',\tau)/\partial\tau = 0$ respectively.
u,v,w	fluctuating velocities in x, y, z directions
u_i or u_j	fluctuating velocities in x, y, z directions (i or j = 1,2,3)
x_1,x_2,x_3	spatial separations of pressure and velocity transducers in x, y, z directions
x_1',x_2',x_3'	spatial separations of two velocity measuring points in x, y, z directions
x	distance parallel to wall, increasing in stream direction
y	distance normal to wall, increasing away from wall
z	distance parallel to wall and perpendicular to stream, forming a right-hand Cartesian coordinate system with x and y
α	temperature coefficient of resistivity
α'	$\alpha' = \alpha R_o$
δ	boundary layer thickness
δ^*	boundary layer displacement thickness
μ	viscosity

ν	kinematic viscosity
ζ	fluctuating vorticity component in x_3-direction in viscous sublayer
ρ	density
ρ_a	density of air
τ	time delay
τ'	time delay equal to transducer spacing divided by convection speed U_c
τ_1	fluctuating shear stress
τ_w	fluctuating wall shear stress
ω	circular frequency; $\omega = 2\pi f$
$\overline{(\ )}$	time average

CHAPTER I

INTRODUCTION

Historically, the background for new investigations of the structure of turbulent shear flow are the extensive investigations of the turbulent velocity field made first by Townsend[24] (1951) and later by Schubauer and Klebanoff[20] (1951), Laufer[15] (1953), Klebanoff[9] (1954), etc. Most of our knowledge about the structure of turbulence in a shear flow rests on their measurements of the spatial correlations between turbulent velocities and the power spectra of turbulent velocity components. In recent years, quite a number of new investigations were reported, among which the more representative are Favre, Gaviglio, and Dumas[5] (1958), Grant[6] (1958), and Willmarth and Wooldridge[26,27] (1962). In this period a new technique using a tape recorder for the measurement of spatial correlations with variable time delay was developed by Favre, et al.,[5] so that one is able to study the correlation between the fluctuations of wall pressures and/or velocity components at one point and those of earlier or later history at the same or another point. This is the so called space-time correlation, which makes it possible to investigate the evolution of turbulent eddies.

In the measurement of space-time correlations between the fluctuating wall pressure and the fluctuating velocities reported by Willmarth and Wooldridge,[27] the interesting result that they pointed out is that near the wall in the planes $\frac{x_2}{\delta^*} = 0.20$ and 0.10 the constant cor-

relation contours of $\overline{pv}$ show a curious swept-back behavior (see Ref. 27, Fig. 37). In the beginning of the present work we made a few measurements of R_{vv} with hot-wires at various distances from the wall and found that near the wall at $\frac{x_2}{\delta^*} \approx 0.2$ there was a change of sign of R_{vv} from positive to negative (see Fig. 15). Grant[6] in his study of large eddies in the boundary layer measured the spatial correlations of each of the three components of the fluctuating velocity; however, he did not report any measurements of R_{vv} for $\frac{x_2}{\delta^*} < 0.29$. With these results it appeared to us that in the wall region there is a definite structure that is worth understanding; and therefore our measurements were mostly performed near the wall.

The measurements described in the present work include space-time correlations between the fluctuating wall pressure and the span-wise velocity component w, and between the various velocity components. The velocity correlations include measurements of the space-time correlation of the streamwise component of the fluctuating wall shear stress. With these measurements we are able to propose a qualitative model for the structure of turbulence near the wall.

The measurements of the correlation between the fluctuating wall pressure and the velocity components by Willmarth and Wooldridge[27] include $\overline{pu}$ and $\overline{pv}$. In the present work we have continued the program and measured the correlation of $\overline{pw}$ and constructed its constant correlation contours. Interest was found in these contours of constant $\overline{pw}$, which gave support to the proposed model of the structure of turbulence

near the wall. We shall discuss the details of this in Chapter IX and describe the measurements in Chapters VI and VII. A rough comparison of the present $\overline{pw}$ measurements with Kraichnan's[12] wall pressure theory was also made, and given in Chapter VIII.

In Chapter IV, we have described the measurement of the mean wall shear stress with a single hot-wire using Wills'[28] experimental method to correct for the effect of wall heat transfer.

We have used hot-wires to measure the correlation between the fluctuating streamwise velocity very near the wall. We have also studied the existence of the instantaneous linear velocity profile in the sublayer (see Appendix I). With the instantaneous linearity of the velocity profile near the wall confirmed, we are able to interpret our correlation measurements of $\overline{uu}$ performed in the sublayer region as the correlation of the fluctuating streamwise wall shear stress or fluctuating spanwise vorticity component, and to deduce the correlation distribution and the propagation in the wall region. These results are included in Chapter V, VII, and VIII.

The present investigation was carried out in a 5-in. thick turbulent boundary layer at a nominal free stream velocity of 206 fps. The ratios of pressure transducer diameter and hot-wire length to boundary layer thickness were approximately 1:80 and 1:100, respectively, allowing a study of the detailed structure of the fluctuations in the layer.

Corrections and errors of the present measurements are described in Appendix II.

CHAPTER II

EXPERIMENTAL APPARATUS AND PROCEDURE

A. WIND TUNNEL FACILITY

The experiments were carried out in the fully developed turbulent boundary layer on the floor of the 5 by 7 ft low speed wind tunnel facility at the Aeronautical Engineering Laboratories, The University of Michigan. The wind-tunnel test section is 25 ft long and is indoors. The settling chamber, fan, and steel ducting that recirculates the air are out of doors. The total distance around the wind-tunnel circuit is 332 ft. The contraction ratio of the nozzle is 15:1.

A schematic diagram showing the general layout is given in Fig. 1. Natural transition took place in the contraction section (approximately 24 ft ahead of the measuring point) and no tripping device was required to make the boundary layer fully turbulent. A varnished and waxed sheet of masonite extending 14 ft upstream from the point of measurement was installed to make the wall aerodynamically smooth. In order to eliminate the undesirable effects of wind tunnel vibration, measurements were made on a 1 in. thick smooth (oil-lapped) steel plate, 20 in. in diameter and mounted on a heavy pedestal, which was inserted flush with the floor. The 0.0625 in. gap which was allowed between the plate and the wind-tunnel floor was sealed on the outside of the tunnel with a strip of rubber. The mounting pedestal was vibration-isolated from the floor by means of rubber shock pads. Holes were drilled in the plate to

accept the pressure crystal assembly and the hot-wire plug. The hole for the former is 0.3125 in. in diameter while that for the latter is 1 in. in diameter.

B. INSTRUMENTATION

The fluctuating wall pressure was measured with a pair of 0.060 in. diameter lead-zirconate disks mounted back to back in a brass plug which was supported in the steel plate by a screw-controlled holder attached underneath the plate. The sensitive area of the pressure transducer which was newly made by Willmarth, is about 7.4 times smaller than that used in the former measurements by Willmarth and Wooldridge,[26,27] thus spatial attenuation caused by the finite size of pressure transducer is decreased and the resulting pressure measurement is more representative for the point to be measured. As shown in a schematic diagram of the transducer installation (see Fig. 2), rubber O-rings were used to prevent air leakage around the transducer body. The transducer was connected through a low-noise cable to a low-noise preamplifier having a cathode follower input with an input impedance of 1.2×10^8 ohms. The capacity of the lead zirconate disks connected in parallel was 60 micro-microfarads, allowing a low frequency response down to approximately 25 cps. The gain of the preamplifier was approximately 50; it was followed by a two-stage amplifier which gave the entire system a maximum gain of 100,000. The bandwidth of the amplifier circuitry was adjustable between 1 cps and 160 kcps.

The fluctuating velocities were measured with constant current hot-wire equipment manufactured by Shapiro and Edwards. The frequency response of the uncompensated amplifier was flat from 1.3 cps to 320 kcps. Adjustable filters in the amplifier were used to cut out frequencies above and below the range needed in the experiments (1.3 cps < f < 80 kcps) to eliminate unnecessary noise. In the measurements of velocity-velocity correlations one additional amplifier made according to the design of Kovasznay[32] was used. Its frequency response without compensation was flat from 5 cps to 25 kcps when its filter adjusting switch was set at the widest band position (1 cps < f < 50 kcps). Both platinum and tungsten wires of 0.00015 in. or 0.0002 in. in diameter were used. Their lengths ranged from 0.03 to 0.05 in, and in any case a slenderness ratio greater than 150 was employed to take care of the effect of finite wire length.[13] The wires were attached to the supports by the usual method of copper plating and soldering. In case of velocity measurements very near the wall, silver-coated platinum wires were glued directly on the smooth surface of a plug 1 in. in diameter (see Fig. 3). Then the sensitive parts of the wires were obtained by the method of etching with dilute nitric acid and electrolysis. The plug was made of insulating material such as, bakelite and Plexiglas. The time constant of the wires was approximately from 0.35 to 0.50 msec. The compensation required to correct for the time lag of the wires was determined by the square wave method and accomplished by a resistance-capacitance network in the amplifier. No wire length corrections were applied to any of the data. As

reported by Willmarth and Wooldridge[27] the microscale of the turbulence near the wall was calculated from the measured spectra and found to be approximately twice the hot wire length (ℓ = 0.05 in.). Moreover, the upper frequency limit on the tape recorder described below limits the smallest eddy which can be studied to a scale of approximately the hot wire length.

For the measurements of fluctuating velocity at a distance greater than 0.05 in. from the wall, a probe made of 0.19 in. brass tube and strengthened by thin sheet metal was used to support the hot-wire needles; see Fig. 2. Measurements very near the wall were obtained by fastening the hot wire probes directly on the wall. In case of the measurement of streamwise wall shear correlations and wall shear-cross flow correlations the wire itself was glued on the surface of a plug as described above to reach the points inside or near the edge of the viscous sublayer ($\delta_{SL} \approx 0.0043\ \delta^*$). For the closest spacing to the wall, a microscope with a filar eye piece was used to measure the distance between the wire and its surface reflection.

The signals from the pressure and velocity transducers were recorded on a three-channel Ampex Model FR-1100 magnetic tape recorder which utilized 0.5 in. wide tape travelling at 60 in. per sec. The recorder had a bandwidth extending from d-c to 10 kcps. In the present measurements special filters were used to replace the original 10 kcps filters in the record and reproduce units for each channel. Thus the limiting upper frequency for the measurements was extended to 20 kcps

so as to be able to measure small eddies of approximately the same size as the hot wire length. A special movable play-back head was used to replace the original recorder head to allow the introduction of time delay between a pair of signals. The smallest incremental time delay which could be obtained was 0.017 msec.

The correlator used in the measurement of the space-time correlations worked on the mean-square principle. A thermocouple was used to measure the mean-square values of each of the two signals to be correlated, of their sum, and of their difference. The sum was obtained from a simple resistive summing circuit built into the apparatus, and the difference was obtained by first sending one signal through an electronic phase inverter and then into the summing circuit. A provision for external filtering of the signal before it reached the thermocouple allowed the measurement of correlations in adjustable frequency bands; a Krohn-Hite Model 310-AB filter was used for this purpose (see Section III-B). The output from the thermocouple was measured on a sensitive research d-c millivoltmeter having a time constant of 3 sec.

CHAPTER III

EXPERIMENTAL ENVIRONMENT

A. EXTRANEOUS DISTURBANCES

The accuracy of the measurements made in this report can be affected by the extraneous disturbances which include the vibration of the measuring apparatus, the sound field in the wind tunnel, the free stream turbulence level, and the mean flow conditions in the boundary layer. These disturbances were studied and reported formerly by Willmarth and Wooldridge; the following is quoted from their work (Ref. 27, p. 4-5):

> " A check on the effectiveness of the vibration isolation of the mounting showed that the spurious pressure signals caused by vibration amounted to less than 1/100 of the mean-square turbulent pressure fluctuations.
>
> "The sound field in the test section was first measured by a pressure transducer located on the stagnation line of an airfoil-shaped body exposed to the free stream. The spectrum of the stagnation pressure fluctuations had peaks at 135 and 200 cycles per sec. The wall pressure correlation measurements described in Reference 11 which were made later showed a small peak at negative time delay which was caused by sound propagating upstream. From these data it was finally determined that the mean-square sound pressure in the free stream amounted to approximately 1/20 of the mean-square turbulent wall pressure fluctuations. The mean-square velocity fluctuations associated with the sound were less than 1/2 percent of the mean square turbulent fluctuations near the edge of the boundary layer.
>
> "The settling chamber of the wind tunnel contains four turbulence damping screens. The free-stream turbulence level in the test section increases with velocity and has been measured at 50, 100, and 150 fps. Extrapolation of the data to the 200 fps speed used in this experiment results in a value of $\sqrt{\overline{u^2}}/U_\infty = 1 \times 10^{-3}$ for the turbulence level of the axial velocity component. The level of the transverse velocity component is approximately three times the level of the

axial component.

> "Large-scale flow disturbances in the test section boundary layer were first discovered during the measurements of the wall pressure spectra which are described below. The entire wind tunnel, with the exception of the test section, is exposed to the weather. Heat transfer through the steel walls caused by sunlight impinging on the outside of the tunnel produced density stratification near the walls which in turn produced vorticity when accelerated into the test section. Observations of streamers of smoke near the concave surface of the contraction section showed large-scale oscillations which were swept into the test section. It is believed that the large-scale disturbances observed in the test section are caused by a combination of the Taylor-Goertler boundary layer instability on the concave walls of the contraction and the density stratification."

The wind tunnel condition has not been changed except that one of the four turbulence damping screens in the settling chamber of the wind tunnel had been damaged and removed sometime before the present measurements were made. We remeasured the free-stream turbulence level and found that $\sqrt{\overline{u^2}}/U_\infty = 2.5 \times 10^{-3}$ in axial flow direction. The level of the transverse velocity component is $\sqrt{\overline{v^2}}/U_\infty = 3.2 \times 10^{-3}$. Both were measured at an air speed of 200 fps, which was used to obtain a fully turbulent boundary layer for all measurements in the present work.

B. THE NATURE OF THE TURBULENT BOUNDARY LAYER USED IN THE INVESTIGATION

The mean velocity profile, velocity intensity profile, wall pressure spectrum and velocity spectra of the turbulent boundary layer used for the present investigation, were measured and reported by Willmarth and Wooldridge.[27] So, no such experiment has been repeated. The properties of the boundary layer profile measured by them are tabulated in Table I and reprinted in Fig. 4 together with the properties of Coles'

ideal boundary layer at the same value of R_θ, the Reynolds number based on momentum thickness. Figure 4 and Table I show that their measurements agree satisfactorily with the ideal case.

TABLE I

PROPERTIES OF THE ACTUAL AND IDEAL TURBULENT BOUNDARY LAYER

T °F	U_∞ fps	R_θ	δ ft	δ^* ft	θ ft	δ^*/θ	U_τ/U_∞	R	Remarks
67	204	38,000	0.42	0.041	0.0315	1.30	0.0326	3.1×10^7	Measured by Willmarth and Wooldridge
		38,000				1.30	0.0318	3.2×10^7	Coles' ideal boundary layer
45	203	43,000	0.42	0.041	0.0315	1.30	0.0325	3.85×10^7	Willmarth and Wooldridge
		43,000				1.295	0.0315	4.0×10^7	Coles' ideal boundary layer

In the measurements of wall pressure spectrum Willmarth and Wooldridge[26] found that the data were not repeatable for $\frac{\omega\delta^*}{U_\infty} < 0.13$. The results varied with the amount of heat transfer to the tunnel by sunlight. Therefore, in the measurements of space-time correlation of pressure-velocity and velocity-velocity the Krohn-Hite filter has been used to reject all frequencies below $\frac{\omega\delta^*}{U_\infty} = 0.13$. The upper limit on the frequency, $\frac{\omega\delta^*}{U_\infty} = 25$, was provided by the tape recorder response.

At the closest spacing of the hot-wire to the wall, 0.002 in., for the streamwise wall shear-wall shear correlation measurements the convection speed of the disturbances is approximately 0.2 U_∞. Since the boundary layer thickness is 5 in. disturbances convected at this speed and at

$\frac{\omega\delta^*}{U_\infty}$ = 0.13 have a wave-length of 0.93 δ. Hence, even with filtering and very near the wall information can be obtained about eddies or disturbances whose scale is about the same as the boundary layer thickness. However, in correlation measurements the filter acts directly to eliminate the correlation in the frequency band below its cut-off point, and indirectly to boost the value of the normalized correlation coefficient at all values of time delay by reducing the magnitude of the denominator. The net effect with filter cut-off frequency at $\frac{\omega\delta^*}{U_\infty}$ = 0.13, as studied by Willmarth and Wooldridge[27] in the pressure-velocity correlation measurements, is not more than 5%. Their analysis also showed that the direct effect of the filtering changes the correlation curves most near their tails. This is to be expected since at large time delay or at large spacing between measuring points the correlation is mainly contributed from the low frequency (large scale) velocity fluctuations. The filter effect also increases with distance from the wall since low frequency fluctuations become increasingly important in the correlation measurement as this distance increases.

CHAPTER IV

THE MEASUREMENT OF MEAN WALL SHEAR STRESS USING A SINGLE HOT-WIRE AND THE CORRECTION FOR THE EFFECT OF WALL HEAT TRANSFER

A. INTRODUCTION

The mean wall shear stress of the turbulent boundary layer used in the present investigation was measured by Willmarth and Wooldridge,[26,27] and reported in the form of a non-dimensional friction velocity $\frac{U_\tau}{U_\infty}$ (see Table I, Section III-B). The measurement was made by them with a Stanton tube using the calibration results reported by Gadd.[30] Other methods such as the "floating" element device developed by Dhawan[31] have been successfully used by different investigators: Hakkinen, Coles, and Korkegi (e.g., see Ref. 7).

In the present work, however, the mean wall shear stress was measured by using a single hot-wire which was set up outside but very near the edge of viscous sublayer. The distance to the wall was determined with the aid of a microscope fitted with a filar eyepiece and was found to be 0.00439 δ^*. A piece of silver-coated platinum wire with a diameter of 0.0002 in. was glued directly on the flat surface of a plug as described in Section II-B. A sensitive length of 0.043 in. was obtained by etching off the silver coating in a very small jet of dilute nitric acid with an electric current of about 0.8 milliampere. Technically there was not much difficulty to place the hot-wire even closer to the wall to ensure that it was in the sublayer region, $\frac{x_2 u_\tau}{\nu} < 5$; but when the wire was too

close to the wall the Reynolds number of the wire, $(Rey)_w$, would be near unity and thus King's linear relation would not be valid (Ref. 13, p. 231). There were also difficulties in calibrating the hot-wire at a speed as low as 20 fps with the present equipments.

B. CALIBRATION

At the beginning of measurements the hot-wire was calibrated and a curve was plotted with I^2R_w vs $\sqrt{U}$. Since, according to the usual form of King's formula for incompressible subsonic flow, we have

$$Q = I^2R_w = (T_w - T_e)(A + B\sqrt{U})$$

where A,B = constants

However, the calibration curve obtained was not quite a straight line; it became curved in the region where $\sqrt{U} > 10(\text{fps})^{1/2}$. After a study of the flow parameters involved in the present problem the above calibration curve was replotted with I^2R_w vs $\sqrt{\rho U}$ to include the effect of compressibility and then it turned out to be linear (see Fig. 5). This would be quite clear if one was guided in the study by a more general relation of the heat transfer of a thin wire with forced convection[13] (Prandtl No. = const.),

$$Nu = a + b\sqrt{(Rey)_w}$$

where a, b = constants.

In the present measurement, a linear calibration curve was found very convenient to use, especially when correction was necessary in case that the ambient temperature and the density of air during calibration were different from those during measurement.

C. THE MEASUREMENT OF MEAN WALL SHEAR STRESS

Difficulties were experienced by many investigators when using a hot wire for velocity measurements close to a solid boundary. Besides setting up the wire at an adequate distance to the wall to ensure the validity of King's linear relation and measureing this distance accurately, one must also correct for the effect of wall heat transfer. Wills[28] (1962) made a comprehensive study of the latter problem and conducted a series of experiments. The results were plotted into curves which can be used to correct, at different heights, the errors introduced by the effect of wall heat transfer. Because of its simplicity and convenience Will's correction method was successfully employed in the present work to compute the mean wall shear stress. The result (see Appendix III for details) that we found was:

$$\bar{f}_w = 0.0912 \quad \text{lb/sq ft}$$

where $\bar{f}_w$ = mean wall shear stress,

or the non-dimensional wall friction velocity,

$$\frac{U_\tau}{U_\infty} = \frac{1}{U_\infty}\sqrt{\frac{\bar{f}_w}{\rho_a}}$$

$$= 0.032 ,$$

which agrees very well with the result by Willmarth and Wooldridge with Stanton tube,

$$\frac{U_\tau}{U_\infty} = 0.0326 \qquad \text{(see Table I);}$$

and by Coles' ideal boundary layer based on same R_θ,

$$\frac{U_\tau}{U_\infty} = 0.0318 \qquad \text{(see Table I).}$$

In calculation of the mean velocity, a correction for the error due to nonlinear effects of the turbulent velocity fluctuations was also studied. The correction found by our analytical method was 3% (see Appendix II-A), which was checked with the result by a graphical method.

CHAPTER V

SPACE-TIME CORRELATIONS OF WALL SHEAR-WALL SHEAR, OF WALL SHEAR-VELOCITY, AND OF VARIOUS VELOCITY-VELOCITY COMPONENTS

A. INTRODUCTION

In recent years different investigators,[4,6,9,14,17,19,21,23,27,etc.] either theoretical or experimental, have been interested in studying the turbulence near the wall in a boundary layer. The main purposes of their work may be summarized as:

(1) To determine the structure of turbulence in the wall region;

(2) To determine whether the so called "laminar sublayer" exists or not and to determine its structure;

(3) To determine the mechanism which maintains the turbulence in a boundary layer.

Many brilliant investigations have been carried out; however, to the author's knowledge, we are still far from reaching a general conclusion or a complete understanding.

In the previous measurements by Willmarth and Wooldridge the contour diagrams of constant correlation $\overline{pv}$ in the planes which are parallel to the $x_1 - x_3$ plane and near the wall (see Ref. 27, Fig. 37, p. 52) showed a very interesting behavior. It was observed that in the plane $\frac{x_2}{\delta^*} = 0.20$ a protruding part of the positive contour of R'_{pv} started to appear in the negative region ($x_1 < 0$). The protruding part became even sharper and extended further into the negative area when $\frac{x_2}{\delta^*} = 0.10$.

Naturally, this phenomenon suggests that in the horizontal plane near the wall ($\frac{x_2}{\delta^*} \lesssim 0.20$) the vertical component of fluctuating velocity changes its sign at certain distance along x_3-axis and it seems that only the existence of a certain type of eddies may serve to explain it satisfactorily.

All these previous investigations greatly stimulated the present work in an attempt to understand the turbulence in the wall region. A number of velocity-velocity correlation measurements in different directions and either at the edge or outside the viscous sublayer were carried out. The results revealed many interesting points, of which more discussions and a study related particularly to the structure of turbulence near the wall will be given in Chapter IX.

B. MEASUREMENTS

The fluctuating velocities in the turbulent boundary layer are stationary random functions of time and space. The velocity-velocity correlation coefficients which have been measured are defined by

$$R_{u_i u_j}(x_2;x_1',x_2',x_3';\tau) = \frac{\overline{u_i(x_1,x_2,x_3;t)\, u_j(x_1+x_1',x_2+x_2',x_3+x_3';t+\tau)}}{\sqrt{\overline{u_i^2}\,(x_1,x_2,x_3;t)}\sqrt{\overline{u_j^2}(x_1+x_1',x_2+x_2',x_3+x_3';t)}} \quad \text{(V-1)}$$

In case both u_i and u_j in the direction of free stream ($i = 1$, $j = 1$) are measured in the linear viscous layer, then since

$$\tau_w \doteq \mu \frac{u(\vec{x},t)}{x_2}$$ [The existence of instantaneous linearity in the viscous sublayer will be discussed in Appendix I]

one can obtain

$$R_{\tau_w\tau_w}(x_1', 0, x_3';\tau) \doteq \frac{\overline{\mu \frac{u(x_1,x_2,x_3;t)}{x_2} \cdot \mu \frac{u(x_1+x_1',x_2+x_2',x_3+x_3';t+\tau)}{x_2 + x_2'}}}{\sqrt{\overline{\left[\mu \frac{u(x_1,x_2,x_3;t)}{x_2}\right]^2}}\sqrt{\overline{\left[\mu \frac{u(x_1+x_1',x_2+x_2',x_3+x_3';t)}{x_2 + x_2'}\right]^2}}}$$

$$= \frac{\overline{u(x_1,x_2,x_3;t)\ u(x_1+x_1',x_2+x_2',x_3+x_3';t+\tau)}}{\sqrt{\overline{u^2}(x_1,x_2,x_3;t)}\sqrt{\overline{u^2}(x_1+x_1',x_2+x_2',x_3+x_3';t)}} \qquad \text{(V-2)}$$

where $x_2 \leq \delta_{SL}$ (thickness of viscous sublayer)

$x_2 + x_2' \leq \delta_{SL}$

similarly, we have

$$R_{\tau_w u_j}(x_1', x_2', x_3';\tau) \doteq \frac{\overline{u\ (x_1,x_2,x_3;t)\ u_j(x_1+x_1',x_2+x_2',x_3+x_3';t+\tau)}}{\sqrt{\overline{u^2}(x_1,x_2,x_3;t)}\sqrt{\overline{u_j^2}(x_1+x_1',x_2+x_2',x_3+x_3';t)}} \qquad \text{(V-3)}$$

where $x_2 \leq \delta_{SL}$

Hence, one defines the wall shear-wall shear or the wall shear-velocity correlation coefficient in terms of a velocity-velocity correlation coefficient.

The measurements of $R_{\tau_w\tau_w}$, $R_{\tau_w u}$, $R_{\tau_w w}$, R_{uu}, R_{vv}, R_{ww}, R_{uw} and R_{vw} are shown in Figs. 6 through 28 as functions of the non-dimensional time delay $\frac{U_\infty(\tau-\tau')}{\delta^*}$ where τ' is the time delay for maximum correlation of any particular curve. An additional vertical axis stands on each curve,

except those with $\frac{x_1'}{\delta^*} = 0$ (or $\frac{U_\infty \tau'}{\delta^*} = 0$), and shows the true origin $\frac{U_\infty \tau}{\delta^*} = 0$. In each case the non-dimensional convection speed $\frac{U_c}{U_\infty}$ can be computed by dividing the longitudinal spacing $\frac{x_1'}{\delta^*}$ by the corresponding non-dimensional time delay $\frac{U_\infty \tau'}{\delta^*}$. Since τ' is the time delay for maximum correlation, the convection speed determined in this way is defined by $\frac{\partial R_{u_i u_j}(x_1', \tau)}{\partial \tau} = 0$. According to Wills[33](1964), in measurements in a shear flow the convection speed, U_c, is a function of spacing δ (between two measuring points) and time delay τ; when U_c is defined by $\frac{\partial R(\delta,\tau)}{\partial \tau}$ or $\frac{\partial R(\delta,\tau)}{\partial \delta} = 0$ a slight difference in magnitude was observed. However, for practical reasons the convection speed defined by $\frac{\partial R_{u_i u_j}}{\partial \tau} = 0$ was used in the present work.

C. RESULTS

The convection speed U_c in each case was computed by using the following relation,

$$\frac{x_1}{\delta^*} = - \frac{U_\infty \tau}{\delta^*} \frac{U_c}{U_\infty} \qquad (V\text{-}4)$$

and was marked in the corresponding figures.

The measured correlation curves of $R_{\tau_w \tau_w}$ are symmetrical about the vertical axis passing through the origin of the time delay axis. The symmetry was destroyed when one of the measuring points was raised from $\frac{y}{\delta^*} = 0.005$ to 0.204. When $y/\delta^* > \delta_{SL}$, we actually measured $R_{\tau_w u}$ instead of $R_{\tau_w \tau_w}$ since one of these two measuring points was not in the linear viscous region. The peak value of the correlation curve of $R_{\tau_w u}$ was found

to increase slightly and shifted to the left side ($\tau < 0$) with the increasing y/δ^*. Such a destruction of symmetry and the shift of the peak of the correlation curves, which appear clearer in the contour diagrams of the constant correlation $R_{\tau_w u}$ (see Figs. 7, 40 and Section VII-C), will be explained in Section VIII-A.

In the R_{vv} measurements at zero time delay a change of sign from positive to negative was observed when the two probes approached the wall as near as $\frac{x_2}{\delta^*} = 0.16$ (see Fig. 15). Grant[6] (1958) did not report any measurements of R_{vv} for $\frac{x_2}{\delta^*} < 0.29$. In his reported measurements near the wall, also no negative R_{vv} has been observed.

The change of sign was also found in the present measurements of R_{wv} near the wall at zero time delay when the two hot-wires which were set up at the same values of x_1 and x_2 but different x_3 were interchanged [e.g., $\frac{x_3'}{\delta^*} = \pm 0.223$ for R_{wv} (see Fig. 26)]. Furthermore, when one studies the measurement of R_{wv} (see Fig. 28) one finds that R_{wv} changes from a negative to a positive value as $\frac{x_1'}{\delta^*}$ varies from + 1.52 to - 1.52. The change of sign in the above mentioned measurements and the unusual behavior of R_{wv} show that there is a definite structure of turbulent eddies in the wall region. We shall study this structure in more detail in Chapter IX.

CHAPTER VI

SPACE-TIME CORRELATION OF PRESSURE-SPANWISE VELOCITY, R_{pw}

A. INTRODUCTION

The pressure-velocity correlation measurements of R_{pu} and R_{pv} reported by Willmarth and Wooldridge[27] were quite extensive and revealing. In the present work a number of measurements of R_{pw} were made for the following purposes:

(1) To study how the turbulent velocity w is correlated to the wall pressure fluctuation;

(2) To study the relation between $\overline{pw}$ and $\overline{vw}$ using Kraichnan's[12] theory for the wall pressure fluctuations (see Section VIII-B); and

(3) To construct contours of constant R_{pw} in order to study the turbulent structure near the wall.

B. MEASUREMENTS

The pressure-velocity cross-correlation coefficient, R_{pw} is defined by

$$R_{pw}(x_1,x_2,x_3;\tau) = \frac{\overline{p(x,y,z;t)\ w(x+x_1,y+x_2,z+x_3;t+\tau)}}{\sqrt{\overline{p^2}(x,y,z;t)}\sqrt{\overline{w^2}(x+x_1,y+x_2,z+x_3;t)}} \qquad \text{(VI-1)}$$

The experimental measurements are shown in Figs. 30 through 38 as functions of the non-dimensional time delay $\frac{U_\infty(\tau-\tau')}{\delta^*}$. The shift of the origin on the time delay axis, given by $\frac{U_\infty\tau'}{\delta^*}$, is defined in the same way as

has been explained in Section V-B above.

In consideration of the symmetry of R_{pw} about the x_1-x_2 plane, let us refer to Fig. 29 where the point of measurement of pressure fluctuations coincides with the origin and the points A and B are symmetrical with respect to the x_1-x_2 plane. The flow direction is into the plane of the figure along x_1-axis which is not shown. Assume that a homogeneous turbulence exists in the plane which is parallel to the wall as is the case the boundary layer used in the present study. Then, if one defines the positive sign of velocity component w being along the positive direction of x_3-axis, it will be quite obvious that +w at point A or -w at point B should give the same pressure response at point p merely because of geometrical symmetry. One can write

$$R_{pw}(x_1,x_2+x_3) = -R_{pw}(x_1,x_2,-x_3) \qquad \text{(VI-2)}$$

and infer that when $x_3 = 0$

$$R_{pw}(x_1,x_2,0) = 0 \qquad \text{(VI-3)}$$

from an argument of R_{pw} being unable to be either positive or negative. Consequently, in measuring R_{pw}, one can confine oneself to the quarter space between positive x_2-axis and positive x_3-axis and reduce the amount of work required.

C. RESULTS

The convection speed, U_c, of the disturbance as defined in Section

V-B was found equal to the local mean speed when spacing is not too large, or

$$U_c = U.$$

Since the same result was also found in R_{pu} and R_{pv} measurements formerly made by Willmarth and Wooldridge,[27] one may conclude experimentally that all the three pressure-velocity correlations (i.e., R_{pu}, R_{pv} and R_{pw}) are convected with the local mean speed when spacing is not too large.

Measurements of R_{pw} (see Figs. 30-31) showed that R_{pw} is an odd function of x_3, which supports the discussion made in Section VI-B above.

The measurements have been used also to construct contour diagrams of constant R_{pw}, which will be presented in Chapter VII.

CHAPTER VII

CONTOURS OF CONSTANT CORRELATION OF $\overline{\tau_w \tau_w}$, OF $\overline{\tau_w u}$ AND OF $\overline{pw}$

A. INTRODUCTION

Owing to the existence of the linearity (see Appendix I) in the viscous sublayer, the longitudinal fluctuating velocity u implies a fluctuating slope of the velocity profile in that region. Physically, a fluctuating slope of the velocity profile means a fluctuating local wall shear stress. Thus, we measured the streamwise wall shear-wall shear and streamwise wall shear-velocity correlations with hot-wires and plotted them as functions of nondimensional time delay. Since the fluctuating wall shear stress

$$\tau_w \doteq \mu \frac{u}{x_2} \qquad (x_2 \leq \delta_{SL})$$

where $\frac{u}{x_2}$ can be interpreted as the fluctuating vorticity component in x_3-direction in viscous layer, these measurements can also be interpreted as the correlations of vorticity-vorticity (ζ-ζ) and of vorticity-velocity (ζ-u) where ζ=fluctuating vorticity component in x_3-direction in the viscous layer. With these results we constructed contour diagrams of constant $R_{\tau_w \tau_w}$ (or $R_{\zeta\zeta}$) and of constant $R_{\tau_w u}$ (or $R_{\zeta u}$) in order to obtain a clear picture of the correlation field of the fluctuating streamwise wall shear stress or the fluctuating vorticity component in x_3-direction in the viscous sublayer.

The contours of constant correlations, $\overline{pu}$ and $\overline{pv}$ were measured and reported by Willmarth and Wooldridge.[27] In the present work the results of the measurement of correlation, $\overline{pw}$ have also been used to construct

similar contours of constant correlations. Thus, together with the former work, we have a complete set of constant correlation contours of $\overline{pu}$, $\overline{pv}$ and $\overline{pw}$ which may help those working on the similar problems to get better understanding of how the three fluctuating velocity components in the semi-space above the wall produce the pressure fluctuations at the wall.

B. THE CONSTRUCTION OF THE CONTOURS

A direct measurement of enough data points to allow the construction of the contours of constant correlations of $\overline{\tau_w \tau_w}$, of $\overline{\tau_w u}$, and of $\overline{pw}$ would require tremendous tunnel work; furthermore, it was found during the experimental measurements that interference effects between the hot wire probe and the pressure transducer made it impossible to obtain reliable data when the pressure transducer was located in the wake behind the hot wire probe. Hence, the spatial correlation contours were obtained from the measured time-delay correlations at zero longitudinal separation by using the convection transformation

$$\frac{x_1}{\delta^*} = -\frac{U_\infty \tau}{\delta^*} \frac{U_c}{U_\infty} \qquad \text{(VII-1)}$$

The correlation contours obtained by the use of this transformation are shown in Figs. 39 through 46 where in case of $\overline{pw}$ measurements the origin of the corrdinate system is located at the point where the wall pressure was measured, and in case of $\overline{\tau_w \tau_w}$ or $\overline{\tau_w u}$ measurements the origin is located at the wall and directly beneath one of the two hot-wires.

C. RESULTS

The contour diagram of constant $R_{\tau_w\tau_w}$ (or $R_{\zeta\zeta}$) constructed above appeared to be a very narrow strip. It is some $12\delta^*$ in length and $2\delta^*$ in width. The maximum positive correlation was at the point where the fixed u-wire in the viscous layer was located during measurement (see Fig. 39). The contour diagram of $R_{\tau_w u}$ (or $R_{\zeta u}$) for $\frac{x_2'}{\delta^*} = 0.118$ was similar in shape, but elongated along $\frac{x_1'}{\delta^*}$ axis ($29\delta^*$ in length and $1.8\delta^*$ in width) and with the maximum positive value of $R_{\tau_w u}$ located off the origin at $\frac{x_1'}{\delta^*} \approx 0.6$ and $\frac{x_3'}{\delta^*} \approx 0.13$ (see Fig. 40). The angle of sweep of this maximum positive $R_{\tau_w u}$ was measured to be 12° to the $\frac{x_1'}{\delta^*}$ -axis when projected on the $\frac{x_1'}{\delta^*} - \frac{x_3'}{\delta^*}$ plane, and 11° to the $\frac{x_1'}{\delta^*}$ -axis when projected on the $\frac{x_1'}{\delta^*} - \frac{x_2'}{\delta^*}$ plane. It is believed that this sweep represents the effect of convection and turbulent diffusion of the local wall shear fluctuations or the vorticity fluctuation in the x_3-direction. To verify this point, a simple calculation has been made and will be found in Chapter VIII below.

The contours of constant correlation R_{pw} which lie in vertical planes perpendicular to the flow at $\frac{x_1}{\delta^*} = -1, -0.5$ and 0 are positive and are closed curves of constant R_{pw}. These positive contours have a tendency to move upward when $\frac{x_1}{\delta^*}$ increases from negative to positive values. The positive contours are replaced by the negative contours near the wall when $\frac{x_1}{\delta^*} = +1$, and finally break into two separate groups of positive contours with the negative contours near the wall growing even larger when $\frac{x_1}{\delta^*} = +3$ (see Figs. 41 through 46). An explanation of the variation of the

R_{pw} contours along $\frac{x_1}{\delta^*}$ -axis has been attempted and will be included in Chapter IX.

CHAPTER VIII

DISCUSSION OF THE RESULTS OF MEASUREMENTS

A. THE PROPAGATION OF FLUCTUATING WALL SHEAR (OR FLUCTUATING VORTICITY IN x_3-DIRECTION) DUE TO CONVECTION AND DIFFUSION

The contour diagram of constant correlation of $\overline{\tau_w \tau_w}$ (Fig. 39) and that of $\overline{\tau_w u}$ (Fig. 40) show that there is a shift of the maximum positive correlation off the origin when the moving wire has larger distance from the wall than the fixed wire. In Fig. 40, the location of maximum positive correlation was observed to be:

$$\frac{x_1'}{\delta^*} \doteq 0.60 \qquad \frac{x_3}{\delta^*} \doteq 0.13$$

This deviation from the origin of the axes is believed to be caused by convection and turbulent diffusion, and thus shows how the fluctuating wall shear propagates from inside the sublayer region ($\frac{x_2 U_\tau}{\nu} < 5$). According to the theory of turbulent diffusion (Ref. 29, p.48), at small time t diffusion proceeds proportionally with time, or

$$\sqrt{\overline{x_i^2}} \doteq \sqrt{\overline{u_i^2}} \cdot t \qquad \text{(VIII-1a);}$$

and at large time $t \gg t^*$, where t^* is the time for which the Lagrangian correlation $R_L(t^*) = \frac{\overline{u_i(t) u_i(t+t^*)}}{\sqrt{\overline{u_i^2}}} \doteq 0$, diffusion is proportional to the square root of time, or

$$\sqrt{\overline{x_i^2}} \doteq \sqrt{2\mathcal{J}_L} \sqrt{\overline{u_i^2}} \sqrt{t} \qquad \text{(VII-1b)}$$

where

$$\mathcal{T}_L = \int_0^{t^*} d\tau \, R_L(\tau)$$

Assume that very near the wall the turbulence is beginning to diffuse, hence we apply Eqn. (VIII-1a) in the calculation below. Next we refer to Fig. 47 and suppose that a random disturbance first hits the u_1-wire at $x_1 = 0$, $x_2 = 0.002$ in, $x_3 = 0$ (location of the fixed wire during measurement of R_{uu}) and reaches a new point within a time period Δt

$x_1 = d_1$ (unknown)

$x_2 = 0.06$ in (height of the 2nd wire; given)

$x_3 = d_3$ (unknown).

On this basis, we are able to equate the following:

$$\Delta t \doteq \frac{d_1}{(U_c)_{avg}} \doteq \frac{d_2'}{(\sqrt{\overline{v^2}})_{avg}} \doteq \frac{d_3}{(\sqrt{\overline{w^2}})_{avg}} \qquad \text{(VIII-2)}$$

where $d_2' = 0.06 - 0.002$

$= 0.058$ in (difference of height between u_1 - and u_2 - wire).

The convection speed was found from measurements:

$(U_c)_{x_2 = 0.002 \text{ in}} = 36$ fps

$(U_c)_{x_2 = 0.06 \text{ in}} = 110$ fps

hence $(U_c)_{avg} \doteq 73$ fps;

also from measurements

$$\left(\sqrt{\overline{v^2}}\right)_{avg} \doteq 12.4 \text{ fps}$$

$$\left(\sqrt{\overline{w^2}}\right)_{avg} \doteq 14.4 \text{ fps.}$$

Substituting the given values into Eqn. (VIII-2), one finds

$$d_1 = 0.34 \text{ in} \qquad d_3 = 0.068 \text{ in}$$

or $$d_1/\delta^* = 0.69 \qquad d_3/\delta^* = 0.14 \quad \text{(calculated)}$$

where δ^* = displacement thickness of the B.L.

$$= 0.041 \text{ ft.}$$

This result can be compared with what we observed from the location of the maximum positive correlation of $R_{\tau_w u}$ (see Fig. 40 and compare with Fig. 39):

$$\frac{x_1'}{\delta^*} \doteq 0.60 \qquad \frac{x_3'}{\delta^*} \doteq 0.13 \quad \text{(observed)}$$

where x_1', x_3' are corresponding to d_1, d_3 respectively.

As shown above agreement was found between the displacement determined by R_{uu} measurements and the displacement calculated on the assumption that the turbulent diffusion is at the initial stage, one naturally believes that the turbulence very near the wall is still very concentrated and is just beginning to diffuse.

B. PHILLIPS' INTEGRAL CONDITION AND THE MEASUREMENT OF THE PRESSURE-VELOCITY CORRELATION, R_{pw}

Phillips[18] in his study of the aerodynamic surface sound in a turbu-

lent boundary layer derived an integral condition which when applied to the present R_{pw} measurements reads

$$\int_{-\infty}^{\infty}\int_{-\infty}^{\infty} R_{pw}\, dx_1\, dx_3 = 0 \qquad \text{(VIII-3)}$$

where x_1 is the axis along stream direction and x_3 the axis normal to the stream and parallel to the wall. Both the present measurement and our theoretical consideration of R_{pw} showed that it is an odd function of x_3 (see Section VI-B and Figs. 30 through 31), therefore for R_{pw} one can even write down a more strict condition than Eqn. (VIII-3)

$$\int_{-\infty}^{\infty} R_{pw}\, dx_3 = 0 \qquad \text{(VIII-4)}$$

In the report of measurements of the correlations $\overline{pu}$ and $\overline{pv}$ by Willmarth and Wooldridge,[27] a qualitative comparison was made between experimental results and the approximate wall pressure theory of Kraichnan.[12] For the present measurement of $\overline{pw}$ one can also infer a similar relation as follows:

$$\overline{p(0,t)\, w(\vec{x},t+\tau)} = \frac{\rho}{\pi} \int_V \frac{d\bar{U}(r_2)}{d\, r_2}\, \overline{vw}\, (\vec{r}-\vec{x},\tau)\, \frac{r_1}{|\vec{r}|^3}\, dV(\vec{r}) \qquad \text{(VIII-5)}$$

where $\vec{x} = \vec{x}(x_1,x_2,x_3)$ -- fixed

$\vec{r} = \vec{r}(r_1,r_2,r_3)$ -- variable

V = semi-space above the wall

However, too much tunnel work is required to obtain enough information

about the correlation $\overline{vw}(\vec{r}-\vec{x},\tau)$ for just making a qualitative comparison of the above equation, since our measurement showed that the $\overline{vw}$ was not conserved by convection. So we have only studied a special case: When $\tau = 0$ and $\vec{x} = \vec{x}(0,x_2,0)$, then we have $\overline{pw} = 0$ ($\overline{pw}$ is an odd function of x_3) at the left hand side of Eqn. (VIII-5). At the right hand side of Eqn. (VIII-5), $\frac{\partial \overline{U}}{\partial r_2}$ is always positive and our measurement of $\overline{wv}$ showed that near the wall, e.g., $\frac{x_2}{\delta^*} = \frac{r_2}{\delta^*} = 0.102$ (see Figs. 26 through 27) $\overline{wv}$ is an odd function of r_3 and therefore the total volume integral at the right hand side of Eqn. (VIII-5) should vanish also.

The further interest we have in studying the pressure-velocity correlation, R_{pw} lies in its relation with the turbulent structure near the wall which will be presented in detail in the next chapter.

CHAPTER IX

THE STRUCTURE OF TURBULENCE NEAR THE WALL IN A TURBULENT BOUNDARY LAYER

A. INTRODUCTION

As discussed briefly in Chapter V above, the question, "What is the real structure of turbulence near the wall and what is the real mechanism which maintains the turbulence in a turbulent boundary layer?" has interested many investigators, both theoretical and experimental, for decades. To the author's knowledge no definite answer has yet been given. This was not only theoretically due to the lack of a complete mathematics which is able to describe the whole history of the turbulence of different stages existing contemporarily in a turbulent boundary layer, but also experimentally due to the difficulty in techniques that it is almost impossible for us to extract any single turbulent eddy or disturbance to study its origin and development. However, it is believed that the statistical method, when it is properly employed, is still one of the best which can describe the average behavior of turbulence.

In the present work the measurements of the correlations R_{vv} and R_{wv} showed that their behavior in the wall region ($\frac{x_2}{\delta^*} \lesssim 0.2$) was completely different from that at greater distance from the wall. As mentioned in Section V-C, Grant[6] did not report any measurements of R_{wv}, or R_{vv} for $\frac{x_2}{\delta^*} < 0.29$. Also, no negative correlation has been observed in his reported measurements of R_{vv} near the wall. The result of the present measurements

of R_{vv} and R_{wv} together with the constant contour diagrams of R_{pw} and $R_{\tau_w u}$ stimulated us to propose a physical structure of the turbulence near the wall as presented in the following section.

B. THE STRUCTURE OF TURBULENCE NEAR THE WALL

In the problem of the transition from laminar to turbulent boundary layer either theoretical or experimental studies(e.g., 2,8,10,11,22) showed that, in the course of development from two-dimensional Tollmien-Schlichting waves to the final stage when the turbulent spots are formed, a necessary intermediate step is the appearance of streamwise vortex components. According to Stuart,(22) it is this streamwise vortex component which produces the vertical convection of the span-wise vorticity component, $\frac{\partial U}{\partial x_2}$, which is at the same time stretched along the x_3-direction so as to be intensified and eventually generate turbulence. We believe that such a streamwise vortex component, or together with the other two components a three-dimensional vortex line of a certain shape, also exists in the turbulent boundary layer and is an important part of the physical mechanisms which maintain the turbulence.

To explain physically how a three-dimensional vortex line is formed and to find what shape it is we first refer to the work by Browand(3) (1965) who studied the behavior of small vortices in a shear flow. As shown in Fig. 48, Browand concluded that a small vortex of opposite circulation (positive) from the mean circulation (negative) always experiences a restoring force, $\pm \rho(U_2-U_1)\Gamma$ (where Γ is the circulation of

the small vortex), when it is displaced either upward or downward; while a vortex with circulation in the same direction (negative) as the mean circulation (negative) always experiences a destabilizing force when displaced. With this result in mind we now study the region near the wall in a turbulent boundary layer. The viscous sublayer next to the wall is usually considered to be equivalent to a Couette flow in which all disturbances are highly damped,[16] therefore an outer region near the edge of the sublayer, where the damping effect is much weaker but the shear flow is yet very strong, would be more suitable for disturbances to grow and develop. Suppose small disturbed waves, which are mainly two-dimensional, first appear and finally become concentrated to form discrete vortex lines around the edge of the sublayer and in the direction of x_3-axis (see Fig. 49a). As discussed at the beginning of this section the vortex line of opposite circulation from the mean circulation will remain one-dimensional along x_3-axis, while the vortex line with circulation in the same direction as the mean circulation will not remain one-dimensional whenever there is a perturbed vertical motion imposed somewhere at a radnom position along this vortex line. Assume that Browand's two-dimensional result can be applied here locally, then the random disturbance may induce an upward or a downward local motion at the latter vortex line and this local motion will continue in the region where the shear flow is very strong. To illustrate these ideas, suppose there are disturbances of the vortex line as shown in Fig. 49b. Once the vortex line is bent vertically the stretching process in the

shear flow starts simultaneously, and finally the vortex line with circulation in the same direction as the mean circulation will take the form as shown in Fig. 49c. With the above physical strcuture in mind it seems that one can explain why an originally two-dimensional wave motion becomes three-dimensional in a strong shear flow and why the vortex flow in x_2-x_3 plane often occurs in pairs with streamwise vorticity components of opposite sign in a transition boundary layer as observed in experimental works (e.g., see Refs. 6 and 10).

A similar physical structure which was predicted in a transition boundary layer by different authors is quite the same as above. Hama[8] (1963) studied the behavior of a single vortex line in a shear flow and pointed out that besides the stretching due to the shear flow the plane of a curved vortex line rotates in a direction opposite to that of its circulation, which gave the same result as we discussed above. However, Hama did not discuss the case when the circulation of a vortex line has different sign from the circulation of the mean flow. Stuart[22] (1965) studied a problem pertaining to boundary layer transition in which longitudinal vortex pairs already exist in a boundary layer, and under his assumptions he linearized the equation of motion and solved the time dependent problem. He emphasized two things in his paper: the vertical convection and the span-wise stretching (due to $\frac{\partial w}{\partial x_3}$) caused by these streamwise vortices. Owing to the vertical convection the span-wise vorticity component, $\frac{\partial U}{\partial x_2}$, travels upward and downward alternatively along the x_3-direction and owing to the stretching it is intensified

in the course of its travelling. On this basis he finally proposed a structure of the vortex line similar to what we have presented above. Benney[1] (1964) also solved a problem mathematically in a boundary layer possessing constant shear, his result showed the existence of a vortex pair in the y-z plane which agrees with the above discussion.

When compared to the work by Stuart the structure discussed in the present work depends more upon the interaction between the vortex line and the mean shear. Besides, we think that the vortex line picks up motion in the plane perpendicular to the flow direction before its longitudinal vortex line component can be formed from stretching. In any case, Stuart's idea of using the convection and the stretching due to longitudinal vortices to explain the occurrence of intensified shear layers is valuable, since it is believed that such shear layers are closely related to the flow finally breaking into turbulence.[10,11,22]

In the present work, the turbulence generating region near the wall but outside the viscous layer is believed to contain a random distribution of vortex lines making an acute angle to the wall and extending downstream. We shall compare this structure of turbulence near the wall with the experimental results in the following section.

C. COMPARISON WITH EXPERIMENTAL RESULTS

1. R_{vv} Measurements

According to the discussion in previous section near the wall in the turbulent boundary layer there exists a region in which the vortex

lines as shown by Fig.(49c) are randomly distributed with respect to time and space. So, in the x_2x_3-plane one would see an average vortex flow as shown by Fig. 50. If we think that an average model exists there, then it is quite obvious that the double velocity correlation $R_{v_A v_B}$ (where v_A = v measured at point A, etc.) is always negative in this region. Indeed, our measurements showed that when the two measuring hot-wire probes approached the wall region ($\frac{x_2}{\delta^*} \approx 0.2$) the sign of R_{vv} was changed from positive to negative (see Fig. 15). One also can refer to the report by Willmarth and Wooldridge (see Ref. 27, Fig. 37, p. 52) to find the corresponding drastic change in the R_{pv} constant contour diagrams as one approaches the wall at $\frac{x_2}{\delta^*} = 0.5$ and 0.2.

2. R_{wv} Measurements

Referring to Fig. 51, with w measured at point A and v measured at B one should find $R_{w_A v_B}$ to be negative, and similarly $R_{w_A v_C}$ to be positive; therefore

$$R_{w_A v_B} = - R_{w_A v_C}$$

when points B and C are in symmetrical position with respect to point A. The above result was found in agreement with our measurements (see Fig. 26).

Next, referring to the average model of the vortex lines in Fig. 52 one finds $R_{w_B v_A}$ to be negative and $R_{w_C v_A}$ to be positive, which was also verified by our measurements as shown in Fig. 28.

3. R_{pw} Constant Contour Diagrams

If we set up an average model of our vortex lines as shown in Fig. 53a with one of the lower loops located at the point where the perturbation pressure, p, is measured then we can see that the distribution of the sign of velocity component w at different vertical planes which are parallel to the x_2-x_3 plane and located one after the other from upstream to downstream of the origin O, will be as shown in Fig. 53b. Since the fluctuating pressure, p, recorded at the origin O which is directly underneath the lower loop of the vortex core should have a negative sign, one can easily find the distribution of the sign of R_{pw} at these vertical planes as shown by Fig. 53c. Again referring to Fig. 53a, if instead of point O we choose point A as the location where the perturbation pressure is measured, then since the pressure recorded there is positive and the sign of w in different vertical planes as shown by Fig. 53b is also reversed the distribution of the sign of R_{pw} as shown by Fig. 53c will still hold without any change.

The present experimental result of R_{pw} (see Fig. 46) was found to be in coincidence with the result as derived from the above discussion. Besides, the model proposed here can also predict that the pressure-velocity correlation, R_{pw}, is an odd function of x_3 (see Fig. 53a), which agrees with the discussion in Section B, Chapter VI as well as with the experimental result presented in Figs. 30 through 31.

In a closer examination of the contour diagrams of constant R_{pw} (see Figs. 44 through 46), one finds that at positive $\frac{x_1}{\delta^*}$ the positive

contours on the top gradually separated into two groups while the negative contours remained unseparated. To explain this, let us refer to Klebanoff's work (see Ref. 10, Fig. 19, p. 21) where the shape of an actual vortex flow in the x_2-x_3 plane during the nonlinear process of transition to turbulence was plotted and let us think that the contributions to R_{pw} are mainly from the average of two cases: either with the pressure measuring point located at O or at A as shown in Fig. 54a. Then one can see that the two vortex flows (see Fig. 54b,c), when correlated with the pressure at point O or A, will agree with the constant contours of R_{pw} at positive $\frac{x_1}{\delta^*}$ as shown by our experimental result, i.e., the positive constant contours on the top gradually separate into two groups while the negative constant contours remain unseparated.

The scale OA in Fig. 53a was measured from direct observation of the constant contours of R_{pw} and found to be $3\delta^*$. Referring to the same figure, the angle of inclination θ between the plane of the sweeping vortex line of our average model and the wall was computed also by using the R_{pw} constant contour diagrams. From the displacement of the zero line between positive and negative R_{pw} contours at two different vertical planes where $\frac{x_1}{\delta^*}$ was equal to 1 and 3, we found this angle θ to be approximately 35 degrees.

4. R_{uv} Measurements

Schubauer and Klebanoff[20] (1951) measured the correlation of velocity components u, v at the same points in a turbulent boundary layer and found

it always negative. One may easily find that from the present proposed structure of turbulence the fluctuating flow field induced by the inclined vortex line as shown in Fig. 53a, has velocity components u, v which also give negative correlations.

CHAPTER X

CONCLUSIONS

The main results of this experimental work and theoretical study near the wall in a fully developed turbulent boundary layer can be summarized as follows:

(1) Near the wall there was found a turbulence generating region which is filled with random vortex lines inclined at an acute angle to the wall when observed along the x_3-direction. These vortex lines were stretched and intensified in a strong shear region near the wall, and owing to the streamwise component of these vortex lines there must be vertical convection and span-wise stretching (due to $\frac{\partial w}{\partial x_3}$) of the span-wise vorticity component, $\frac{\partial U}{\partial x_2}$, to generate strong shear layers (which are thought to be substantial elements for making turbulence).[10,11,22] It is believed that the proposed structure in the wall region is the real mechanism which serves to maintain the turbulence and to produce the wall pressure fluctuations in a turbulent boundary layer. The proposed structure was strongly supported by the present measurements of R_{vv}, R_{wv} and R_{pw} and it was identified to be quite the same as the structure in transition boundary layer recently studied by different investigators,[e.g.,1,8,22] except that in the present case in a turbulent boundary layer the appearance and the distribution of these inclined vortex lines are much more random.

(2) The diffusion of turbulence near the wall was found approximately proportional to time t. Since this is true only at the initial stage of turbulent diffusion, the turbulence generated in the wall region can reasonably be thought of as fresh and new. Both this result and the result presented in (1) above lead to the conclusion that in a turbulent boundary layer the turbulence is generated in the wall region and spreads to the outer region due to convection, diffusion and the interaction with shear flow. Since it is well known from measurements that eddies of small size dominate near the wall, this implies that at least a portion of the small eddies near the wall may become larger when they distend into the more central parts of the boundary layer. However, the physical mechanism of development from small to large eddies is not yet completely understood.

(3) The measurements show that the profile of the viscous sublayer next to the wall is fluctuating. However, the instantaneous linearity of a fluctuating sublayer profile was demonstrated either from a theoretical or from an experimental study (see Appendix I). On this basis, one can make streamwise wall shear-wall shear (or x_3-component of vorticity-vorticity) correlation measurement by using hot wires.

(4) The zero to zero scale in $\frac{x_3'}{\delta^*}$ -direction of the measured R_{uu} contours near the edge of viscous layer (see Fig. 39) can be interpreted as the average period of variation of u-component in x_3-direction. This scale was measured to be some $2\delta^*$ which is comparable to the corresponding optical observation by Runstadler, Kline and Reynolds (1963) (see

Ref. 19, p. 262).

(5) The mean wall shear stress can successfully be measured with a single hot wire set up at the linear region near the wall, using Wills' experimental method to correct for the effect of wall heat transfer. Correction of the mean-velocity measurement with a hot wire in the presence of velocity fluctuations in a turbulent boundary layer was studied. A correction term of first order to the mean square value of the fluctuating resistance of the hot wire was found analytically for constant current measuring equipment (see Appendix II-A). For the present problem the correction was computed to be 3% which agreed with the correction found by an alternative graphical method. In calibrating the hot-wire in the present measurement of wall shear stress in the wind tunnel, it was found that the calibration curve should be plotted with Nu vs. $\sqrt{(Rey)_w}$ (not I^2 vs. $\sqrt{U}$) so that a linear curve can be obtained in order to make necessary correction easily when the ambient temperature and the air density during calibration are different from those during measurement.

(6) In case that the turbulent velocity is not negligibly small when compared with its mean velocity, the calibration of the turbulent intensity measurement is not linear. The correction term of the $\overline{u^2}$ measurement was found approximately in terms of $\overline{r_w^4}$ and $(\overline{r_w^2})^2$ where r_w is the fluctuating hot resitance of the hot-wire (see Appendix II-B). For the present measurements the possible maximum error was estimated to be 6.5%.

APPENDIX I

THE EXISTENCE OF INSTANTANEOUS LINEARITY IN THE VISCOUS SUBLAYER

In the measurement of correlation of the fluctuating wall shear, an instantaneous linear viscous sublayer was assumed beneath the turbulent boundary layer. To verify this, we write the fluctuating part of shear stress in the viscous sublayer and neglect its variation with x_2 $(0 \leq x_2 \leq \delta_{S.L.})$,

$$\frac{\tau_1}{\rho} = [\overline{uv}-uv] + \nu \frac{\partial u}{\partial x_2} , \qquad \text{(I-1)}$$

The boundary conditions at the wall requires that

$$u = v = w = 0 \quad \text{at} \quad x_2 = 0$$

and the continuity equation gives

$$\left[\frac{\partial v}{\partial x_2}\right]_{x_2=0} = 0 \quad .$$

It follows from Eqn. (I-1) that

$$\left[\frac{\partial u}{\partial x_2}\right]_{x_2=0} = \frac{\tau_w}{\mu}$$

$$\left[\frac{\partial^2 u}{\partial x_2^2}\right]_{x_2=0} = \frac{1}{\nu}\frac{\partial}{\partial x_2}[uv-\overline{uv}]_{x_2=0} \qquad \text{(I-2)}$$

$$= \frac{1}{\nu}\left[u\frac{\partial v}{\partial x_2} + v\frac{\partial u}{\partial x_2} - \overline{u\frac{\partial v}{\partial x_2}} - \overline{v\frac{\partial u}{\partial x_2}}\right]_{x_2=0}$$

$$= 0$$

similarly,

$$\left[\frac{\partial^3 u}{\partial x_2^3}\right]_{x_2=0} = \frac{1}{\nu}\frac{\partial^2}{\partial x_2^2}\left[uv-\overline{uv}\right]_{x_2=0}$$

$$= 0$$

but

$$\left[\frac{\partial^4 u}{\partial x_2^4}\right]_{x_2=0} = \frac{1}{\nu}\frac{\partial^3}{\partial x_2^3}\left[uv-\overline{uv}\right]_{x_2=0} \qquad \text{(I-2)}$$

$$= \frac{3}{\nu}\left[\frac{\partial u}{\partial x_2}\frac{\partial^2 v}{\partial x_2^2} - \overline{\frac{\partial u}{\partial x_2}\frac{\partial^2 v}{\partial x_2^2}}\right]_{x_2=0}$$

As the second and third derivatives of the fluctuating velocity component, u, vanish at the wall, the variation of u will be closely linear for an appreciable range in x_2 direction. The above argument was first used by Townsend[25] for the mean velocity profile near the wall in a turbulent channel flow.

Experimentally, the measurements of $\sqrt{\overline{u^2}}/U_\infty$ in turbulent boundary layer by Klebanoff[9] and in turbulent channel flow by Laufer[14] showed that such a linear fluctuating region does exist in the vicinity of the wall which covered the whole region of viscous layer. Since $\sqrt{\overline{u^2}} = \overline{c(x_1,x_3,t)}\cdot x_2$ implies $u = c(x_1,x_3,t)\cdot x_2$, their experimental results lend support to the existence of instantaneous linearity in the viscous layer as discussed above. In the present work no such experiment has been repeated, but our correlation measurement of R_{uu} with zero time delay near the edge of viscous sublayer with one hot-wire varying its height gave approximately the same value, which also showed the agreement as predicted by the instantaneous linearity of the viscous layer (see Fig. 7).

APPENDIX II

ERRORS AND CORRECTIONS

A. CORRECTION OF THE MEAN VELOCITY MEASUREMENT IN A TURBULENT BOUNDARY LAYER

When we measured the mean velocity (see Chapter IV and Appendix III) a fixed mean overheating ratio a_w was used. At constant current the fluctuating velocity causes the wire temperature and therefore the overheating ratio to fluctuate. However, the mean of the fluctuations of the overheating ratio does not correspond to the mean of the velocity fluctuation since the velocity does not vary linearly with the overheating ratio. During measurements we observed a mean overheating ratio, so the corresponding velocity found was in error.

The overheating ratio, a_w, has a linear relation with hot resistance, R_w

$$a_w = \frac{R_w - R_e}{R_e}$$

where R_e = cold resistance (independent of velocity fluctuation).

And since R_w shows up at both sides of King's formula,

$$\begin{aligned} I^2 R_w &= (T_w - T_e)(A + B\sqrt{U}) \\ &= \frac{R_w - R_e}{\alpha R_o}(A + B\sqrt{U}) \end{aligned} \qquad \text{(II-1)}$$

we study the relation between velocity U and R_w. From Eqn. (II-1)

$$B\sqrt{U} = \frac{I^2 R_w \alpha'}{R_w - R_e} - A \qquad (\alpha' = R_o \alpha)$$

or

$$\sqrt{U} = \frac{(I^2\alpha' - A)\, R_w + AR_e}{B\,(R_w - R_e)} \tag{II-2}$$

let

$$R_w = \bar{R}_w + r_w \quad \text{(where } r_w = \text{fluctuating hot resistance)}$$

$$U \doteq \bar{U} + u \qquad \text{(with } v^2 \text{ neglected)}$$

be substituted into Eqn. (II-2), and after squaring both sides of the equation we have

$$\bar{U}+u = \frac{[(I^2\alpha'-A)\bar{R}_w + AR_e]^2 \left[1 + \dfrac{(I^2\alpha'-A)\, r_w}{[(I^2\alpha'-A)\bar{R}_w + AR_e]}\right]^2}{B^2(R_w - R_e)^2 \left[1 + \dfrac{r_w}{\bar{R}_w - R_e}\right]^2}$$

$$\overset{\text{let}}{=} \frac{c_3(1+c_1 r_w)^2}{(1+c_2 r_w)^2}$$

where

$$\left.\begin{aligned} c_1 &= \frac{I^2\alpha'-A}{[(I^2\alpha'-A)\bar{R}_w + AR_e]} \\ c_2 &= \frac{1}{\bar{R}_w - R_e} \\ c_3 &= \left[\frac{(I^2\alpha'-A)\bar{R}_w + AR_e}{B\,(\bar{R}_w - R_e)}\right]^2 \end{aligned}\right\} \tag{II-3}$$

then

$$\bar{U}+u = \frac{c_3(1+2c_1 r_w + c_1^2 r_w^2)}{(1+2c_2 r_w + c_2^2 r_w^2)}$$

$$= c_3[1+2(c_1-c_2)r_w+(c_1-c_2)(c_1-3c_2)r_w^2$$
$$-2c_2(c_1-c_2)(c_1-2c_2)r_w^3 \qquad \text{(II-4)}$$
$$+c_2^2(c_1-c_2)(5c_1-11c_2)r_w^4+\ldots]$$

Taking average at both sides of Eqn. (II-4) and assuming u and r_w to be waves symmetrical to their mean values, respectively, then

$$\bar{U} = c_3[1+[(c_1-c_2)(c_1-3c_2)]\overline{r_w^2} + O(\overline{r_w^4}) + \ldots\}$$

$$\doteq c_3+c_3[(c_1-c_2)(c_1-3c_2)]\overline{r_w^2} \qquad \text{(II-5)}$$

After using the value of c_1, c_2, and c_3 from Eqns. (II-3) and simplifying, Eqn. (II-5) becomes

$$\bar{U} \doteq \left[\frac{(I^2\alpha'-A)\overline{R_w}+AR_e}{B\,(\overline{R_w}-R_e)}\right]^2 + \frac{1}{B^2}\left[\frac{2I^2\alpha'R_e(I^2\alpha'-A)}{(\overline{R_w}-R_e)^3}\right.$$
$$\left. + \frac{3(I^2\alpha'R_e)^2}{(\overline{R_w}-R_e)^4}\right]\overline{r_w^2}$$

$$\text{where} \quad \left[\frac{(I^2\alpha'-A)\overline{R_w}+AR_e}{B(\overline{R_w}-R_e)}\right]^2 = U_{\substack{\text{mean}\\ \text{in error}}}$$

so, the correction for the mean velocity is

$$\Delta\bar{U} = \bar{U} - U_{\substack{\text{mean}\\ \text{in error}}}$$
$$\doteq \frac{1}{B^2}\left[\frac{2I^2\alpha'R_e(I^2\alpha'-A)}{(\overline{R_w}-R_e)^2} + \frac{3(I^2\alpha'R_e)^2}{(\overline{R_w}-R_e)^4}\right]\overline{r_w^2} \qquad \text{(II-6)}$$

The value of B and the parameters in the bracket of Eqn (II-6) were given by measurements or calibration, and $\overline{r_w^2}$ can be obtained by measuring

$\overline{e^2}$ since

$$\overline{e^2} = I^2 \cdot \overline{r_w^2} \quad (I=\text{const.}) \tag{II-7}$$

Computation: In the present measurement of the mean wall shear stress (see Chapter IV and Appendix III), we have the following information from measurements:

$$U_{\text{mean in error}} = 39 \text{ fps}$$

$$\overline{r_w^2} = 0.0722 \ (\Omega^2) \ .$$

After using these figures and other given values in Eqn. (II-6), we find

$$\Delta \bar{U} = 1.16 \text{ fps}$$

therefore

$$\text{error } \frac{\Delta \bar{U}}{\bar{U}} = \frac{1.16}{39+1.16}$$

$$= 2.9\% \ .$$

A graphical correction method tried by us gave the error

$$\frac{\Delta \bar{U}}{\bar{U}} = 3\% \tag{II-8}$$

B. THE ERROR OF THE $\sqrt{\overline{u^2}}$ MEASUREMENT

The error of the $\sqrt{\overline{u^2}}$ measurement is estimated as follows:

From Eqn. (II-4) in Section A above

$$\bar{U}+u = c_3[1+2(c_1-c_2)r_w+(c_1-c_2)(c_1-3c_2)r_w^2 - 2c_2(c_1-c_2)(c_1-2c_2)r_w^3+ \ldots] \tag{II-4}$$

where the coefficients c_1, c_2, and c_3 are defined by Eqns. (II-3).

With the aid of Eqn. (II-5), we have from Eqn. (II-4)

$$u \doteq c_3(c_1-c_2)[2r_w+(c_1-3c_2)(r_w^2-\overline{r_w^2})-2c_2(c_1-2c_2)r_w^3+\ldots] \quad \text{(II-9)}$$

Equation (II-9) is squared at both sides and computed up to the 4th order of r_w, then

$$\begin{aligned} u^2 \doteq\ & c_3^2(c_1-c_2)^2\{4r_w^2+(c_1-3c_2)^2[r_w^4-2r_w^2\overline{r_w^2}+(\overline{r_w^2})^2] \\ & +4(c_1-3c_2)r_w(r_w^2-\overline{r_w^2})-8c_2(c_1-2c_2)r_w^4 \\ & +\ldots\} \quad . \end{aligned}$$

Taking average of the above and assuming u and r_w to be waves symmetrical to their mean values as we did in Section A, then

$$\begin{aligned} \overline{u^2} \doteq\ & c_3^2(c_1-c_2)^2\{4\overline{r_w^2}+[(c_1-3c_2)^2-8c_2(c_1-2c_2)]\overline{r_w^4} \\ & -(c_1-3c_2)^2(\overline{r_w^2})^2\} \end{aligned} \quad \text{(II-10)}$$

Usually, in measuring small velocity fluctuations a linear relation was assumed between velocity fluctuations and electronic signals, i.e.,

$u = se$ where s = sensitivity coefficient of the hot wire

e = fluctuating voltage

$= Ir_w$,

hence

$$\begin{aligned} \overline{u^2} &= s^2\overline{e^2} \\ &= (sI)^2\overline{r_w^2} \quad (I = \text{constant}) \end{aligned}$$

Comparing this equation with Eqn. (II-10), we find the correction term approximately

$$\Delta\overline{u^2} = c_3^2(c_1-c_2)^2\{[(c_1-3c_2)^2-8c_2(c_1-2c_2)]\overline{r_w^4}-(c_1-3c_2)^2(\overline{r_w^2})^2\} \quad \text{(II-11)}$$

To compute the possible maximum error in the present measurements, we use $(\sqrt{\overline{u^2}}/\bar{U})_{max} \approx 0.35$, $\bar{U} = 40$ fps. Correspondingly, in our measurements we have $\overline{r_w^2} = 0.168\ (\Omega^2)$, and if r_w is assumed to follow a sine wave variation, then

$$\overline{r_w^4} = 0.042\ (\Omega^4) \quad .$$

Using these values and other information from measurements in Eqn. (II-11), we find

$$\frac{\Delta\ \overline{u^2}}{\overline{u^2}} = 0.12$$

Hence,

$$\text{error } \frac{\Delta \sqrt{\overline{u^2}}}{\sqrt{\overline{u^2}}} = \frac{\sqrt{1.12}-1}{\sqrt{1.12}}$$

$$= 5.7\%$$

C. OTHER ERRORS IN THE MEASUREMENT

(1) From Meter Reading—The averages involved in computing the correlation were obtained by visual observation of the output meter reading. As the meter had a time constant of 3 sec, the fluctuations in the needle reading were small and the probable error in the correlation arising from this source is about ±5% of the maximum value.

(2) From the Filtering Effect—See Section III-B.

(3) From the Hot-Wire Alignment—In measuring v- or w-component of the fluctuating velocity an X-type hot-wire probe with a gap between the two cross wires, about 0.02 in. was used. The two wires have different orientations when they changed side gave an effect to the measurement.

Such an effect was examined in the R_{wv} measurements ($x_2/\delta^* = 0.102$, $x_3'/\delta^* = \pm 0.223$), using hot-wire probes with opposite wire orientations (See Figs. 26-27).

(4) From Using the Convection Hypothesis—When we constructed the contours of constant correlation of τ_w-τ_w, of τ_w-u and of p-w the convection hypothesis was used (see Chapter VII). The amount of error introduced from this source can be determined at those values of x_1/δ^* for which data were taken by comparing the measured values of the spatial correlation at zero time delay with the values predicted by the convection hypothesis. The maximum error in the correlation near the peak value of $R_{\tau_w\tau_w}$ or $R_{\tau_w u}$ is approximately ±20% of the peak value. In constructing the contours of R_{pw} in x_2x_3-plane at $x_1/\delta^* = 0$, actual measurements were made at every point, hence no error resulted from the convection hypothesis was noted. However, the two R_{pw} contours at negative values and two at positive values of x_1/δ^* were constructed by using the convection hypothesis in order to make a qualitative study of the variation of the R_{pw} contour along x_1/δ^* axis. Therefore, the maximum error in the correlation near the peak value of R_{pw} can be as high as ±40% for these four contours.

APPENDIX III

CALCULATION OF THE MEAN WALL SHEAR STRESS

In Chapter IV the measurement of the wall shear stress was introduced and the result was reported. Here we give the details of calculation procedure as follows:

A. INDIRECT APPLICATION OF WILLS'[28] CORRECTION FOR THE WALL HEAT TRANSFER

From the present hot-wire measurements we have the following information:

b = distance between the hot-wire and the wall

= 0.00216 in.

a = radius of the hot-wire

= 0.0001 in.

ℓ = length of the hot-wire

= 0.043 in. (0.00358 ft)

ρ_a = density of air at test section

= 0.00207 slug-ft^{-3}

μ = coefficient of viscosity

= 0.406 x 10^{-6} lb - sec - ft^{-2} (for air at 113°F)

k = coefficient of thermal conductivity

= 4.7 x 10^{-3} watt - ft^{-1} - °R^{-1} (for air at 113°F)

I = electric current through hot-wire

= 53.34 x 10^{-3} ampere

$\overline{R_w}$ = average resistance of heated wire

= 8.78 ohms

R_e = cold resistance of hot wire

= 5.85 ohms

θ_e = ambient temperature

= 318°K (573°R)

α = temperature coefficient of resistivity

= 0.00392 $(°C)^{-1}$ or 0.00218 $(°F)^{-1}$ for Pt wire

U_∞ = free stream velocity

= 206 fps

First, we compute

$$\text{rate of heat loss} = I^2\overline{R_w}$$

$$= (53.34\times10^{-3})^2\times8.78$$

$$= 24.97\times10^{-3} \text{ watt},$$

then, from hot-wire calibration curve, we find

$$\sqrt{\rho_a \bar{U}} = 0.302 \quad ,$$

hence, one can calculate the flow velocity

$$\bar{U} = \frac{0.302^2}{0.00207}$$

$$= 44.1 \text{ fps}$$

and the hot-wire Reynolds number

$$(Rey)_w = \frac{\bar{U}\cdot(2a)\rho_a}{\mu}$$

$$= \frac{44.1\times0.0002\times0.00207}{0.406\times10^{-6}\times12}$$

$$= 3.76$$

or

$$(\mathrm{Rey})_w^{0.45} = (3.76)^{0.45}$$

$$= 1.82$$

Referring to Fig. 2 Wills' report (p. 392) for

$$(\mathrm{Rey})_w^{0.45} = 1.82 \qquad \frac{b}{a} = 21.6$$

we have

$$\Delta\ \mathrm{Nu}\left(\frac{\overline{\theta_w}}{\theta_e}\right)^{-0.17} = 0.116$$

The above value was found by measuring the vertical distance between the curves b/a = 21.6 and b/a = ∞ (when b/a → ∞ the wall effect is absent). Physically, this vertical distance is equivalent to the amount of additional heat loss of the hot-wire due to the effect of heat transfer to the wall.

The value of $\mathrm{Nu}\ (\overline{\theta_w}/\theta_e)^{-0.17}$ can either be measured from the same figure or can be calculated as follows: since one can write the relation between resistance and temperature of the wire,

$$R_e = R_o\ [1+\alpha(\theta_e-\theta_o)] \qquad \text{(III-1)}$$

similarly,

$$\overline{R_w} = R_o\ [1+\alpha(\overline{\theta_w}-\theta_o)] \qquad \text{(III-2)}$$

subtract Eqn. (III-1) from Eqn. (III-2) and rearrange the result, we have

$$\overline{\theta_w} = \theta_e + \frac{R_e}{\alpha R_o}\, a_w \qquad \text{(III-3)}$$

where a_w = overheating ratio of hot-wire

$$= \frac{\overline{R_w}-R_e}{R_e} = 0.5\ .$$

From Eqn. (III-1), R_o was found to be 4.98 ohms, which together with other known values was substituted into Eqn. (III-3), hence

$$\overline{\theta_w} = 318 + \frac{5.85 \times 0.5}{0.00392 \times 4.98}$$

$$= 468°K \text{ (or } 843°R)$$

Then, one can compute

$$Nu\left(\frac{\overline{\theta_w}}{\theta_e}\right)^{-0.17} = \frac{I^2\overline{R_w}}{\pi K \ell(\overline{\theta_w}-\theta_a)} \left(\frac{\overline{\theta_w}}{\theta_e}\right)^{-0.17}$$

$$= \frac{24.97 \times 10^{-3}}{\pi 4.7 \times 10^{-3} \times 0.00358 \times (843-573)} \left(\frac{468}{318}\right)^{-0.17}$$

$$= 1.64$$

and the percentage of correction of heat loss,

$$\frac{\Delta\ Nu\left(\frac{\overline{\theta_w}}{\theta_e}\right)^{-0.17}}{Nu\left(\frac{\overline{\theta_w}}{\theta_e}\right)^{-0.17}} = \frac{0.116}{1.64} = 7.07\%$$

or

$$\frac{\Delta\ I^2\overline{R_w}}{I^2\overline{R_w}} = 7.07\%$$

Therefore, after the correction is applied

$$(I^2\overline{R_w})_{after} = 24.97 \times 10^{-3} \times (1-0.0707)$$

$$= 23.2 \times 10^{-3} \text{ watt}$$

Referring to the hot-wire calibration curve again, we found $\sqrt{\rho\bar{U}} = 0.262$ and $\bar{U} = 33.2$ fps. Thus,

before correction $\bar{U} = 44.1$ fps

after correction $\bar{U} = 33.2$ fps

This result gave the correction of $\overline{U}$ for a laminar boundary layer. In case of a turbulent boundary layer Wills found empirically that a factor 0.5 should be applied to the correction for a corresponding laminar boundary layer (see Wills, p. 395), so

$$(\bar{U})_{\substack{\text{corrected} \\ \text{for turbulent B.L.}}} = \frac{44.1+33.2}{2}$$

$$= 38.7 \text{ fps.}$$

The error in the mean velocity measurement caused by velocity fluctuations was studied in Appendix II-A. The error was +3% for the present measurement, therefore the corrected mean velocity

$$\bar{U} = 38.7 \times 1.03$$

$$= 39.8 \text{ fps}$$

Finally, the mean wall shear stress can be computed

$$\bar{f}_w = \mu \frac{d\bar{U}}{dx_2}$$

$$\doteq \mu \frac{\bar{U}}{x_2} \qquad \text{since wire was set up near the edge of viscous sublayer, } x_2=0.00216 \text{ in.}$$

$$= 0.406 \times 10^{-6} \times \frac{39.8 \times 12}{0.00216}$$

$$= 0.09 \text{ lb/sq ft}$$

or the non-dimensional wall friction velocity,

$$\frac{U_\tau}{U_\infty} = \frac{1}{U_\infty} \sqrt{\frac{\bar{f}_w}{\rho_a}}$$

$$= \frac{1}{206} \sqrt{\frac{0.09}{0.00207}}$$

$$= 0.032$$

B. DIRECT APPLICATION OF WILLS' CORRECTION METHOD

As computed in Section A we have

$$(\mathrm{Rey})_w^{0.45} = 1.82 \quad ,$$

and referring to Fig. 4 Wills' report (p. 394) for b/a = 21.6 we found the correction constant, K_w to be 0.2, hence

$$(\mathrm{Rey})_{w\ \mathrm{corrected}}^{0.45} = (\mathrm{Rey})_w^{0.45} - K_w$$

$$= 1.82 - 0.2$$

$$= 1.62 \quad .$$

And after correction $(\mathrm{Rey})_{w\ \mathrm{corr.}} = 2.92$

$$(\bar{U})_{\mathrm{corr.}} = \frac{(\mathrm{Rey})_w\ \mu}{2a \cdot \rho_a}$$

$$= \frac{2.92 \times 0.406 \times 10^{-6} \times 12}{0.002 \times 0.00207}$$

$$= 34.4 \ \mathrm{fps} \quad .$$

Similar to what was mentioned in Section A this result would only meet the case of laminar boundary layer. For a turbulent boundary layer a factor 0.5 should be applied, thus with

$\bar{U} = 44.1$ fps (without correction)

and

$\bar{U} = 34.4$ fps (with correction for laminar boundary layer) ,

we can find

$$(\bar{U})_{\substack{\text{corrected for} \\ \text{turbulent boundary} \\ \text{layer}}} = \frac{44.1+34.4}{2}$$

$$= 39.3 \ \mathrm{fps} \quad .$$

Since the correction of error due to turbulent velocity fluctuations was 3% as stated in Section A,

$$\bar{U} = 39.3 \times 1.03 = 40.5 \text{ fps}$$

Finally, one can compute the mean wall shear stress

$$\overline{f_w} \doteq \mu \frac{\bar{U}}{x_2}$$

$$= 0.406 \times 10^{-6} \times \frac{40.5 \times 12}{0.00216}$$

$$= 0.0912 \text{ lb/sq ft}$$

and the non-dimensional wall friction velocity,

$$\frac{U_\tau}{U_\infty} = \frac{1}{U_\infty} \sqrt{\frac{\bar{f}_w}{\rho_a}}$$

$$= \frac{1}{206} \sqrt{\frac{0.0912}{0.00207}}$$

$$= 0.0322$$

This result agrees very well with the result found in Section A.

BIBLIOGRAPHY

1. Benney, D. J., "Finite Amplitude Effects in an Unstable Laminar Boundary Layer," Phys. Fluids, 7, 1964, p. 319.

2. Benney, D. J. and Lin, C. C., "On the Secondary Motion Induced by Oscillations in a Shear Flow," Phys. Fluids, 3, 1960, p. 656.

3. Browand, F. K., "An Experimental Investigation of the Instability of an Incompressible, Separated Shear Layer," MIT Report ASRL TR92-4, 1965.

4. Einstein, H. A. and Li, H., "The Viscous Sublayer along a Smooth Boundary," Proc. Amer. Soc. Civ. Engrs., Paper No. 945, 1956.

5. Favre, A. J., Gaviglio, J. J. and Dumas, R., "Space-Time Double Correlations and Spectra in a Turbulent Boundary Layer," J. Fluid Mech., 2, 1957, p. 313; J. Fluid Mech., 3, 1958, p. 344.

6. Grant, H. L., "The Large Eddies of Turbulent Motion," J. Fluid Mech., 4, 1958, p. 149.

7. Hakkinen, R. J., "Measurements of Turbulent Skin Friction on a Flat Plate at Supersonic Speeds," NACA TN 3486, 1955.

8. Hama, F. R., "Progressive Deformation of a Perturbed Line Vortex Filament," Phys. Fluids, 6, 1963, p. 526.

9. Klebanoff, P. S., "Characteristics of Turbulence in a Boundary Layer with Zero Pressure Gradient," NACA TN 3178, 1954.

10. Klebanoff, P. S., Tidstrom, K. D. and Sargent, L. M., "The Three-Dimensional Nature of Boundary-Layer Instability," J. Fluid Mech., 12, 1962, p. 1.

11. Kovasznay, L.S.G., Komoda, H. and Vasudeva, B. R., "Detailed Flow Field in Transition," Proc. 1962 Heat Trans. Fluid Mech. Inst., Stanford Univ. Press, 1962, p. 1.

12. Kraichnan, R. H., "Pressure Fluctuations in Turbulent Flow over a Flat Plate," J. Acoust. Soc. Amer., 28, No. 3, 1956, p. 378

13. Ladenburg, R. W., Physical Measurements in Gas Dynamics and Combustion, High Speed Aerodynamics and Jet Propulsion Series, IX, Princeton Univ. Press, 1954, Section F.

BIBLIOGRAPHY (Continued)

14. Laufer, J., "Investigation of Turbulent Flow in a Two-Dimensional Channel," NACA TN 2123, 1950.

15. Laufer, J., "The Structure of Turbulence in Fully Developed Pipe Flow," NACA TN 2954, 1953.

16. Lin, C. C., The Theory of Hydrodynamic Stability, Cambridge Univ. Press, 1955, p. 11.

17. Lindgren, E. R., Arkiv För Fysik, 12, 1, 1957.

18. Phillips, O. M., "On the Aerodynamic Surface Sound from a Plane Turbulent Boundary Layer," Proc. Roy. Soc. (London), A, 234, 1956, p. 327.

19. Runstadler, P. W., Kline, S. J. and Reynolds, W. C., "An Experimental Investigation of the Flow Structure of the Turbulent Boundary Layer," Ph.D Dissertation of Stanford Univ., also available as AFOSR TN 5241, 1963.

20. Schubauer, G. B. and Klebanoff, P. S., "Investigations of the Separation of Turbulent Boundary Layers," NACA Report No. 1030, 1951.

21. Sternberg, J., "A Theory for the Viscous Sublayer of a Turbulent Flow," J. Fluid Mech., 13, 1962, p. 16.

22. Stuart, J. T., "The Production of Intense Shear Layers by Vortex Stretching and Convection," AGARD Specialists' meeting on "Recent Developments in Boundary Layer Research," Naples, Italy, May 1965.

23. Theodorsen, T., "The Structure of Turbulence," 50 Jahre Granzschichtforschung (Ed. H. Görtler & W. Tollmien), Braunschweig: Veiweg und Sohn, 1955, p. 55.

24. Townsend, A. A., "The Structure of the Turbulent Boundary Layer," Proc. Camb. Phil. Soc., 47, 1951, p. 375.

25. Townsend, A. A., The Structure of Turbulent Shear Flow, Cambridge Univ. Press, 1956, p. 218.

26. Willmarth, W. W. and Wooldridge, C. E., "Measurements of the Fluctuating Pressure at the Wall Beneath a Thick Turbulent Boundary Layer," J. Fluid Mech., 14, 1962, p. 187.

BIBLIOGRAPHY (Concluded)

27. Willmarth, W. W. and Wooldridge, C. E., "Measurements of the Correlation between the Fluctuating Velocities and the Fluctuating Wall Pressure in a Thick Turbulent Boundary Layer," NATO, AGARD Report 456, 1963; also Univ. of Mich., Tech. Report 02920-2-T, 1962.

28. Wills, J.A.B., "The Correction of Hot-Wire Readings for Proximity to a Solid Boundary," J. Fluid Mech., 12, 1962, p. 388.

29. Hinze, J. O., Turbulence, New York: McGraw-Hill Book Company, 1959, p. 48.

30. Gadd, G. E., "A Note on the Theory of the Stanton Tube," Brit. R. and M. 3147, 1960.

31. Dhawan, S., "Direct Measurements of Skin Friction," NACA Rep. 1121, 1953.

32. Kovásznay, L.S.G., "Development of Turbulence-Measuring Equipment," NACA Report 1209, 1954, Fig. 21.

33. Wills, J.A.B., "On Convection Velocities in Turbulent Shear Flows," J. Fluid Mech., 20, 1964, p. 417.

FIGURES

Note: Figures 1, 2, and 4 are reprinted from AGARD Report 456, Figs. 1, 2, and 3 by Willmarth, W. W., and Wooldridge, C. E., 1963

INDEX TO THE POSITION OF PRESSURE-TRANSDUCER AND HOT-WIRES IN THE PRESENT CORRELATION MEASUREMENTS OF $\overline{u_i u_j}$ AND $\overline{pw}$

Note: Coordinate systems are defined as shown by the following figure:

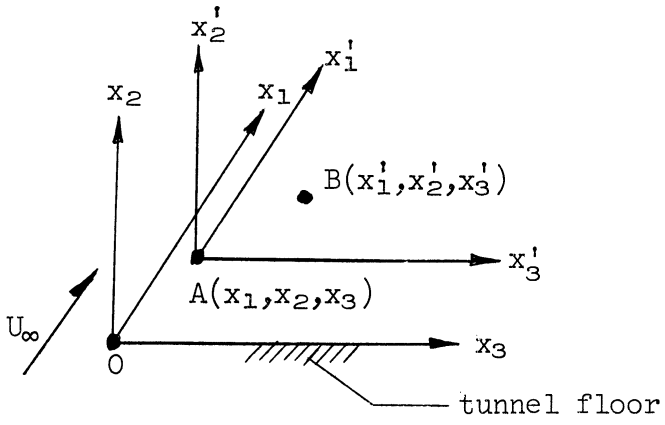

where

(1) the origin 0 is the point at which pressure-transducer measuring p is located;

(2) the point $A(x_1,x_2,x_3)$ is the point at which the first hot-wire measuring u, v, or w is located; and

(3) the point $B(x'_1,x'_2,x'_3)$ is the point at which the second hot-wire measuring u, v, or w is located.

Correlation Measured	Point O Pressure	Point A Velocity Component u	v	w	$\frac{x_1}{\delta^*}$	$\frac{x_2}{\delta^*}$	$\frac{x_3}{\delta^*}$	Point B Velocity Component u	v	w	$\frac{x'_1}{\delta^*}$	$\frac{x'_2}{\delta^*}$	$\frac{x'_3}{\delta^*}$	Figure
R_{uu}		X			0	0.122	0	X			0	0	0	6a
R_{vv}			X		0	0.122	0		X		0	0	0	6b
R_{ww}				X	0	0.122	0			X	0	0	0	6c
R_{uu}		X			0	0.004	0	X			0	0	0	6d
"		X			0	0.004	0	X			0	0.001	0.204	7a
"		X			0	0.004	0	X			0	0.006	0.204	7b
"		X			0	0.004	0	X			0	0.098	0.204	7c
"		X			0	0.004	0	X			0	0.20	0.204	7d
"		X			0	0.004	0	X			0	0	0.095	8a
"		X			0	0.004	0	X			0	0	0.190	8b
"		X			0	0.004	0	X			0	0	0.286	8c
"		X			0	0.004	0	X			0	0	0.518	8d
"		X			0	0.004	0	X			0	0	0.690	8e
"		X			0	0.004	0	X			0	0	0.095	9a
"		X			0	0.004	0	X			0.169	0	0.112	9b
"		X			0	0.004	0	X			0.51	0	0.095	9c
"		X			0	0.004	0	X			0	0.118	0.064	10a
"		X			0	0.004	0	X			0	0.118	0.127	10b
"		X			0	0.004	0	X			0	0.118	0.191	10c
"		X			0	0.004	0	X			0	0.118	0.254	10d
"		X			0	0.004	0	X			0	0.118	0.381	11a
"		X			0	0.004	0	X			0	0.118	0.508	11b
"		X			0	0.004	0	X			0	0.118	0.635	11c
"		X			0	0.004	0	X			0	0.118	0.889	11d
"		X			0	0.004	0	X			0	0.118	0.127	12a
"		X			0	0.004	0	X			1.016	0.118	0.127	12b

Correlation Measured	Point 0 Pressure	Point A Velocity Component u	v	w	$\frac{x_1}{\delta^*}$	$\frac{x_2}{\delta^*}$	$\frac{x_3}{\delta^*}$	Point B Velocity Component u	v	w	$\frac{x_1'}{\delta^*}$	$\frac{x_2'}{\delta^*}$	$\frac{x_3'}{\delta^*}$	Figure
R_{uu}		X			0	0.004	0	X			2.032	0.118	0.127	12c
"		X			0	0.004	0	X			4.064	0.118	0.127	12d
"		X			0	0.004	0	X			0	0.118	0.508	13a
"		X			0	0.004	0	X			2.032	0.118	0.508	13b
"		X			0	0.004	0	X			4.064	0.118	0.508	13c
R_{vv}			X		0	1.89	0		X		0	0.191	0	14a
"			X		0	1.75	0		X		0	0.337	0	14b
"			X		0	0.254	0		X		0	0.406	0	14c
"			X		0	6.14	0		X		0	0	0.35	15a
"			X		0	2.07	0		X		0	0	0.35	15b
"			X		0	1.14	0		X		0	0	0.16	15c
"			X		0	0.16	0		X		0	0	0.35	15d
"			X		0	0.064	0		X		0	0	0.16	15e
"			X		0	6.14	0		X		-0.35	0	0.35	16a
"			X		0	2.03	0		X		-0.35	0	0.35	16b
"			X		0	1.14	0		X		-0.16	0	0.16	16c
"			X		0	0.16	0		X		-0.35	0	0.35	16d
"			X		0	0.064	0		X		-0.16	0	0.16	16e
R_{ww}				X	0	1.04	0			X	0	0	0.203	17a
"				X	0	0.122	0			X	0	0	0.203	17b
"				X	0	0.122	0			X	0	0	0.508	17c
"				X	0	1.67	0			X	0	0.224	0	18a
"				X	0	0.426	0			X	0	0.224	0	18b
"				X	0	0.122	0			X	0	0.224	0	18c
"				X	0	0.004	0			X	0	0	0.284	19a

Correlation Measured	Point O Pressure	Point A Velocity Component u	v	w	$\frac{x_1}{\delta^*}$	$\frac{x_2}{\delta^*}$	$\frac{x_3}{\delta^*}$	Point B Velocity Component u	v	w	$\frac{x_1'}{\delta^*}$	$\frac{x_2'}{\delta^*}$	$\frac{x_3'}{\delta^*}$	Figure
R_{ww}				X	0	0.004	0			X	0	0	0.568	19b
"				X	0	0.004	0			X	0	0	0.852	19c
"				X	0	0.004	0			X	0	0.155	0	19d
R_{uw}		X			0	0.004	0			X	0	0	-0.284	20a
"		X			0	0.004	0			X	0	0	-0.568	20b
"		X			0	0.004	0			X	0	0	-0.852	20c
"		X			0	0.004	0			X	0	0	-1.136	20d
"		X			0	0.004	0			X	0	0	-0.284	21a
"		X			0	0.004	0			X	0	0	0.284	21b
"		X			0	0.004	0			X	0	0	-0.852	22a
"		X			0	0.004	0			X	0	0	0.852	22b
"		X			0	0.127	0			X	2.03	-0.123	-0.284	23a
"		X			0	0.127	0			X	0	-0.123	-0.284	23b
"		X			0	0.127	0			X	-2.03	-0.123	-0.284	23c
"		X			0	0.127	0			X	-4.06	-0.123	-0.284	23d
"		X			0	0.127	0			X	-6.09	-0.123	-0.284	23e
R_{wv}				X	0	0.508	0.508		X		0	0	-0.223	24a
"				X	0	0.508	0.508		X		0	0	0.223	24b
"				X	0	0.508	0.508		X		0	0	0.446	24c
"				X	0	0.508	0.508		X		0	0.254	-0.223	24d
"				X	0	0.508	0.508		X		0	0.254	0.223	24e
"				X	0	0.508	0.508		X		0	0.254	0	24f
"				X	0	0.508	0.508		X		0	-0.286	0.254	24g
"				X	0	0.004	0		X		0	0.155	0.284	25a
"				X	0	0.004	0		X		0	0.155	-0.284	25b

Correlation Measured	Point O	Point A					Point B				Figure
	Pressure	Velocity Component			$\frac{x_1}{\delta^*}$	$\frac{x_2}{\delta^*}$	$\frac{x_3}{\delta^*}$	Velocity Component			$\frac{x_1'}{\delta^*}$	$\frac{x_2'}{\delta^*}$	$\frac{x_3'}{\delta^*}$	
		u	v	w				u	v	w				
R_{wv}				X	0	0.004	0		X		0	0.186	0	25c
"				X	0	0.102	0.508		X		0	0.041	-0.233	26a
"				X	0	0.102	0.508		X		0	0.041	0.223	26b
"				X	0	0.102	0.508		X		0	0.041	0.382	26c
"				X	0	0.102	0.508		X		0	0.041	0.223	27a
"				X	0	0.102	.508		X		0	0.041	-0.223	27b
"				X	0	0.102	0.508		X		0	0.041	-0.223	27c
"				X	0	0.102	0		X		1.52	0.041	0.222	28a
"				X	0	0.102	0		X		0.71	0.41	0.222	28b
"				X	0	0.102	0		X		0	0.041	0.222	28c
"				X	0	0.102	0		X		-0.71	0.041	0.222	28d
"				X	0	0.102	0		X		-1.52	0.041	0.222	28e
R_{pw}	X			X	0	0.127	-0.508							30a
"	X			X	0	0.508	-0.508							30b
"	X			X	0	2.032	-1.016							30c
"	X			X	0	2.032	-2.032							30d
"	X			X	0	0.127	0.508							31a
"	X			X	0	0.508	0.508							31b
"	X			X	0	1.016	0.508							31c
"	X			X	0	1.524	0.508							31d
"	X			X	0	2.032	0.508							31e
"	X			X	0	3.048	0.508							31f
"	X			X	0	0.127	1.016							32a
"	X			X	0	0.508	1.016							32b
"	X			X	0	1.016	1.016							32c

Correlation Measured	Point O	Point A					Point B				Figure
	Pressure	Velocity Component u v w	$\frac{x_1}{\delta^*}$	$\frac{x_2}{\delta^*}$	$\frac{x_3}{\delta^*}$	Velocity Component u v w	$\frac{x_1'}{\delta^*}$	$\frac{x_2'}{\delta^*}$	$\frac{x_3'}{\delta^*}$	
R_{pw}	X	X	0	1.524	1.016					32d
"	X	X	0	2.032	1.016					32e
"	X	X	0	3.048	1.016					32f
"	X	X	0	0.127	1.524					33a
"	X	X	0	0.508	1.524					33b
"	X	X	0	1.016	1.524					33c
"	X	X	0	1.524	1.524					33d
"	X	X	0	2.032	1.524					33e
"	X	X	0	3.048	1.524					33f
"	X	X	0	0.127	2.032					34a
"	X	X	0	0.508	2.032					34b
"	X	X	0	1.016	2.032					34c
"	X	X	0	1.524	2.032					34d
"	X	X	0	2.032	2.032					34e
"	X	X	0	3.048	2.032					34f
"	X	X	0	1.524	2.540					35a
"	X	X	0	2.032	2.540					35b
"	X	X	0	2.540	2.540					35c
"	X	X	0	0.127	0.508					36a
"	X	X	-0.51	0.127	0.508					36b
"	X	X	-1.02	0.127	0.508					36c
"	X	X	-1.53	0.127	0.508					36d
"	X	X	-2.54	0.127	0.508					36e
"	X	X	2.032	0.127	0.508					36f
"	X	X	0	0.508	0.508					37a

Correlation Measured	Point O				Point A				Point B				Figure
	Pressure	Velocity Component u	v	w	$\frac{x_1}{\delta^*}$	$\frac{x_2}{\delta^*}$	$\frac{x_3}{\delta^*}$	Velocity Component u	v	w	$\frac{x'_1}{\delta^*}$	$\frac{x'_2}{\delta^*}$	$\frac{x'_3}{\delta^*}$	
R_{pw}	X			X	-0.51	0.508	0.508							37b
"	X			X	-1.02	0.508	0.508							37c
"	X			X	-1.53	0.508	0.508							37d
"	X			X	2.032	0.508	0.508							37e
"	X			X	2.032	0.127	0.508							38a
"	X			X	2.032	0.508	0.508							38b
"	X			X	2.032	1.524	0.508							38c
"	X			X	2.032	1.524	2.032							38d
"	X			X	2.032	3.048	2.32							38e

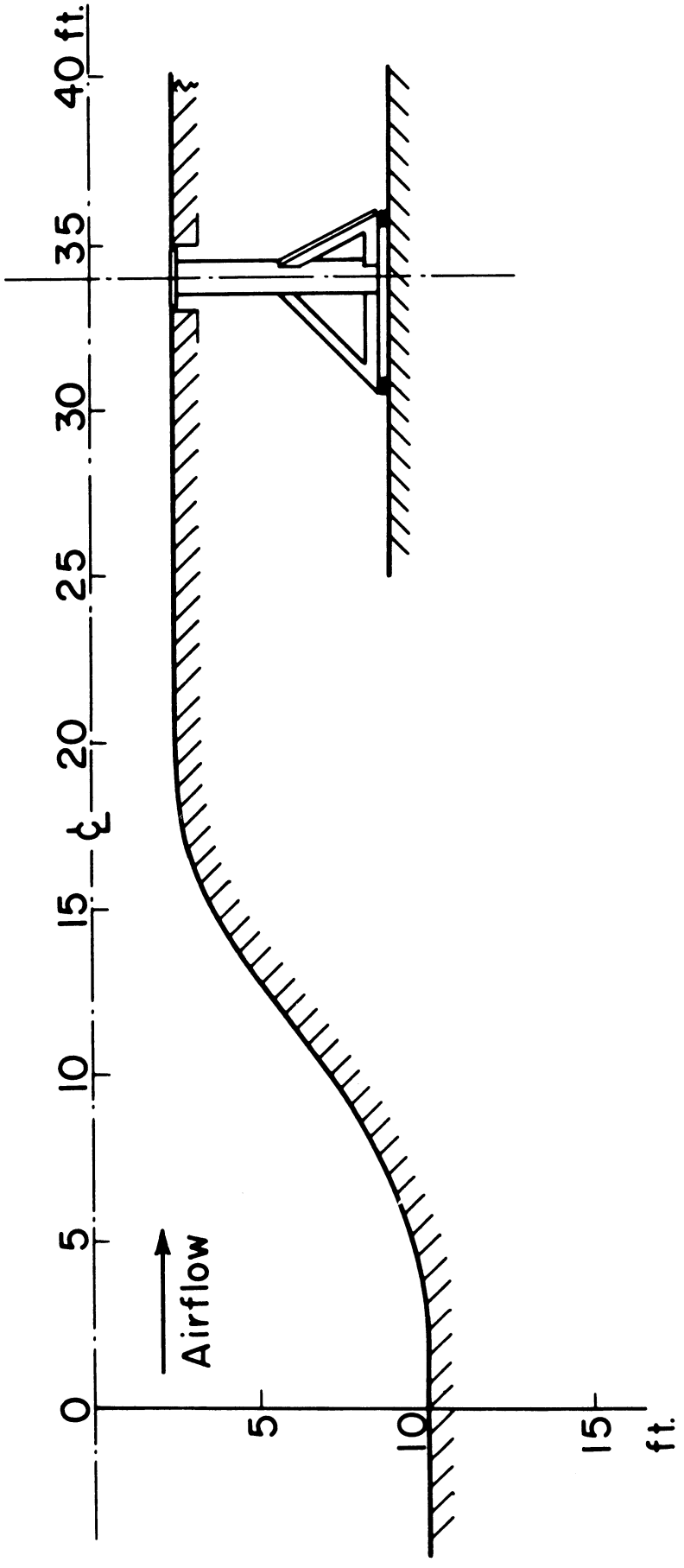

Fig. 1. Scale drawing of wind tunnel test section and massive vibration isolation mounting for the transducers.

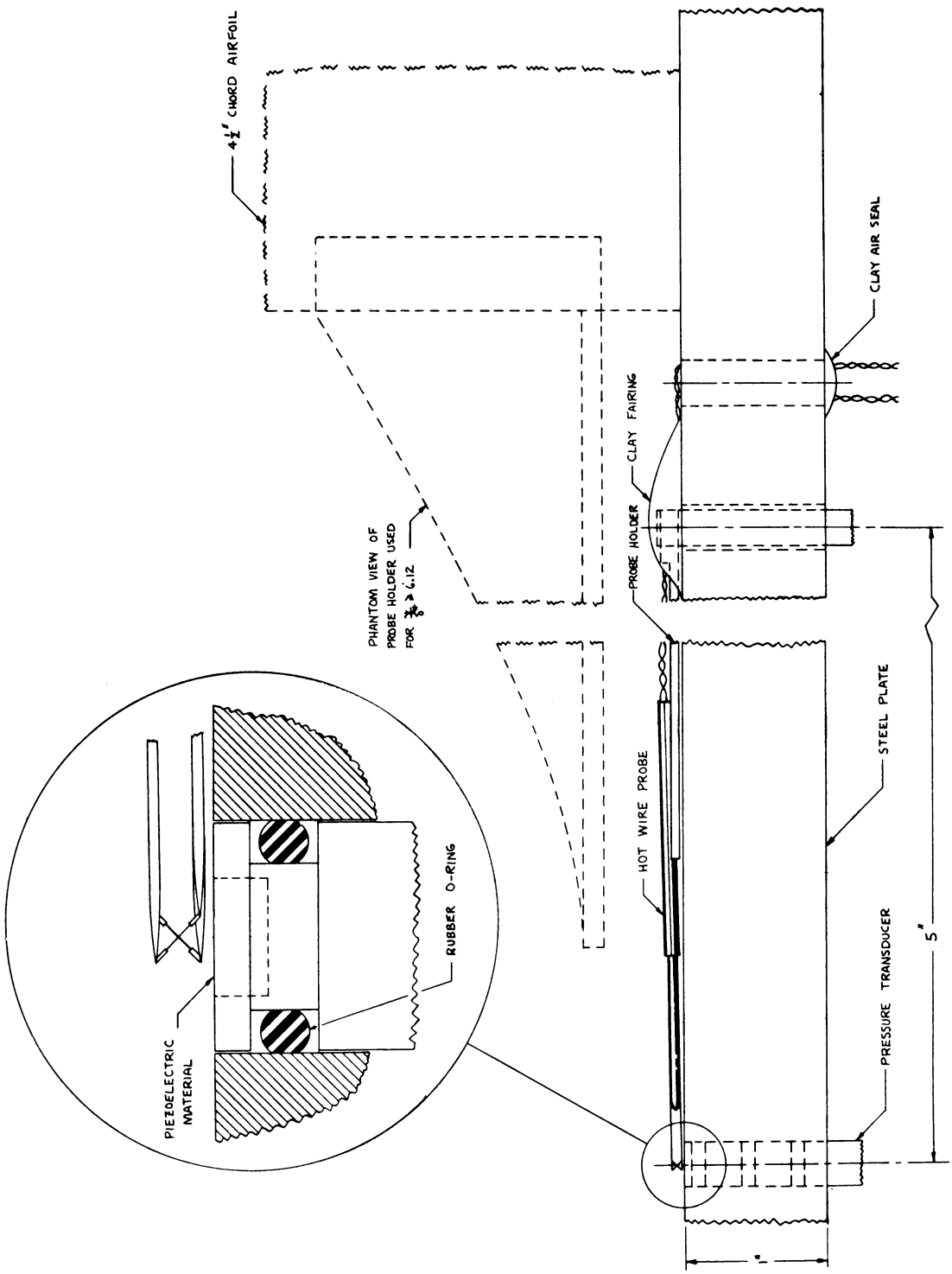

Fig. 2. Pressure transducer and hot-wire installation. Hot-wire shown at closest spacing to plate, 0.05 inch.

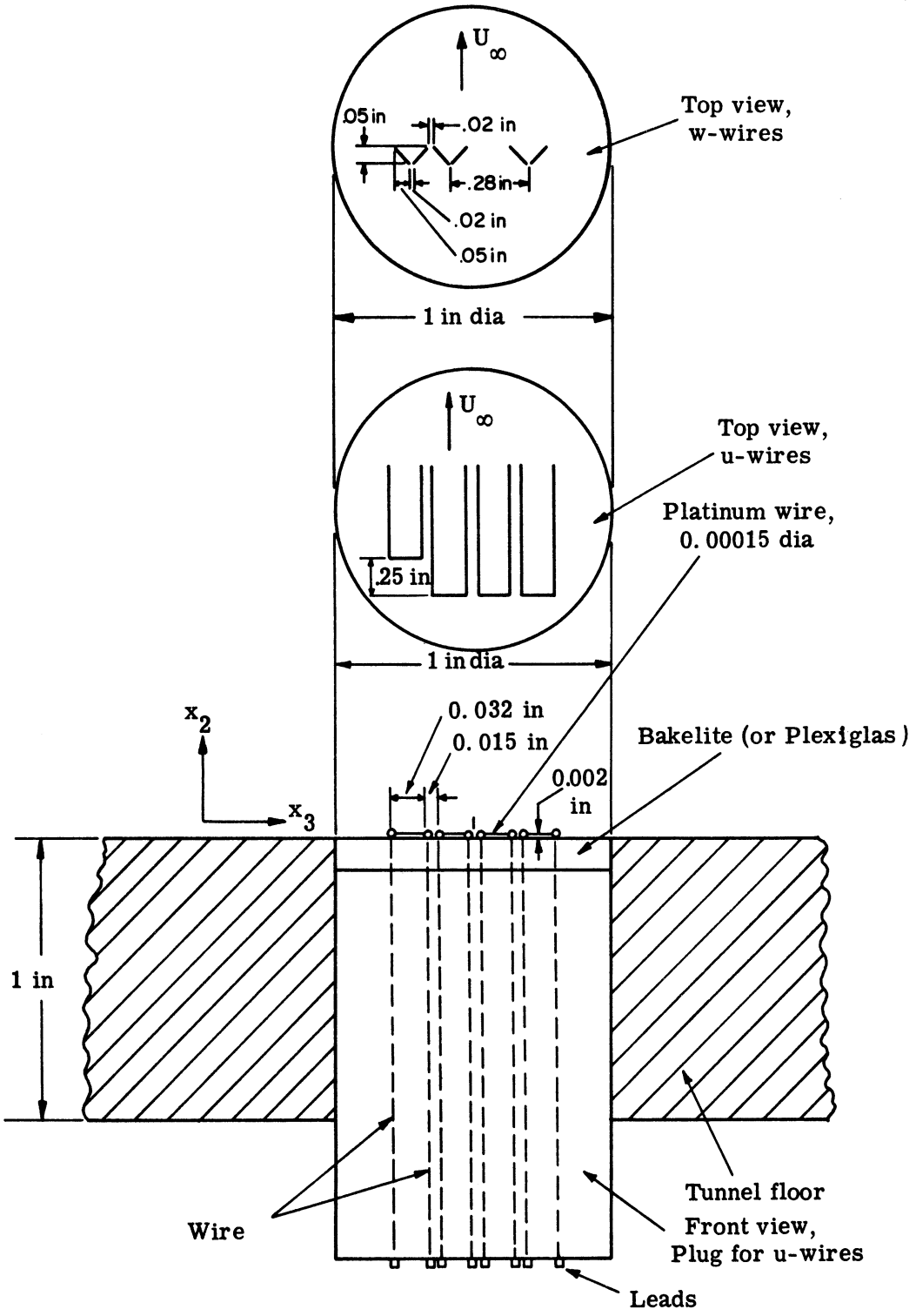

Note: w-wires are arranged in the same horizontal plane owing to the large variation of velocity with x_2 near the wall. This arrangement gives poorer spatial resolution in the x_3 direction than the x-type wires but allows measurements near the wall.

Fig. 3. Hot-wire plug.

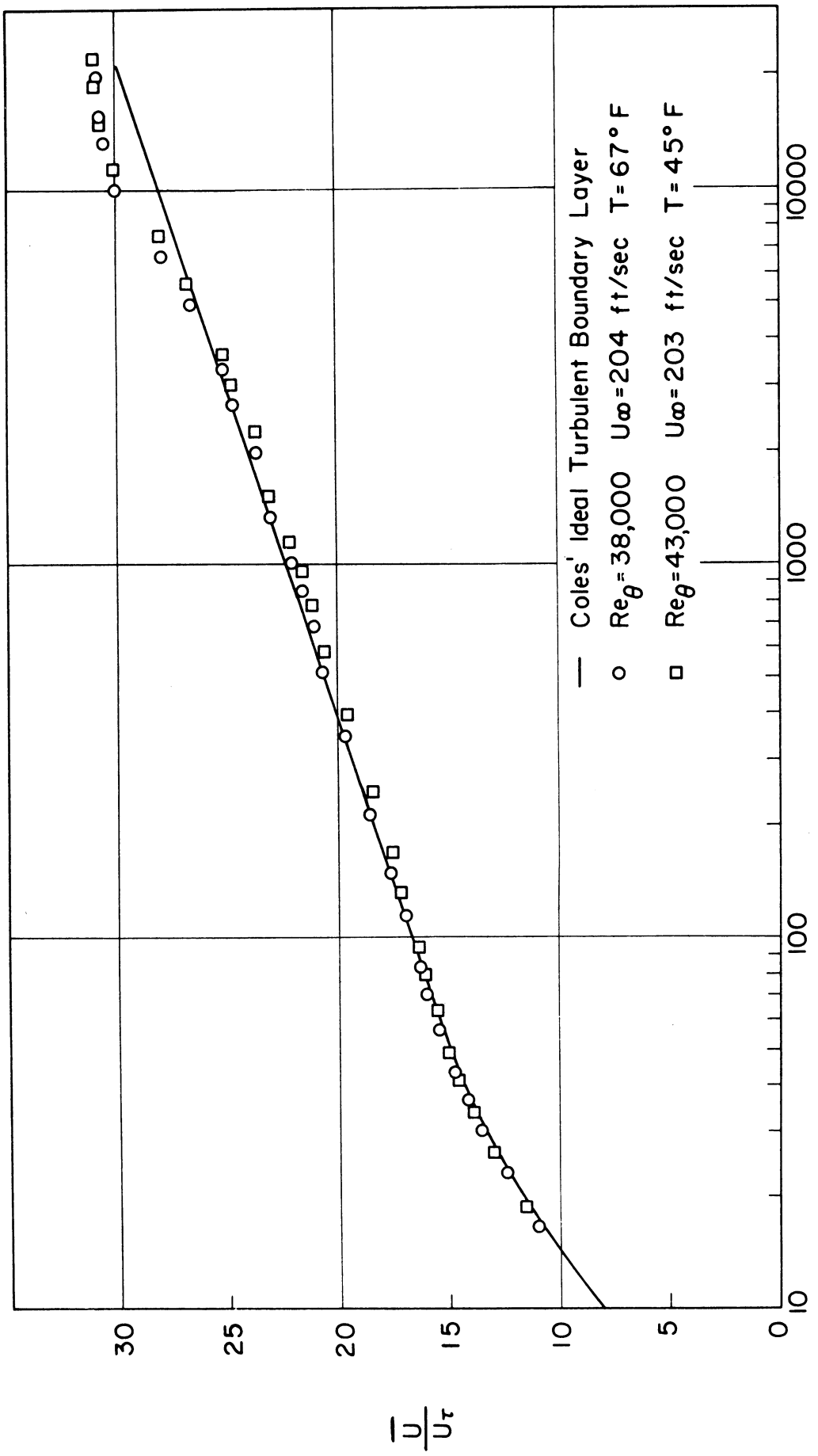

Fig. 4. Mean velocity profiles in the turbulent boundary layer.
Refer to Table I for other boundary layer parameters.

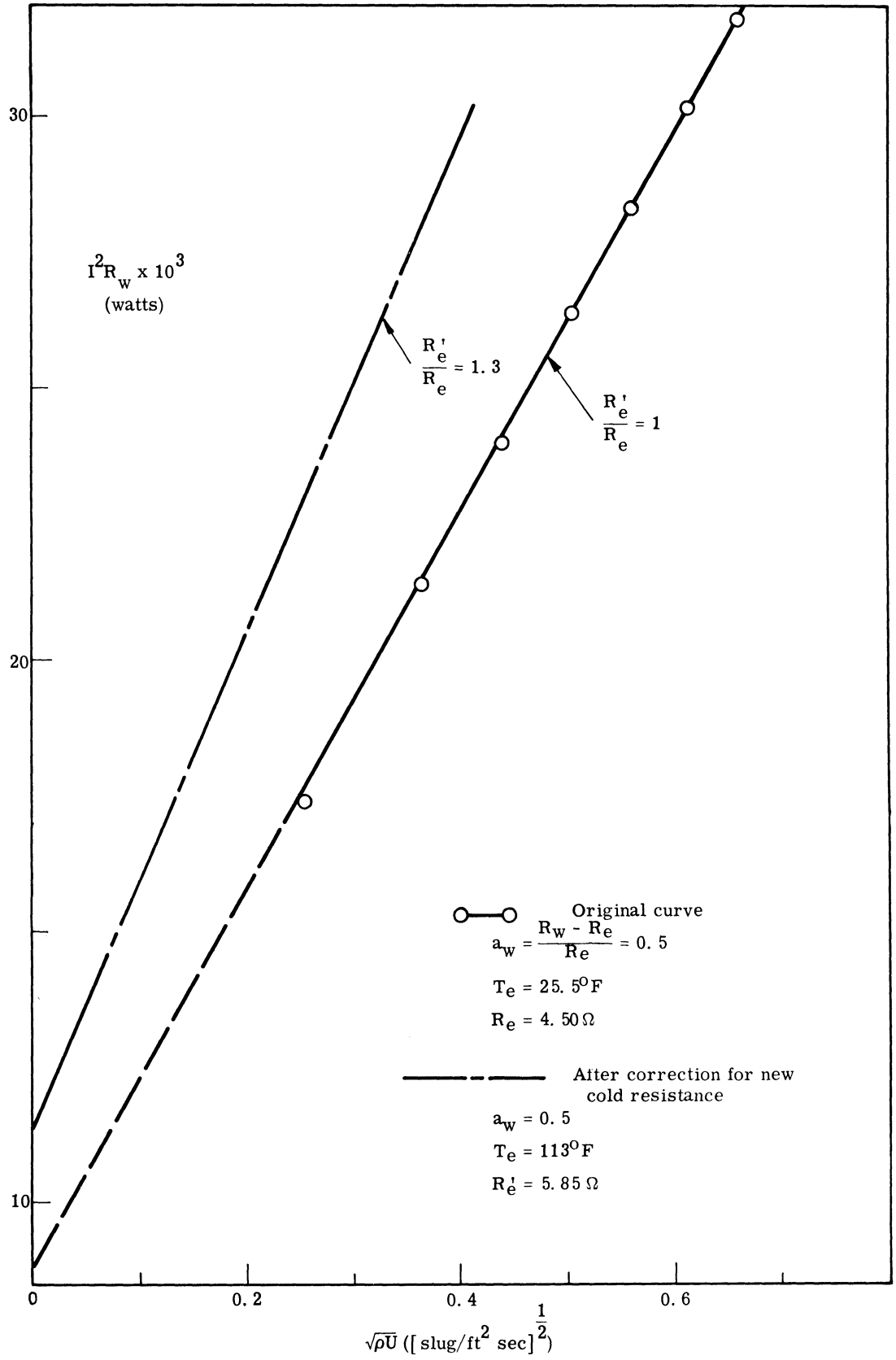

Fig. 5. Hot-wire calibration curve for platinum u-wire.

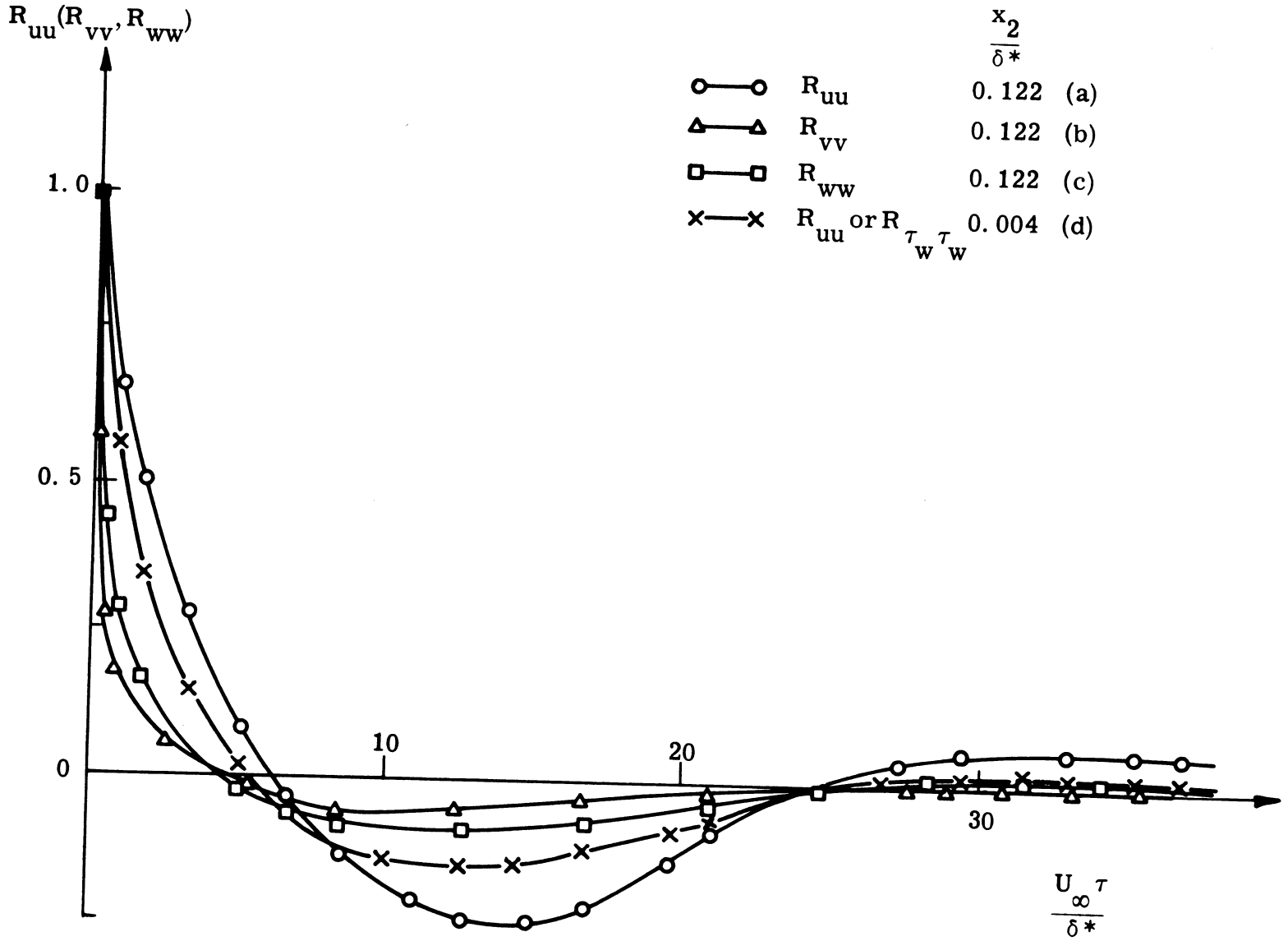

Fig. 6. Comparison of auto-correlations of velocity fluctuations, u, v and w near the wall.

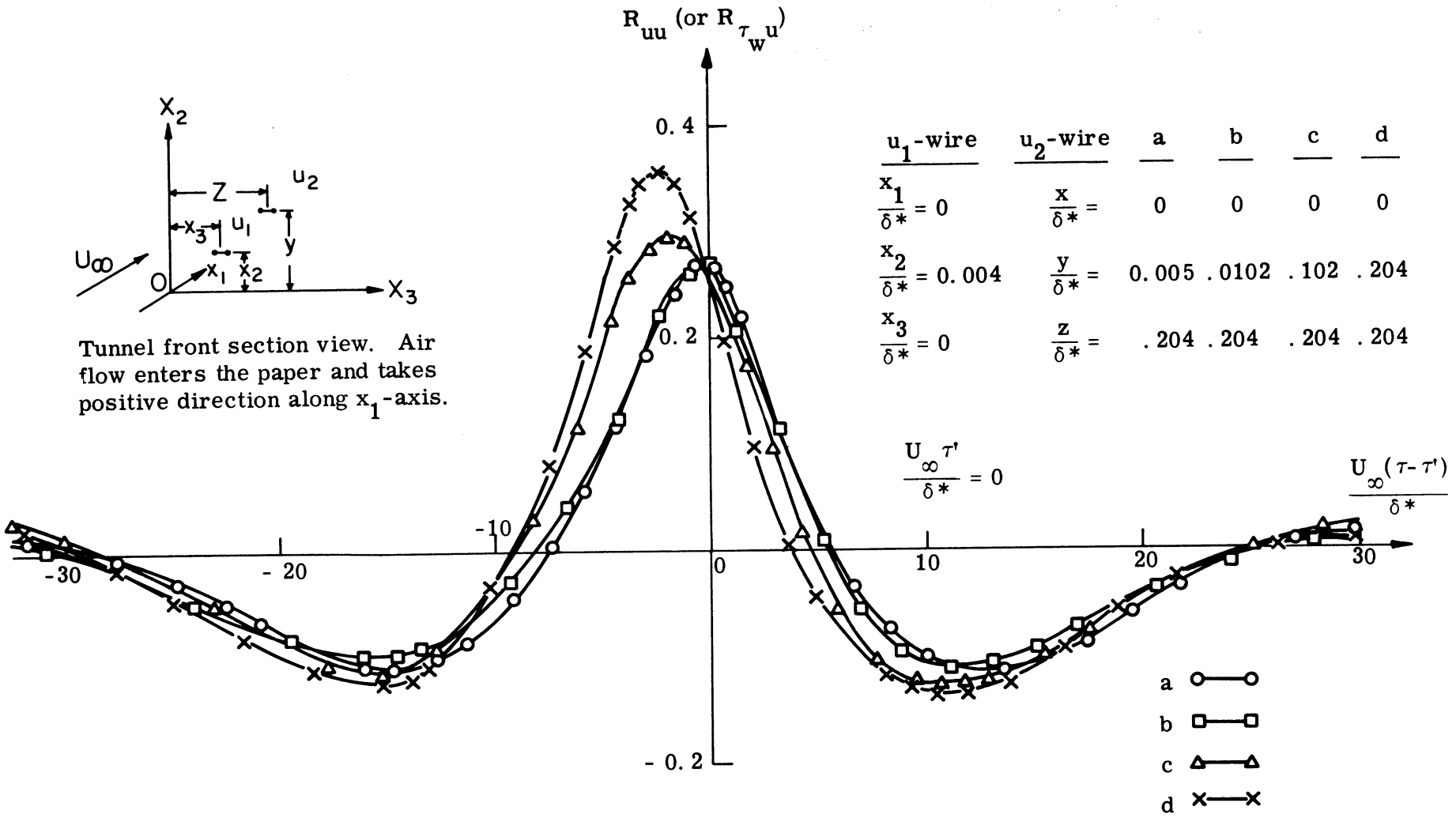

Fig. 7. Comparison of the space-time correlation of u-u near the wall.

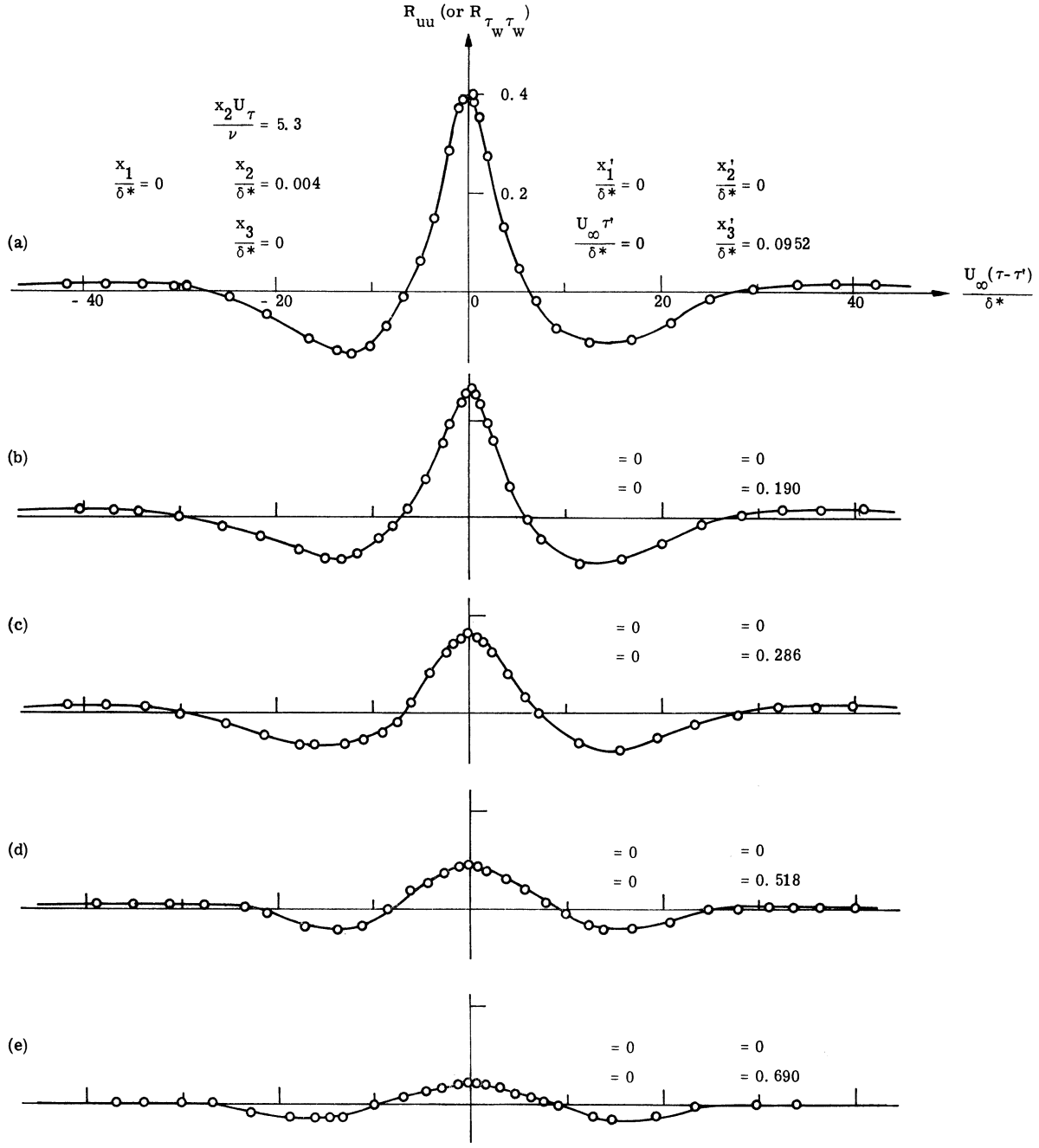

Fig. 8. Measured values of the space-time correlation of u-u very near the wall.

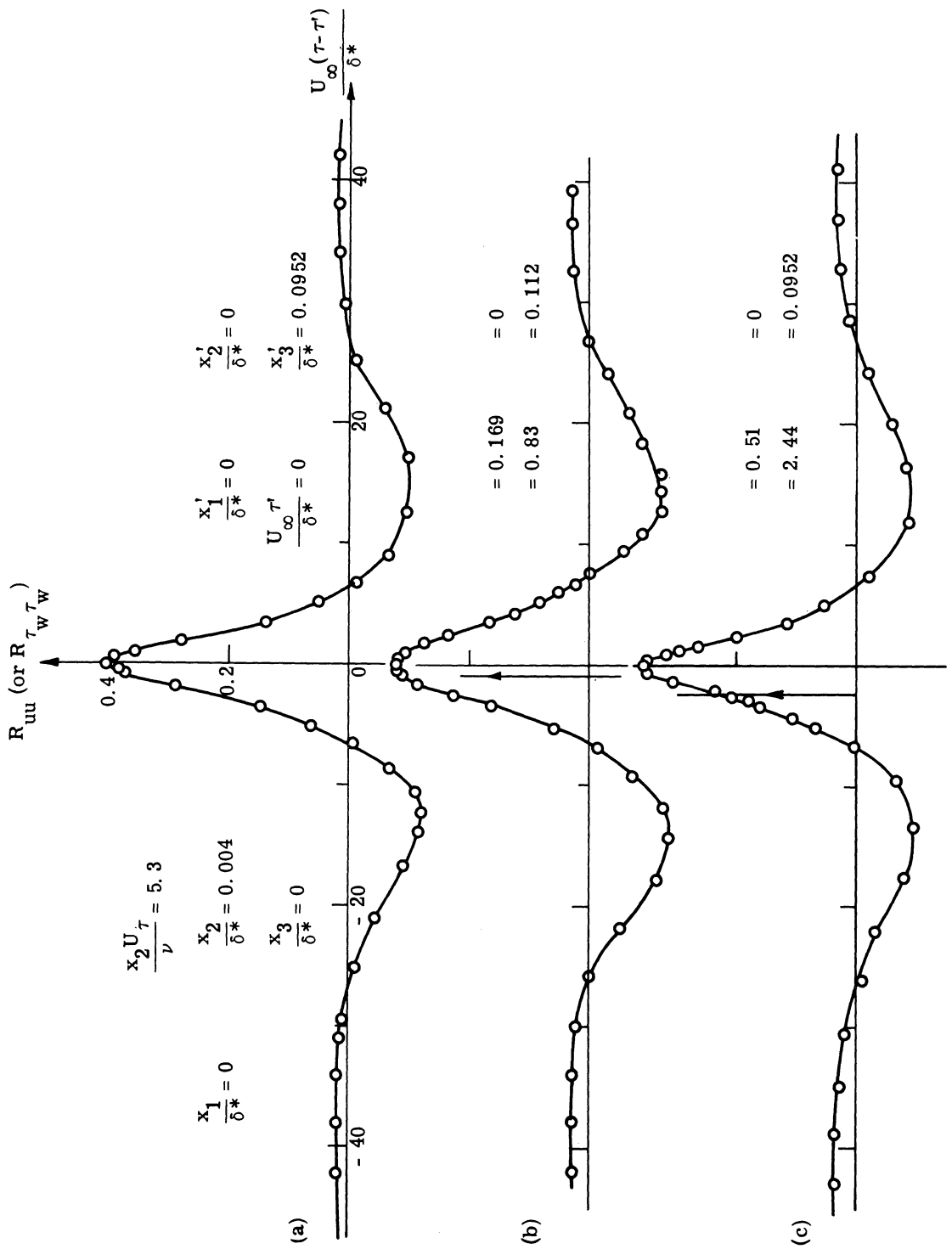

Fig. 9. Measured values of the space-time correlation of u-u very near the wall.

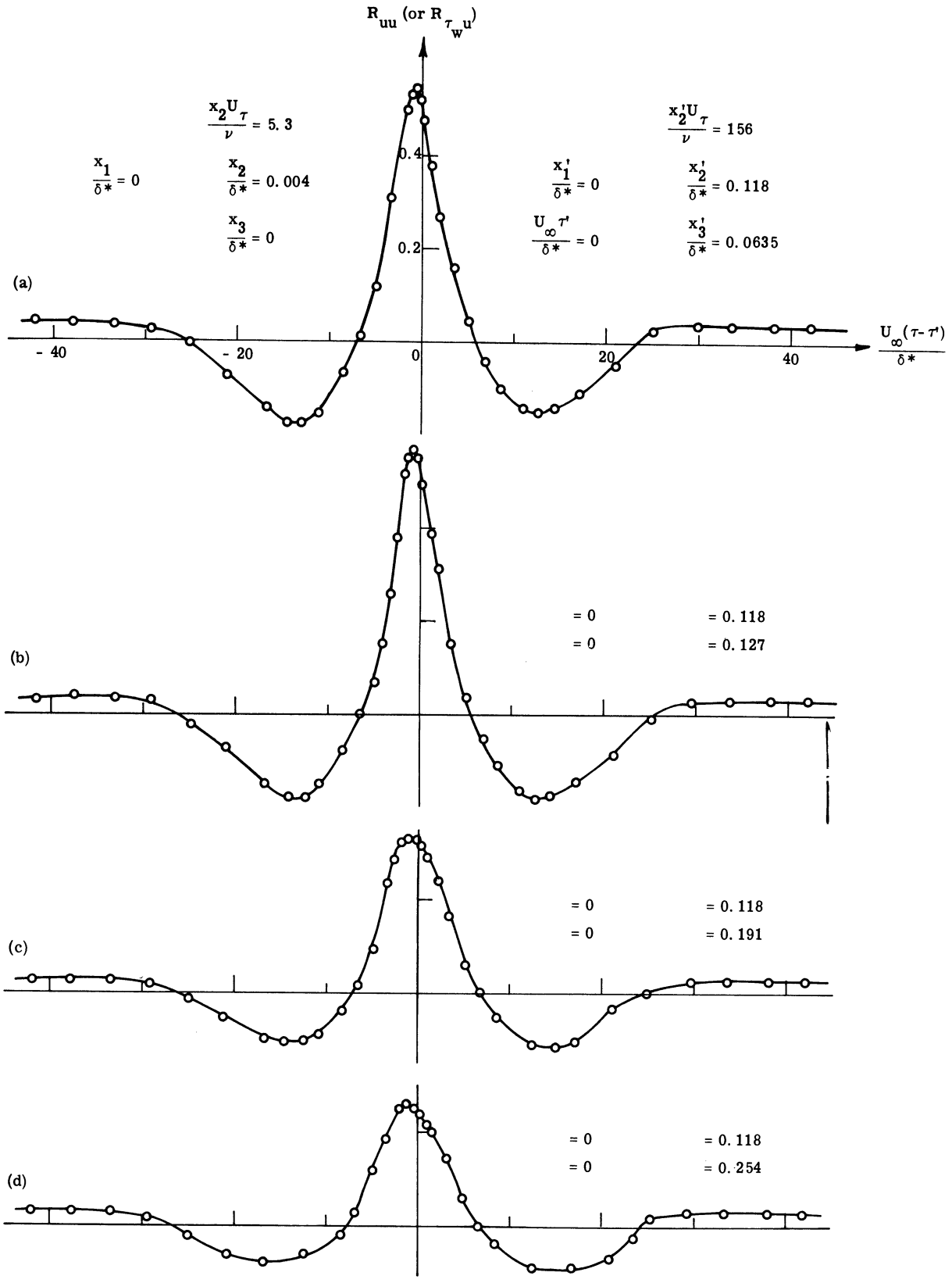

Fig. 10. Measured values of the space-time correlation of u-u near the wall.

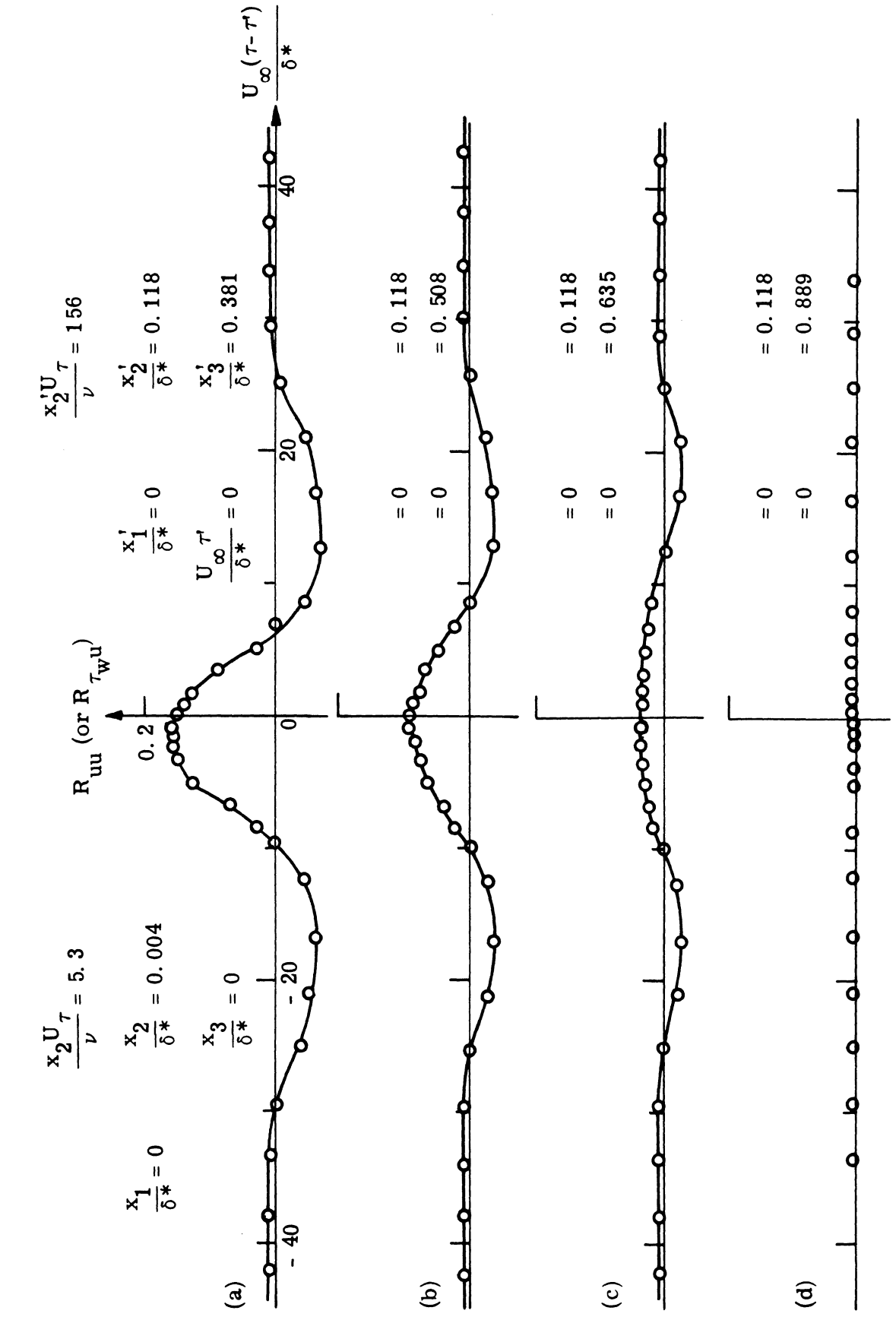

Fig. 11. Measured values of the space-time correlation of u-u near the wall.

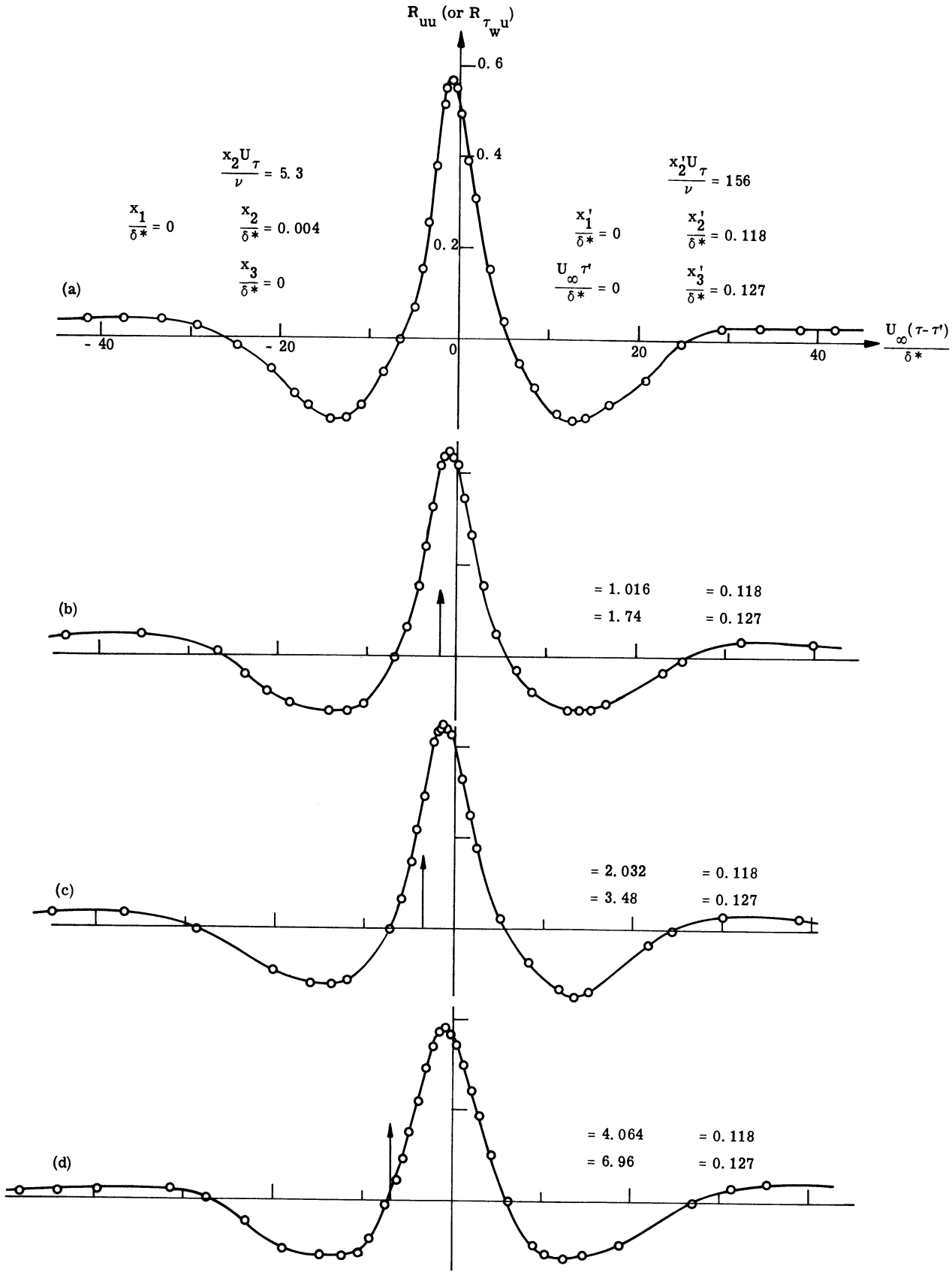

Fig. 12. Measured values of the space-time correlation of u-u near the wall.

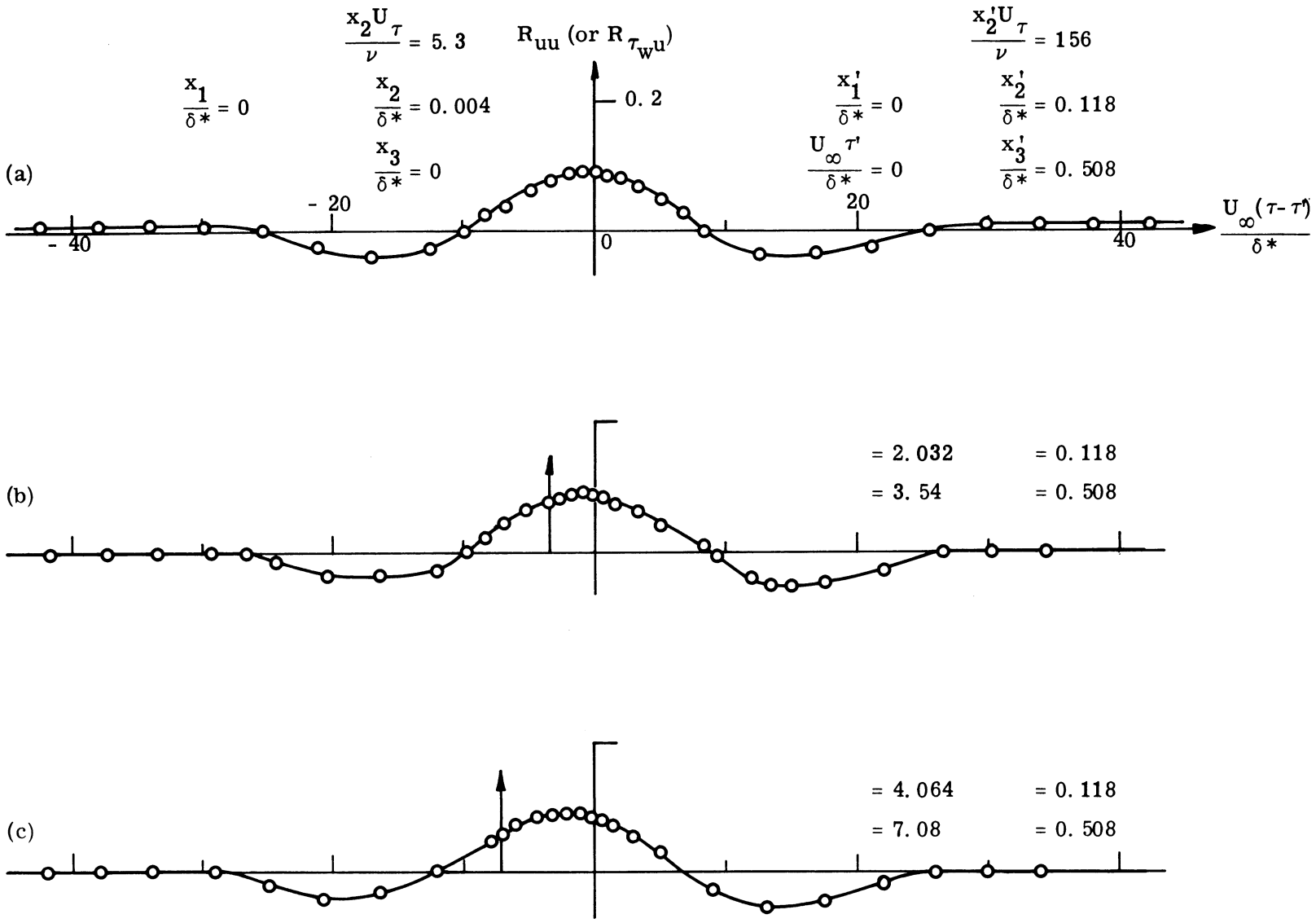

Fig. 13. Measured values of the space-time correlation of u-u near the wall.

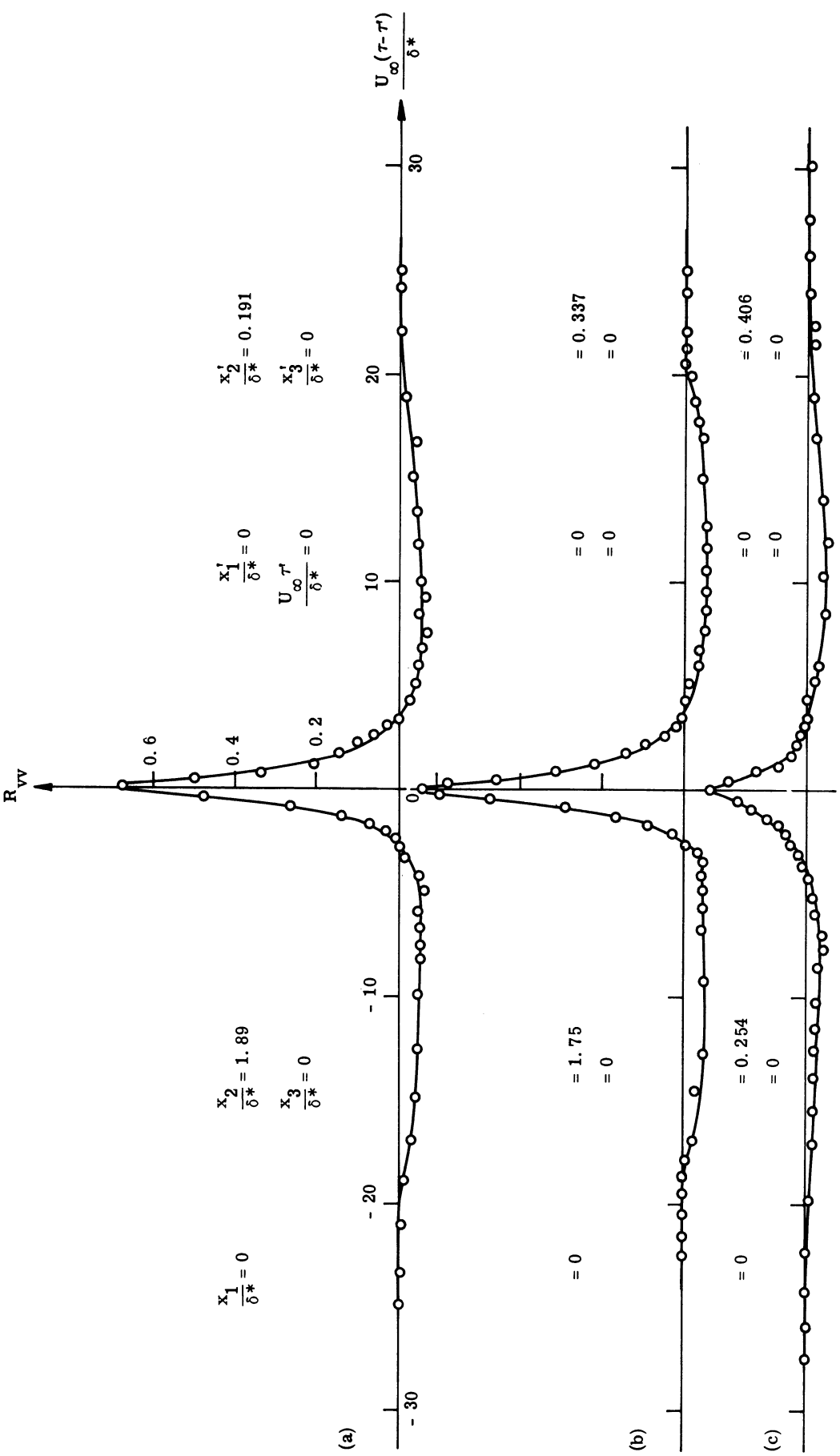

Fig. 14. Measured values of the space-time correlation of v-v.

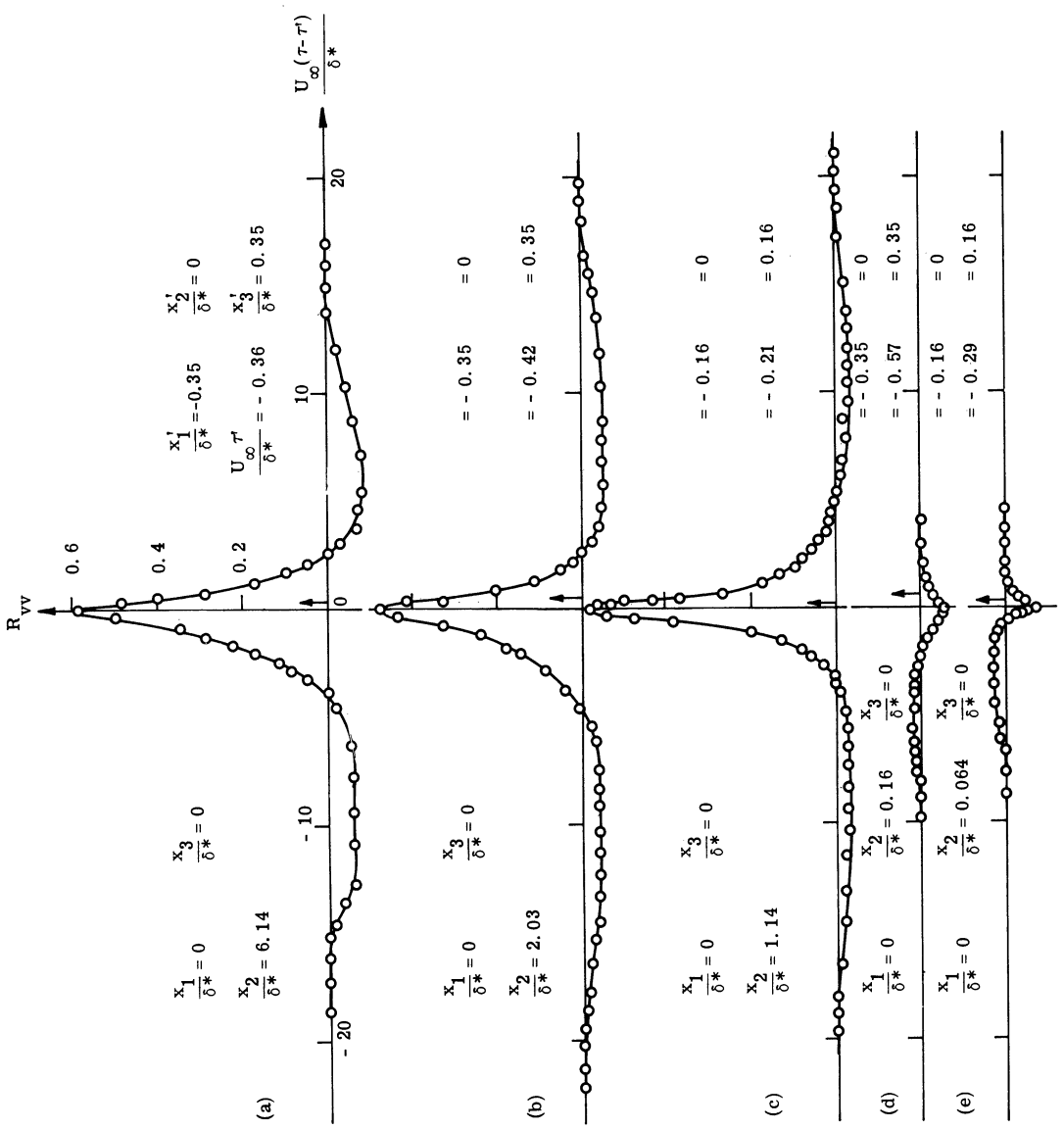

Fig. 15. Measured values of the space-time correlation of v-v.

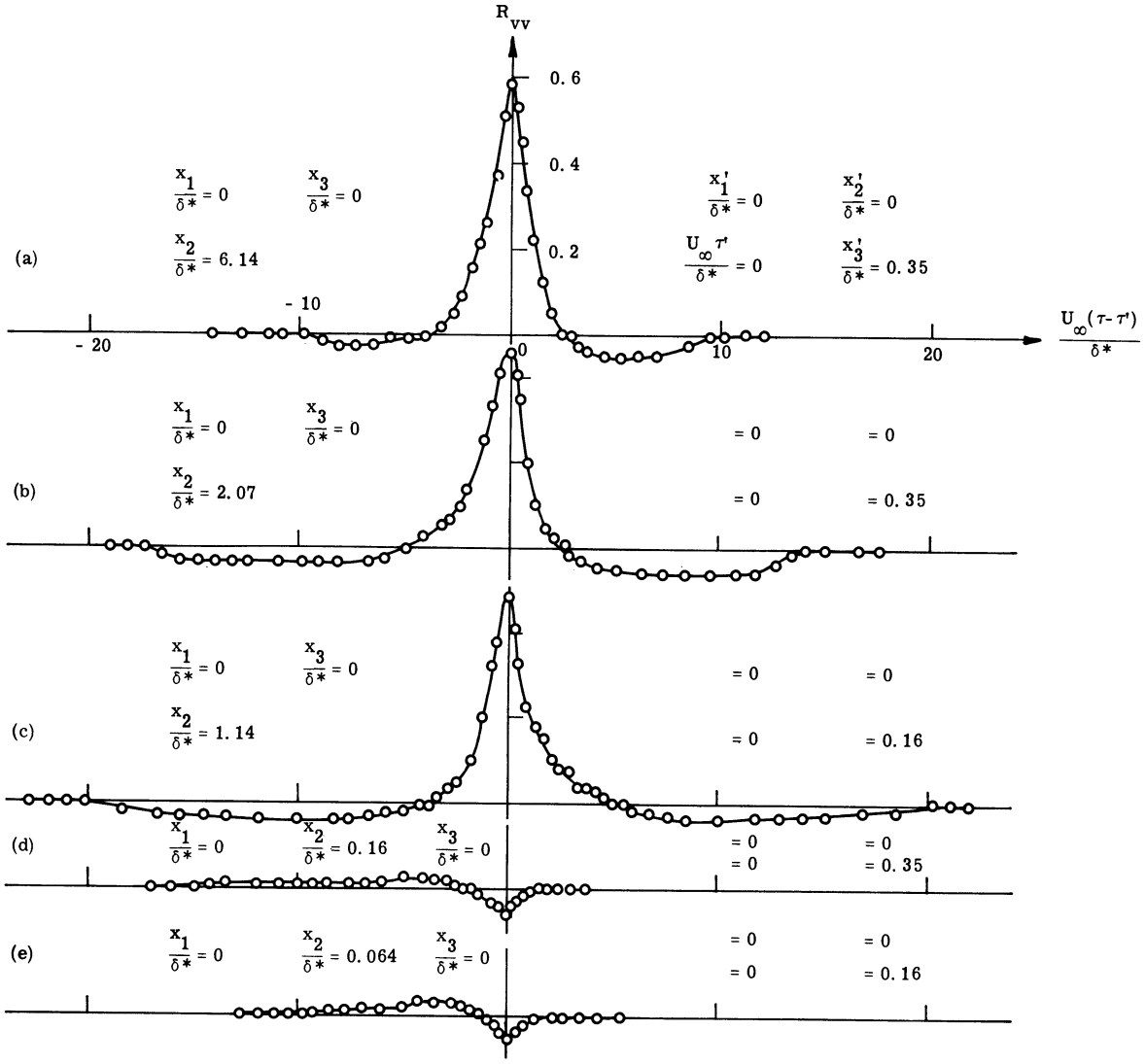

Fig. 16. Measured values of the space-time correlation of v-v.

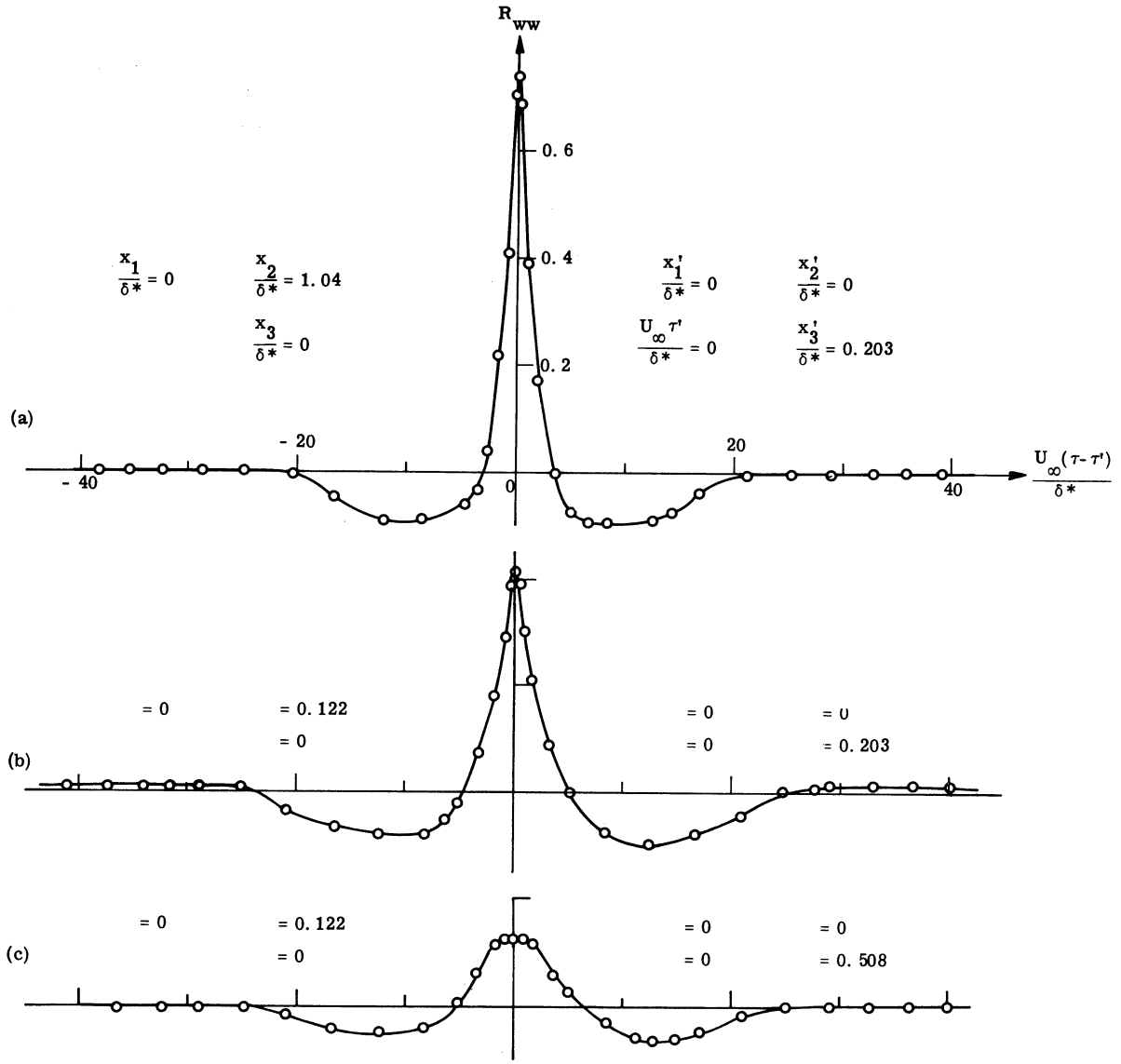

Fig. 17. Measured values of the space-time correlation of w-w near the wall.

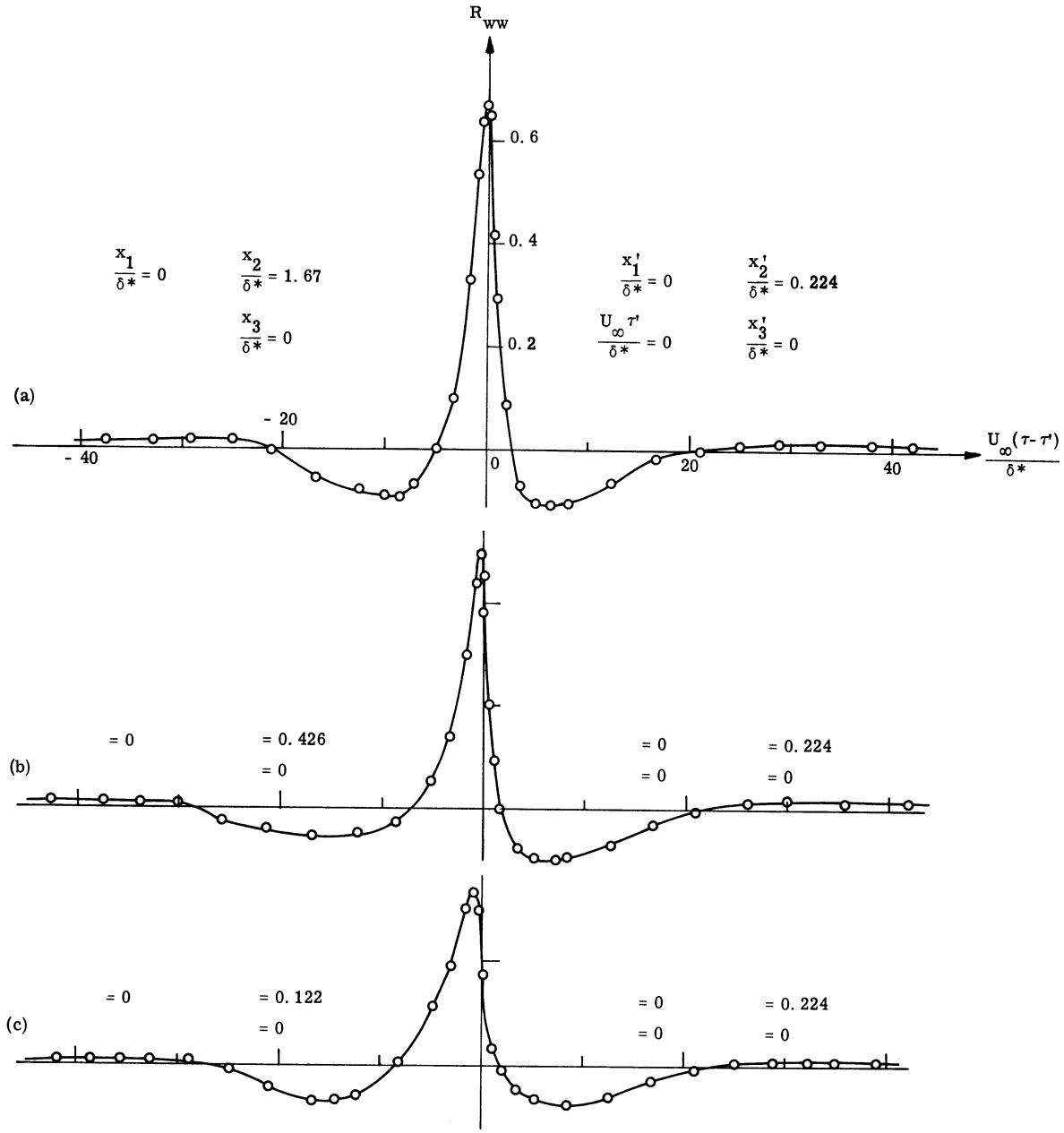

Fig. 18. Measured values of the space-time correlation of w-w near the wall.

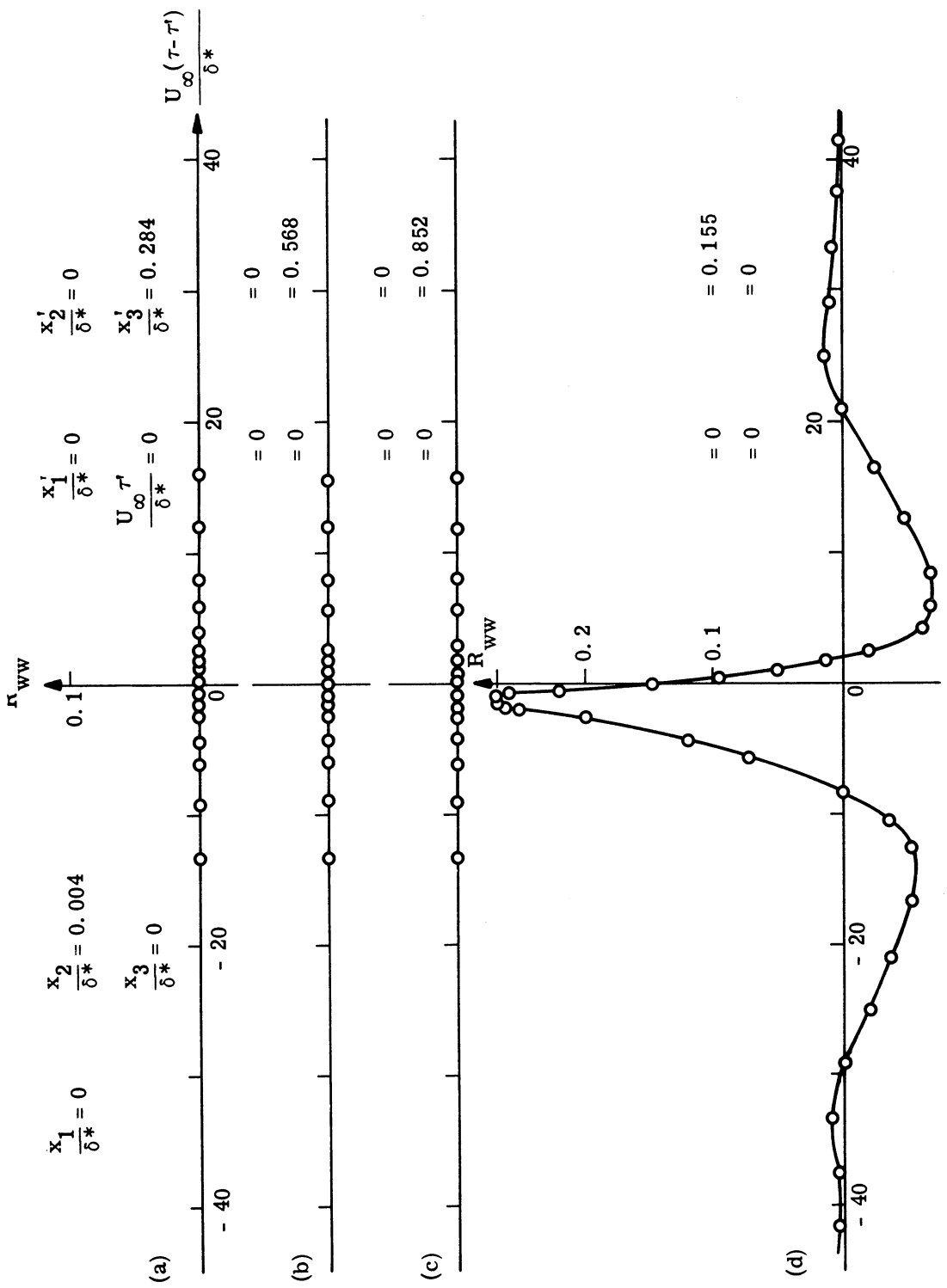

Fig. 19. Measured values of the space-time correlation of w-w very near the wall.

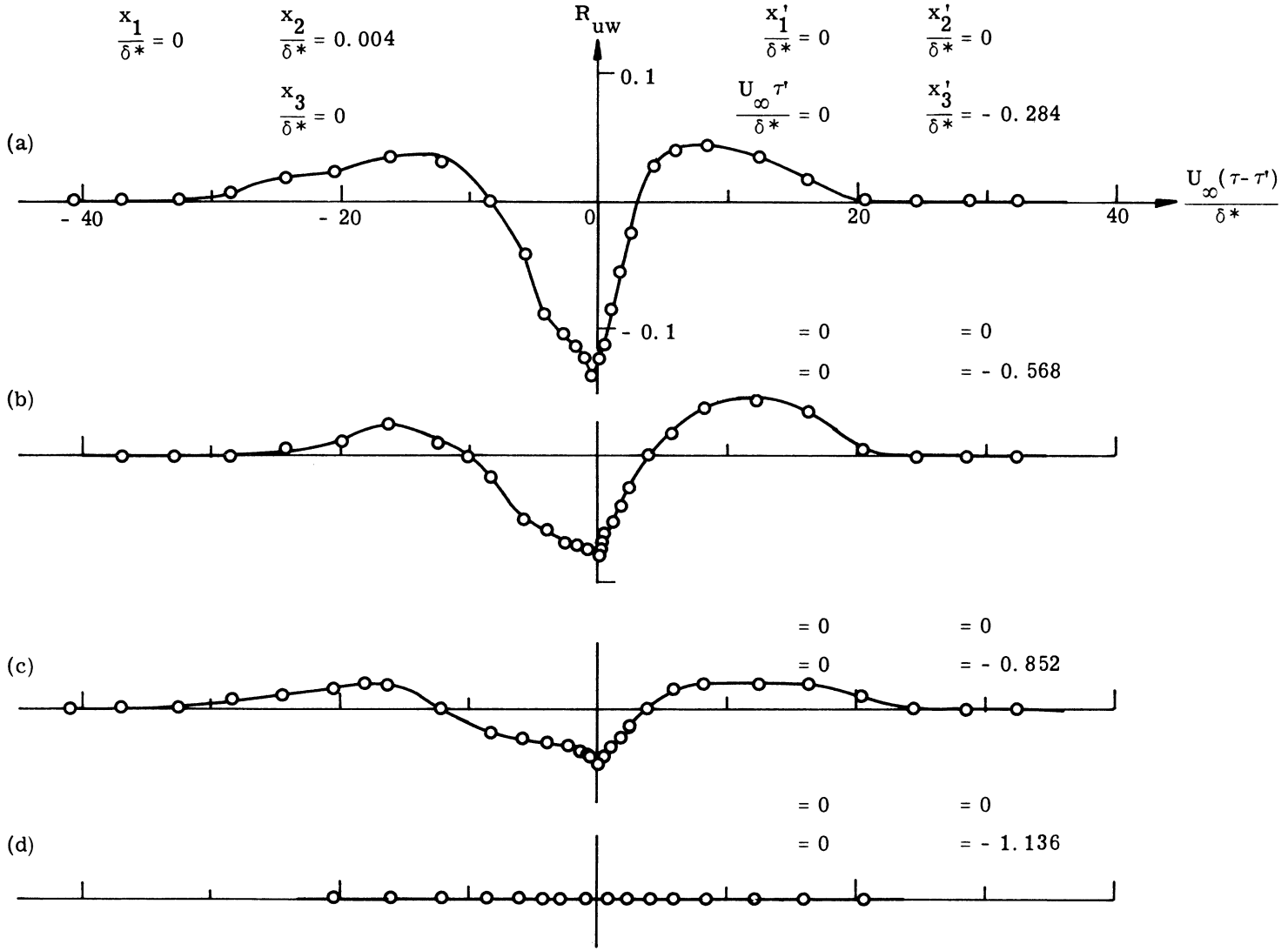

Fig. 20. Measured values of the space-time correlation of u-w very near the wall.

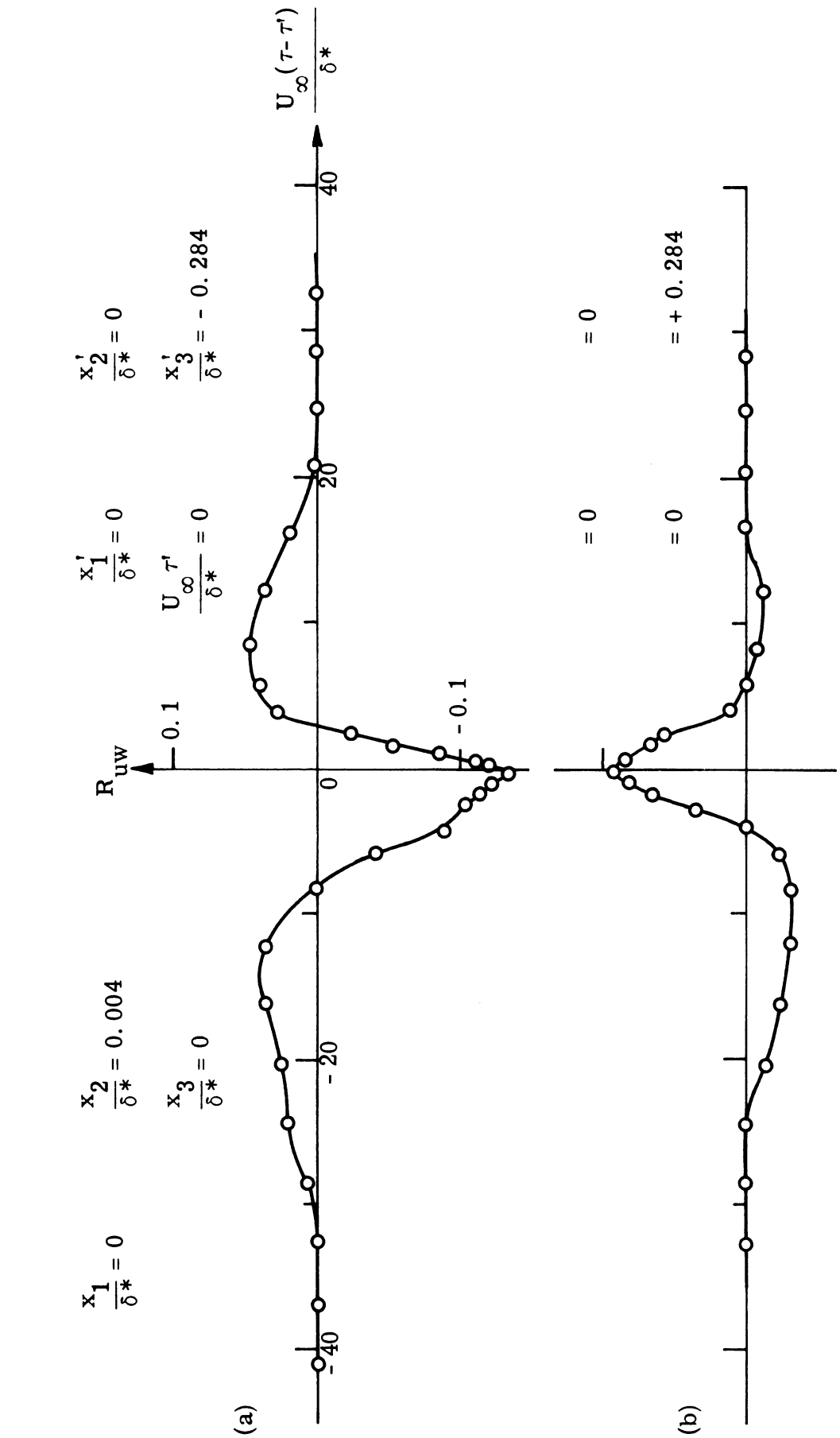

Fig. 21. Measured values of the space-time correlation of u-w very near the wall.

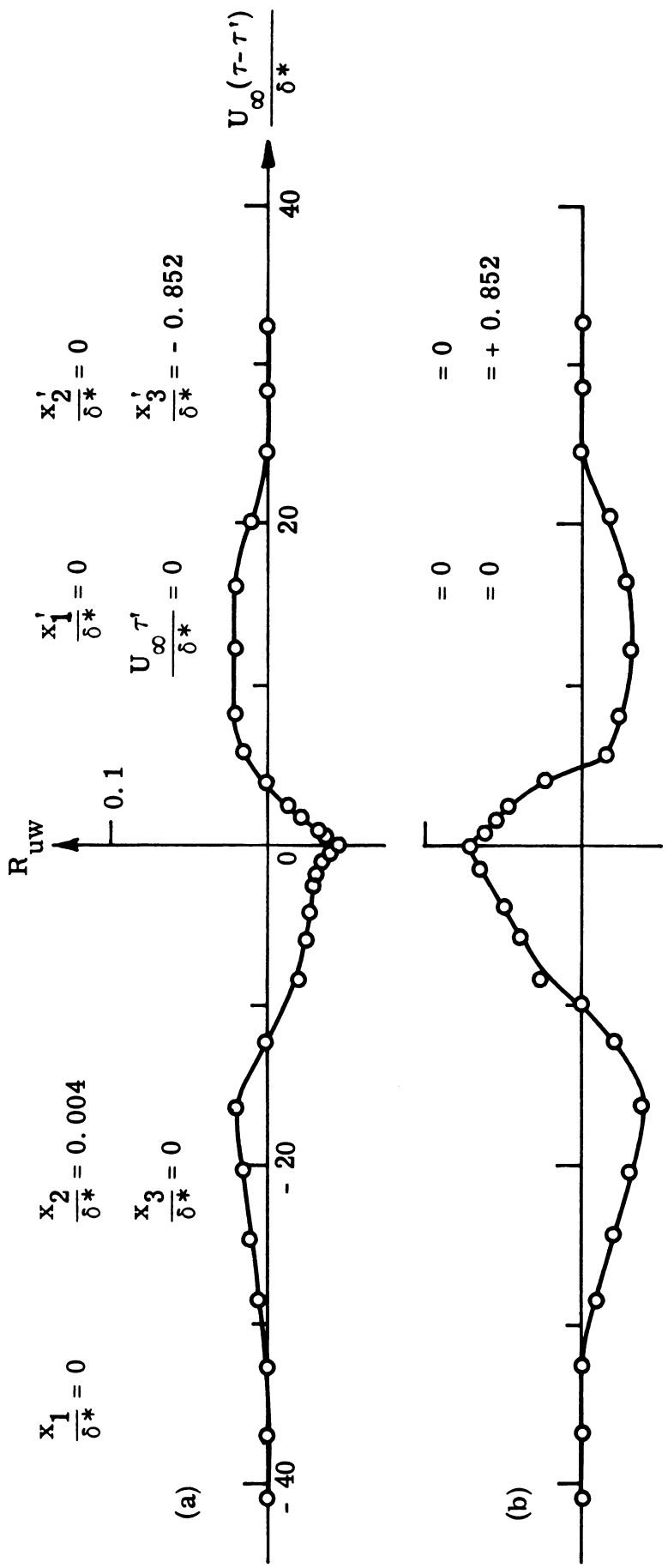

Fig. 22. Measured values of the space-time correlation of u-w very near the wall.

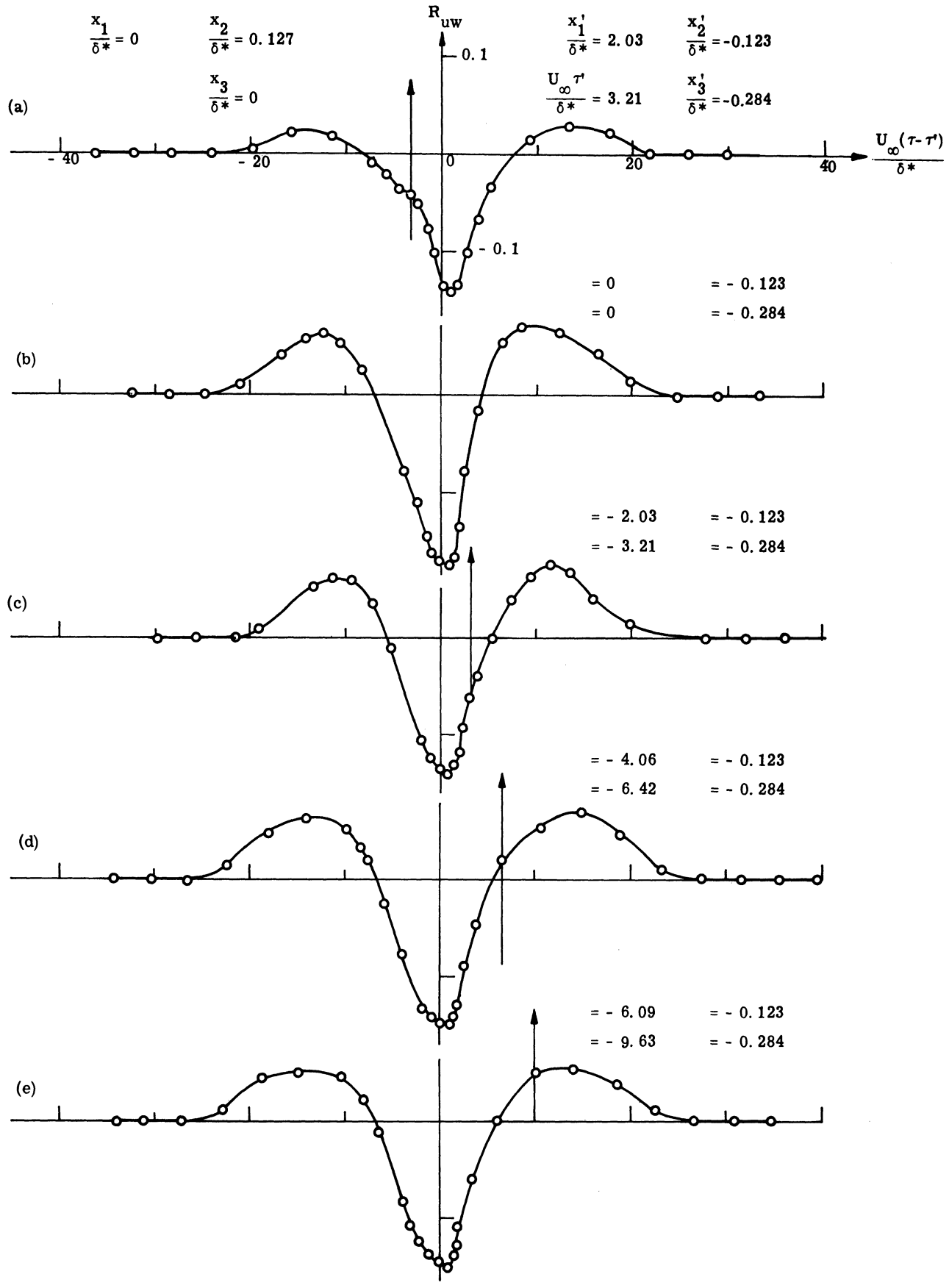

Fig. 23. Measured values of the space-time correlation of u-w near the wall.

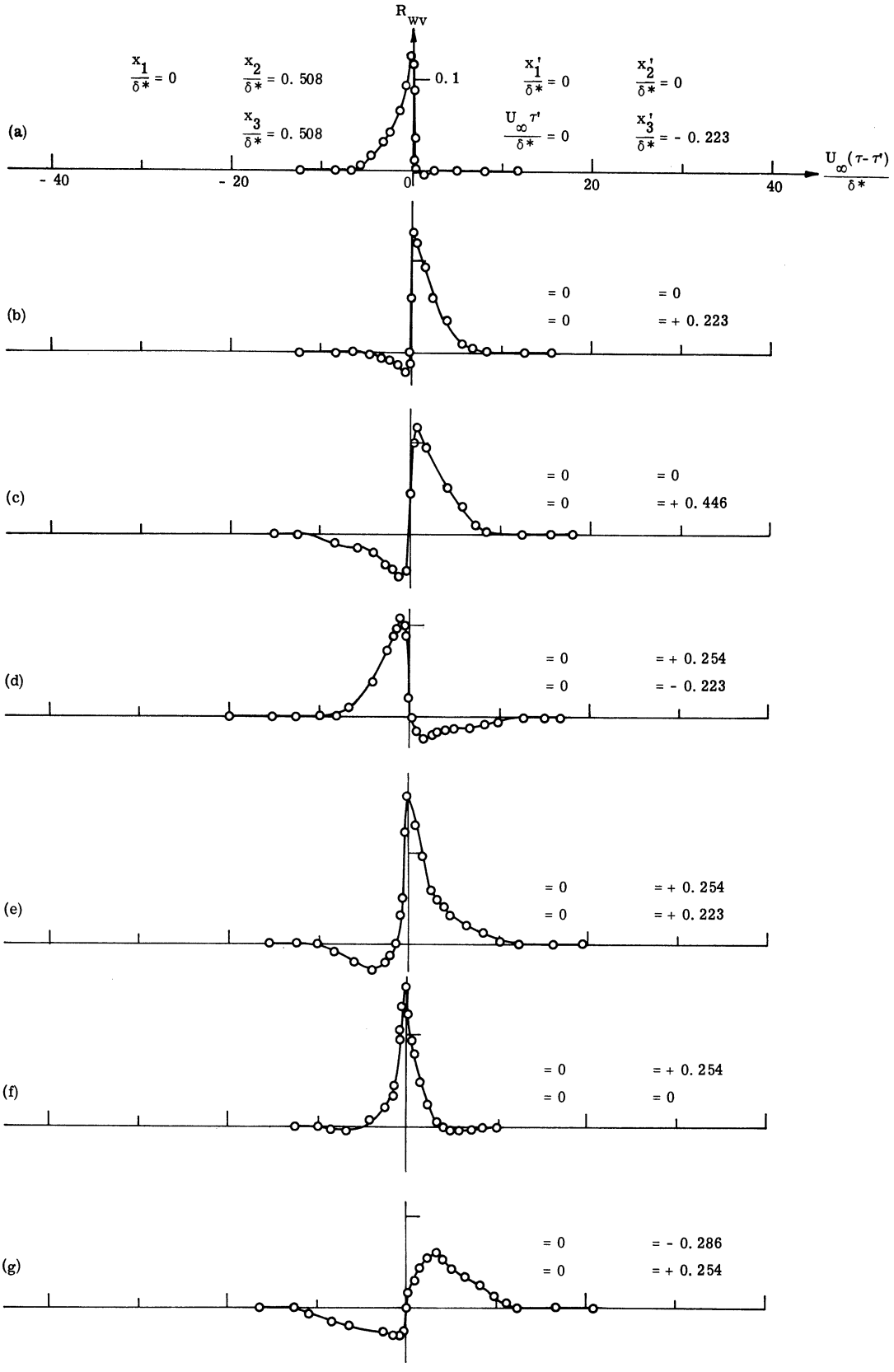

Fig. 24. Measured values of the space-time correlation of w-v.

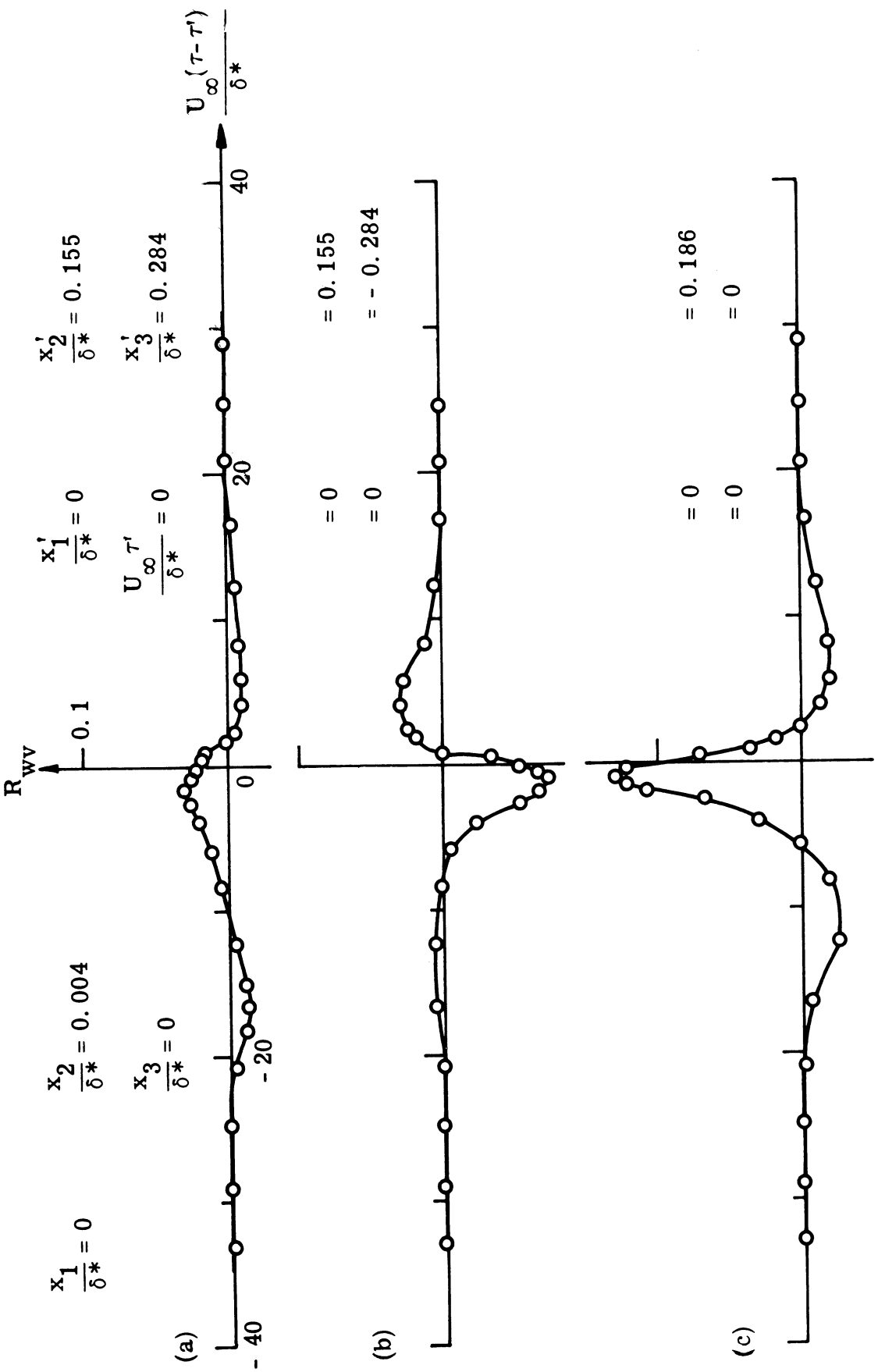

Fig. 25. Measured values of the space-time correlation of w-v near the wall.

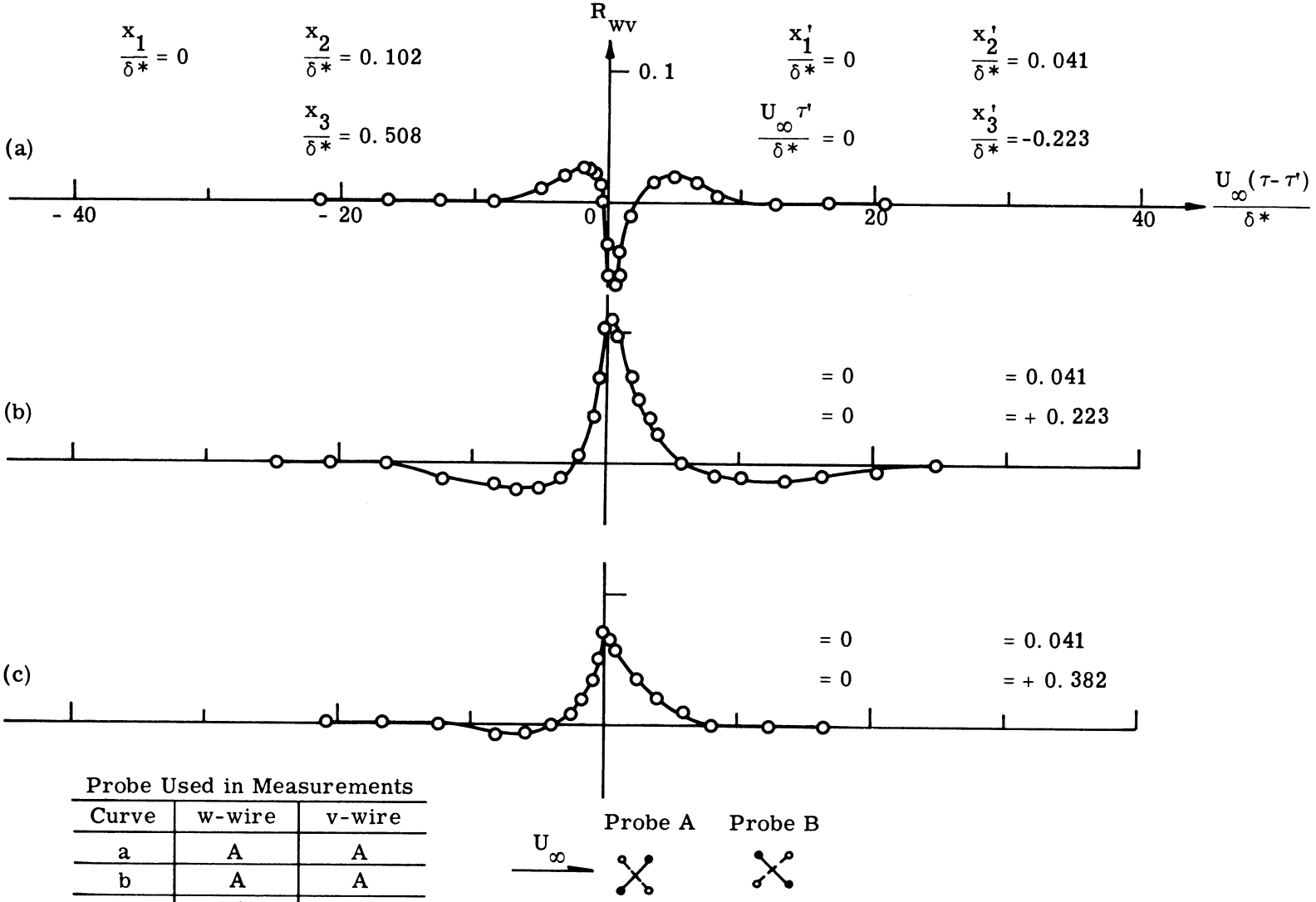

Probe Used in Measurements

Curve	w-wire	v-wire
a	A	A
b	A	A
c	A	A

Fig. 26. Measured values of the space-time correlation of w-v near the wall.

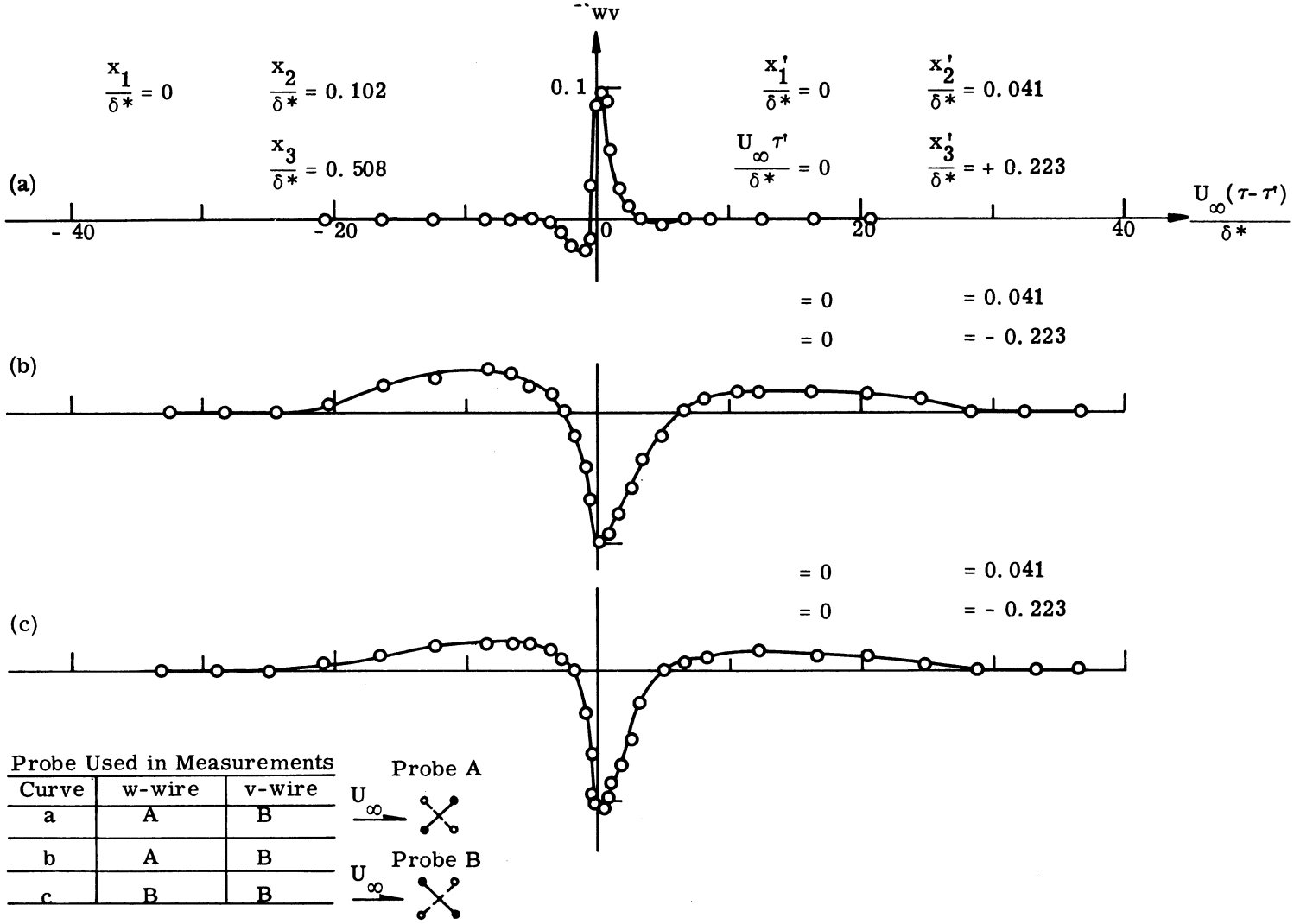

Fig. 27. The measurement of R_{wv} near the wall, using different arrangements of x-type hot-wires (also see Fig. 26 for comparison).

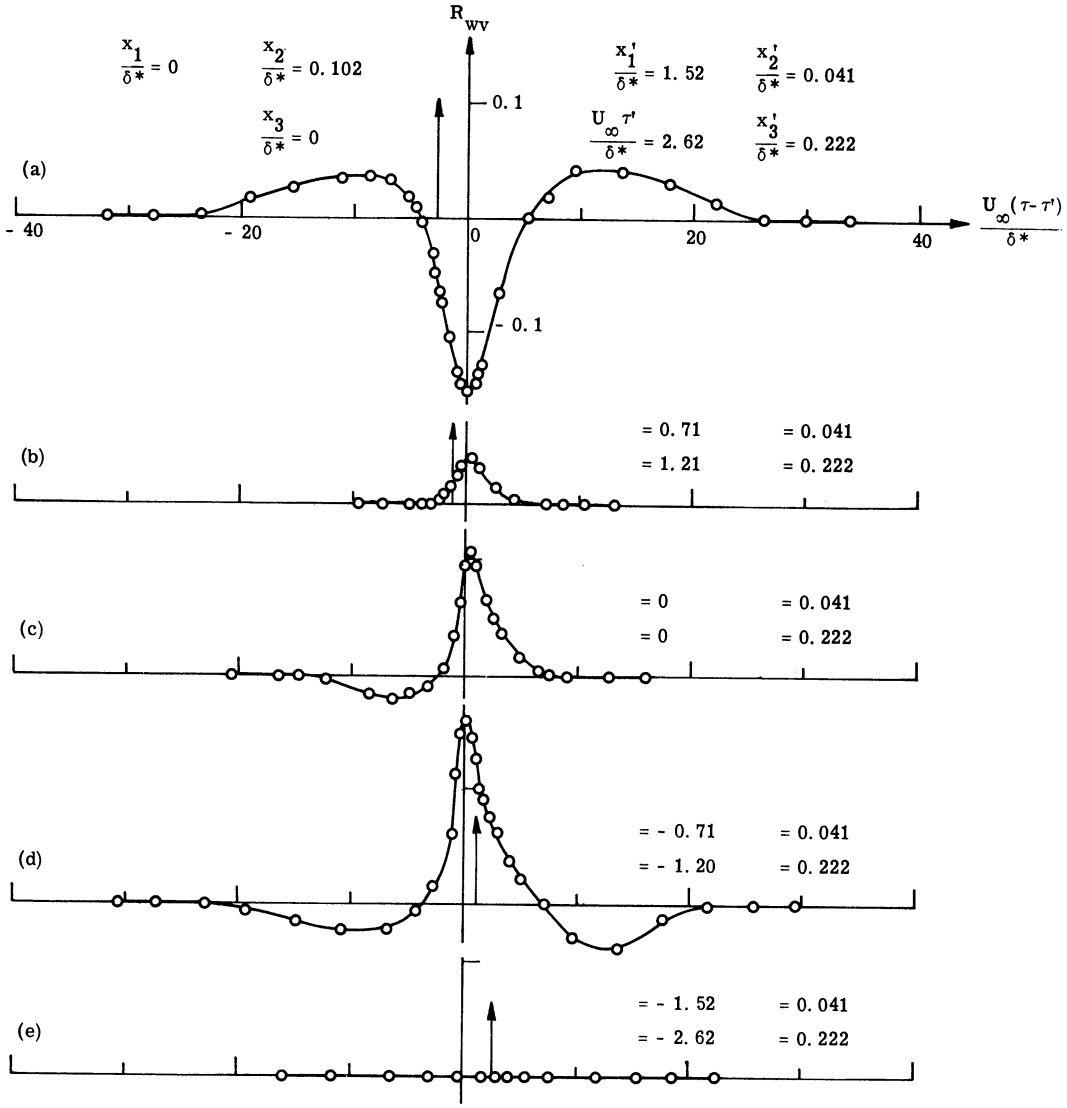

Fig. 28. Measured values of the space-time correlation of w-v near the wall.

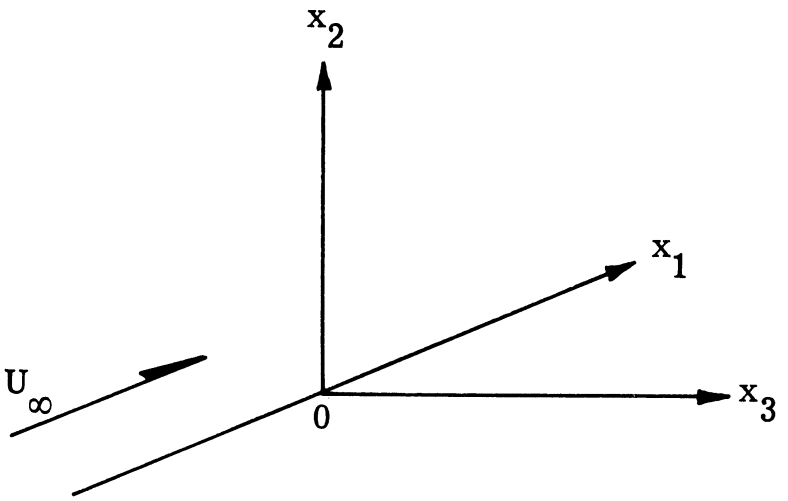

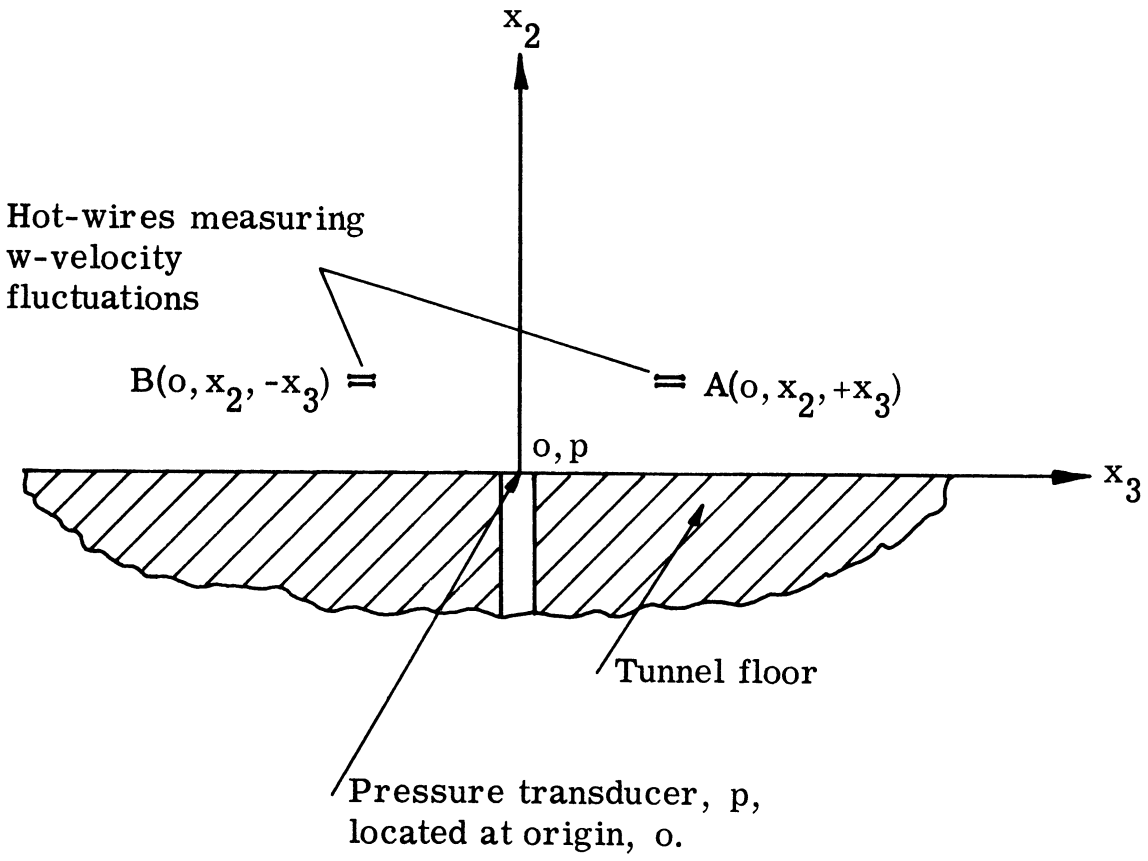

Fig. 29. Preliminary consideration of R_{pw} measurements.

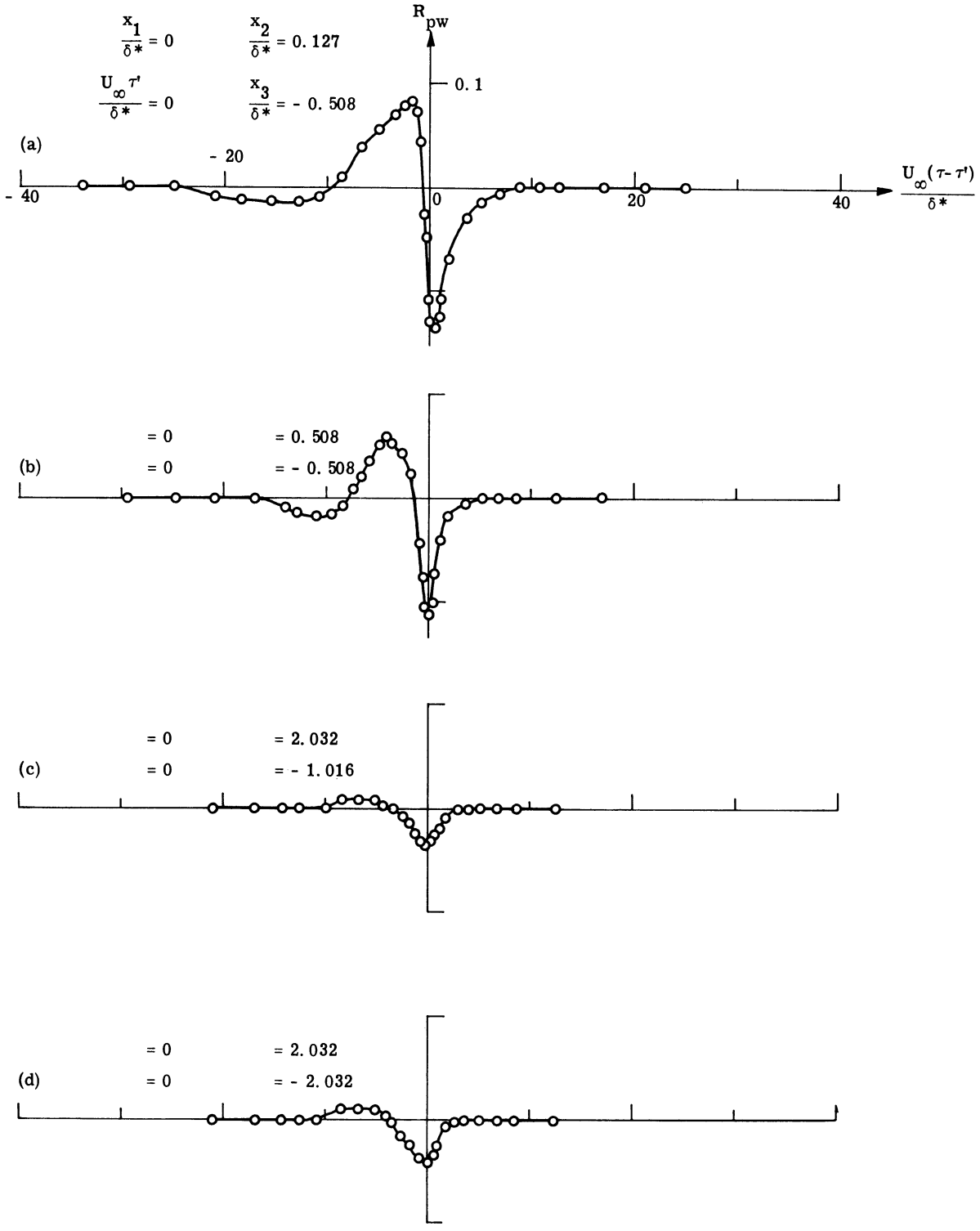

Fig. 30. Measured values of the space-time correlation of fluctuating velocity component w with fluctuating wall pressure ($x_3/\delta^* < 0$).

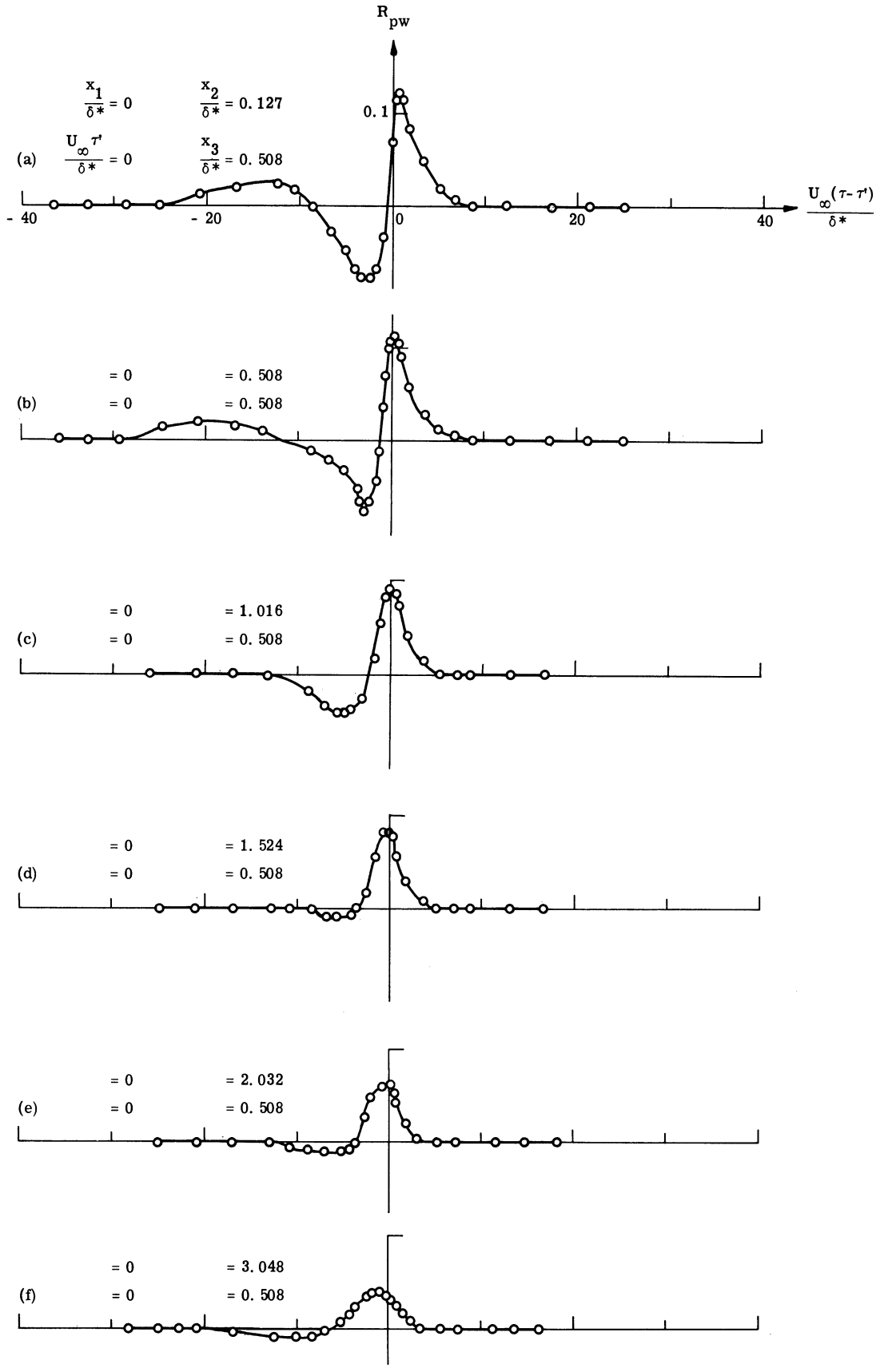

Fig. 31. Measured values of the space-time correlation of fluctuating velocity component w with fluctuating wall pressure ($x_3/\delta^* > 0$).

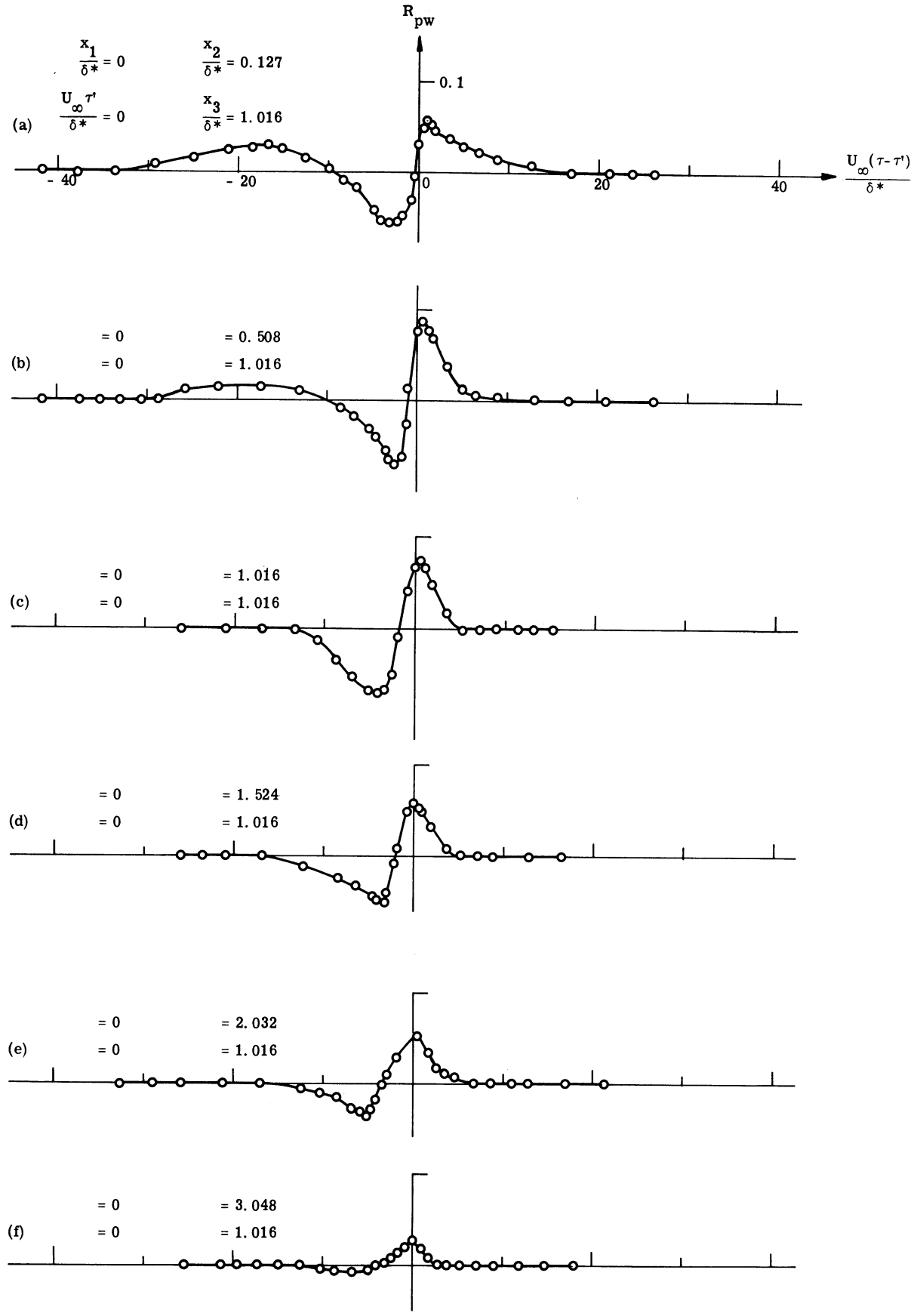

Fig. 32. Measured values of the space-time correlation of fluctuating velocity component w with fluctuating wall pressure ($x_3/\delta^* > 0$).

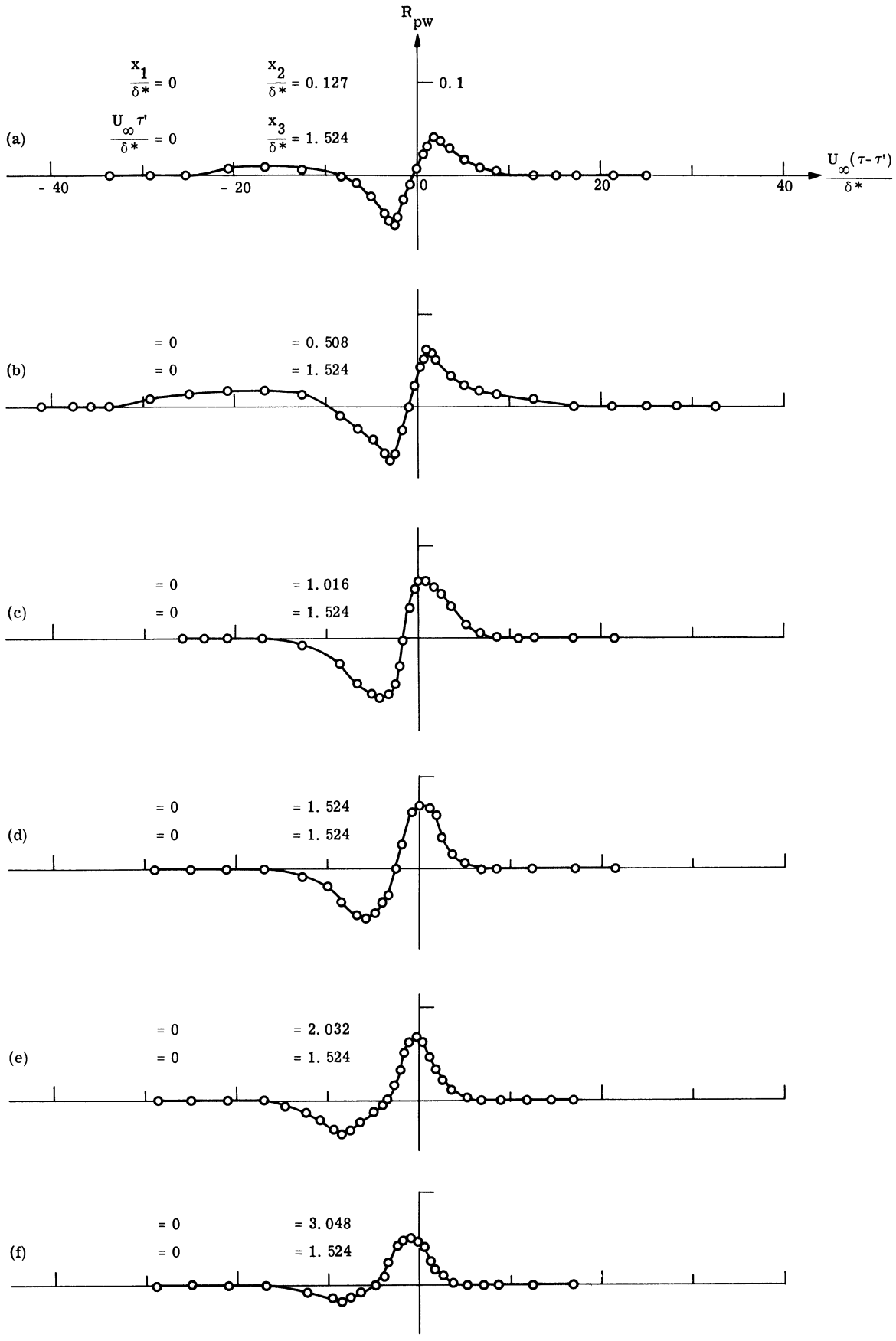

Fig. 33. Measured values of the space-time correlation of fluctuating velocity component w with fluctuating wall pressure ($x_3/\delta^* > 0$).

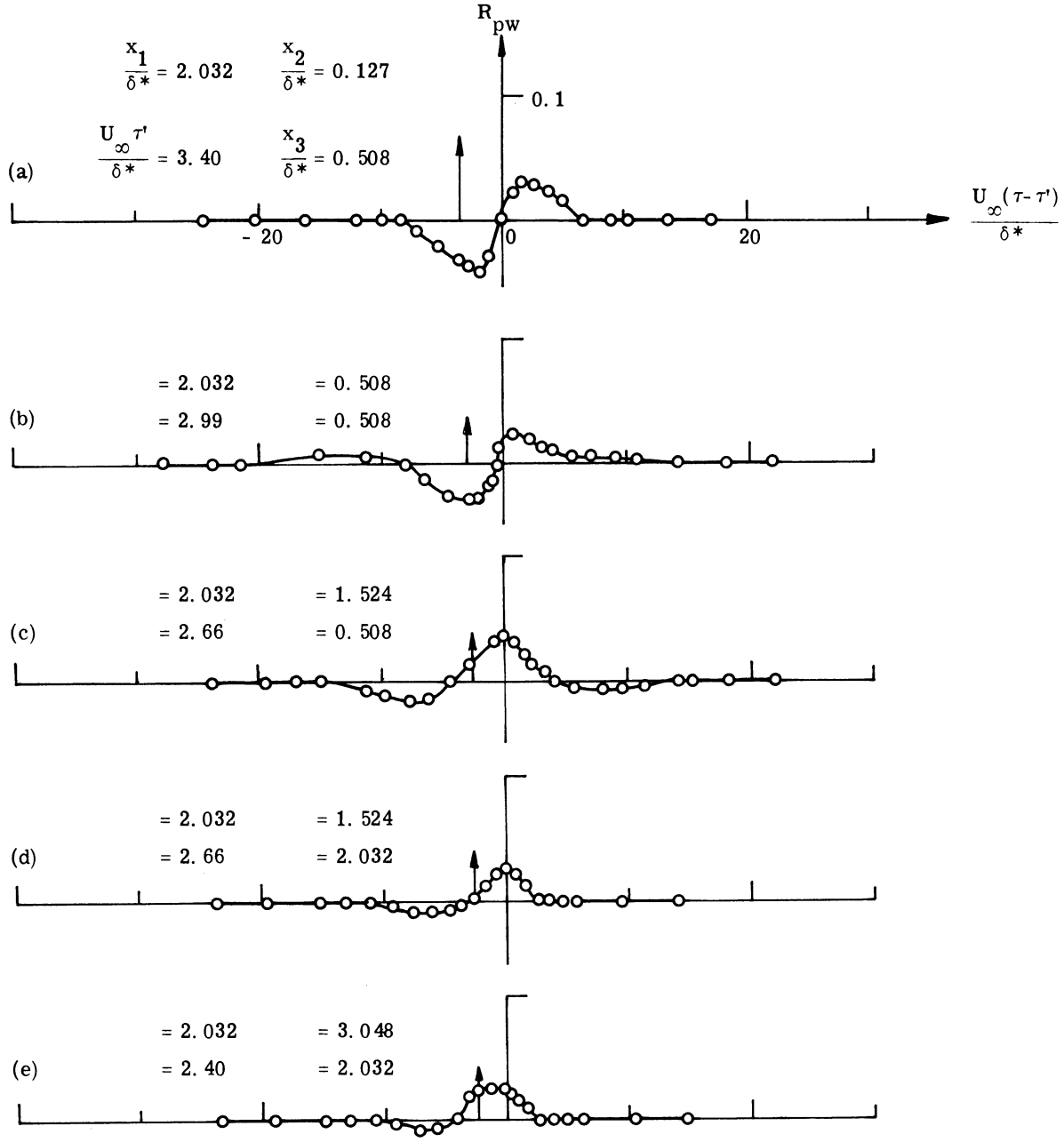

Fig. 34. Measured values of the space-time correlation of fluctuating velocity component w with fluctuating wall pressure ($x_3/\delta^* > 0$).

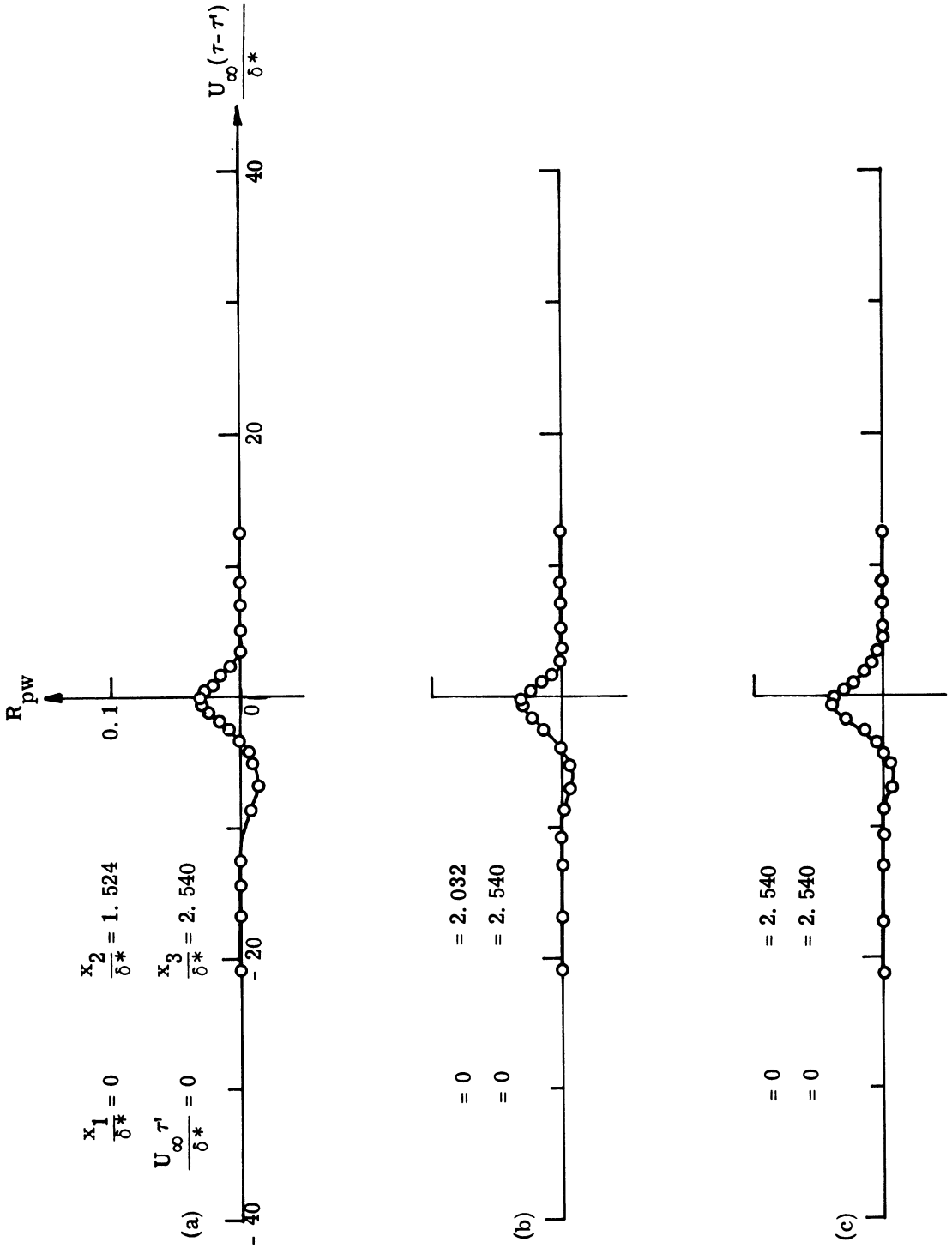

Fig. 35. Measured values of the space-time correlation of fluctuating velocity component w with fluctuating wall pressure ($x_3/\delta^* > 0$).

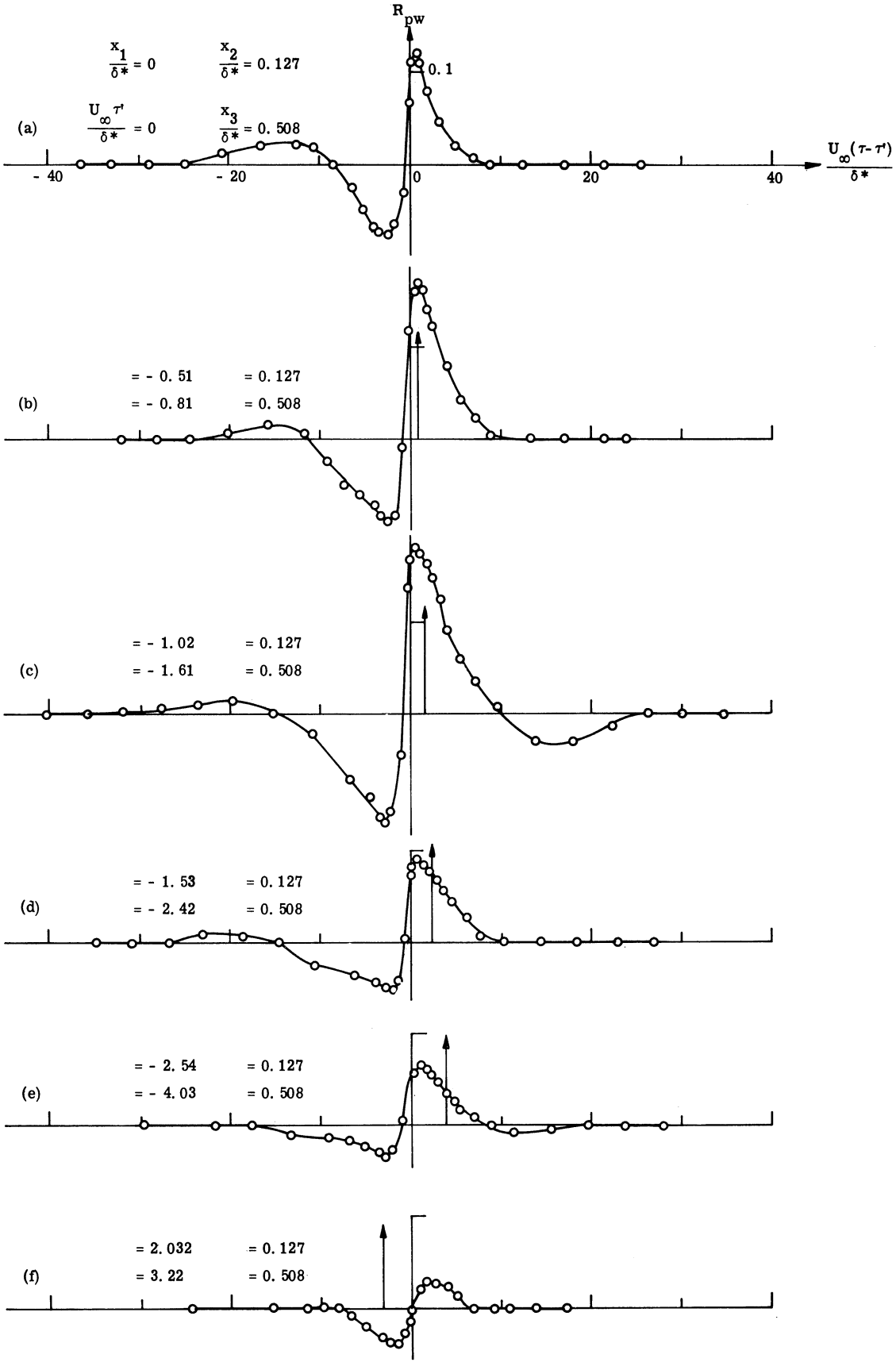

Fig. 36. Measured values of the space-time correlation of fluctuating velocity component w with fluctuating wall pressure ($x_3/\delta^* > 0$).

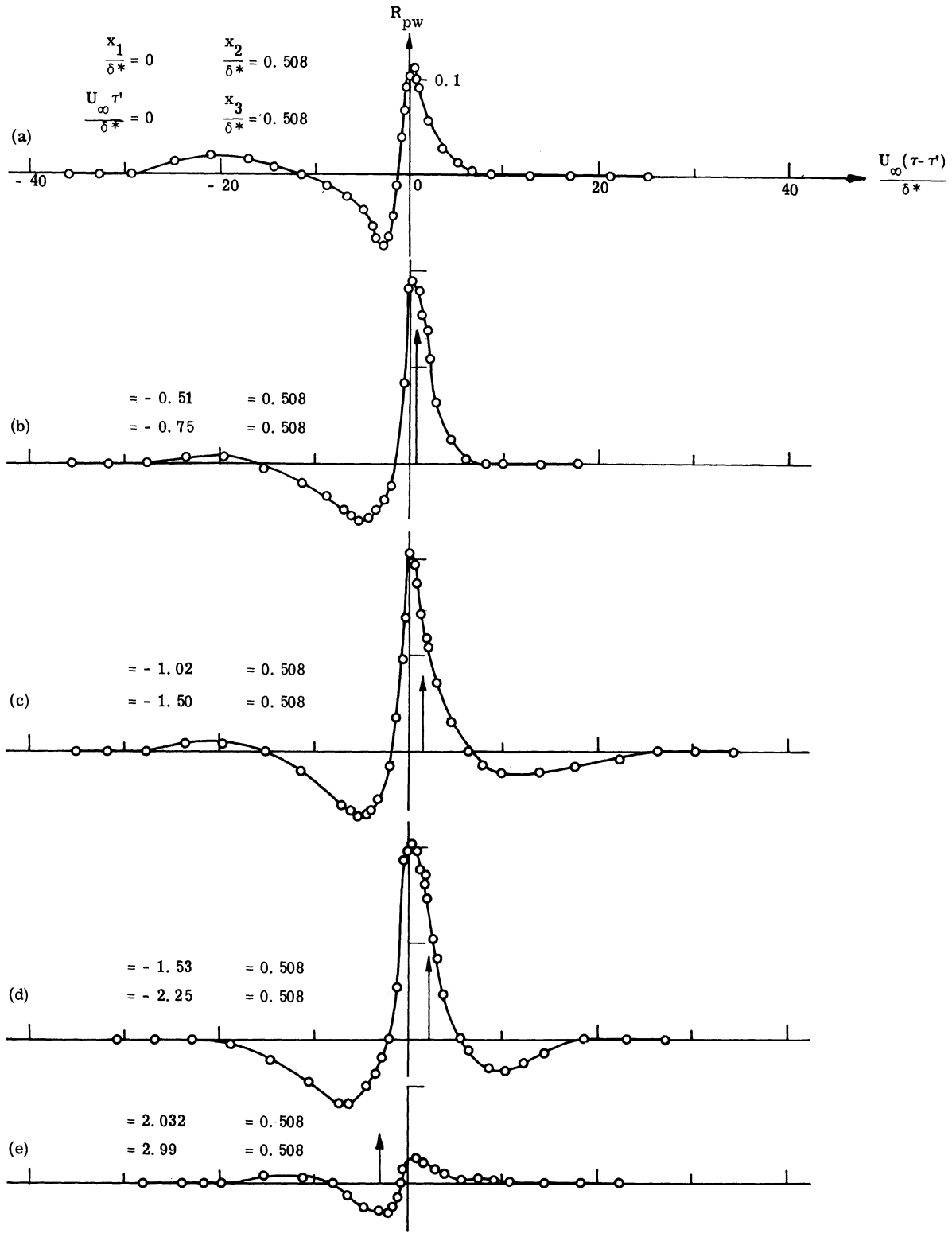

Fig. 37. Measured values of the space-time correlation of fluctuating velocity component w with fluctuating wall pressure ($x_3/\delta^* > 0$).

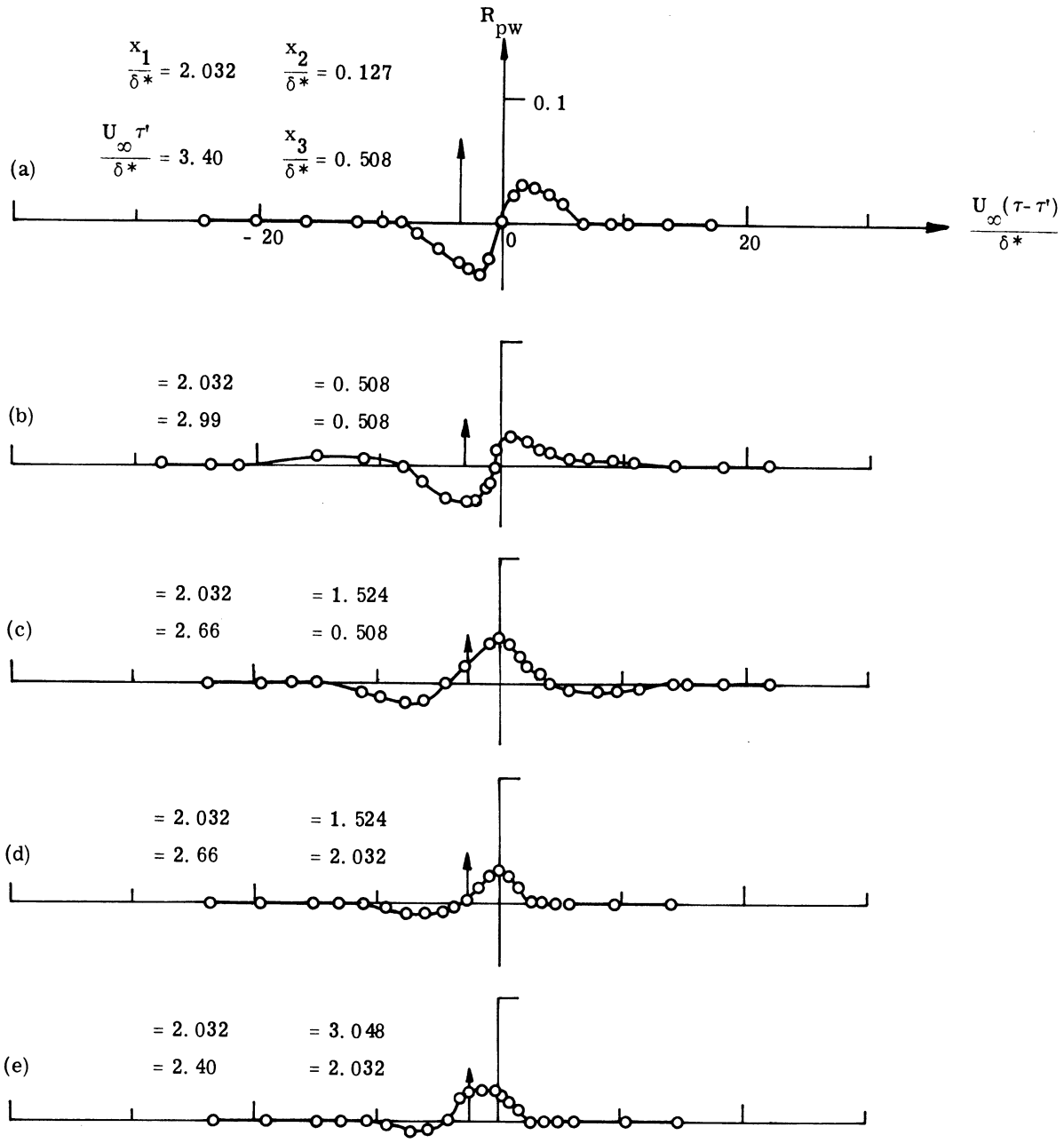

Fig. 38. Measured values of the space-time correlation of fluctuating velocity component w with fluctuating wall pressure ($x_3/\delta^* > 0$).

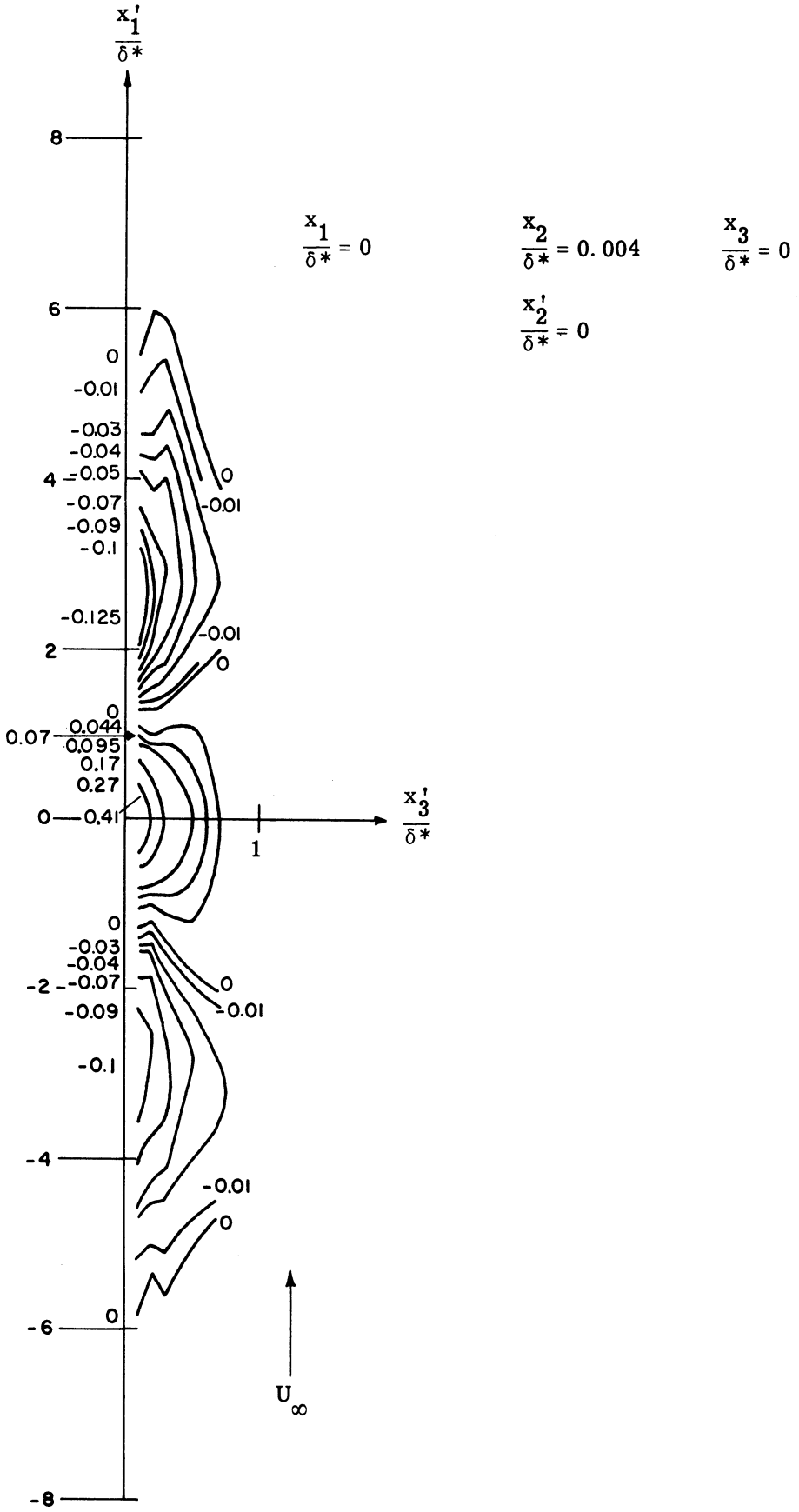

Fig. 39. Correlation contours of constant R_{uu} very near the wall.

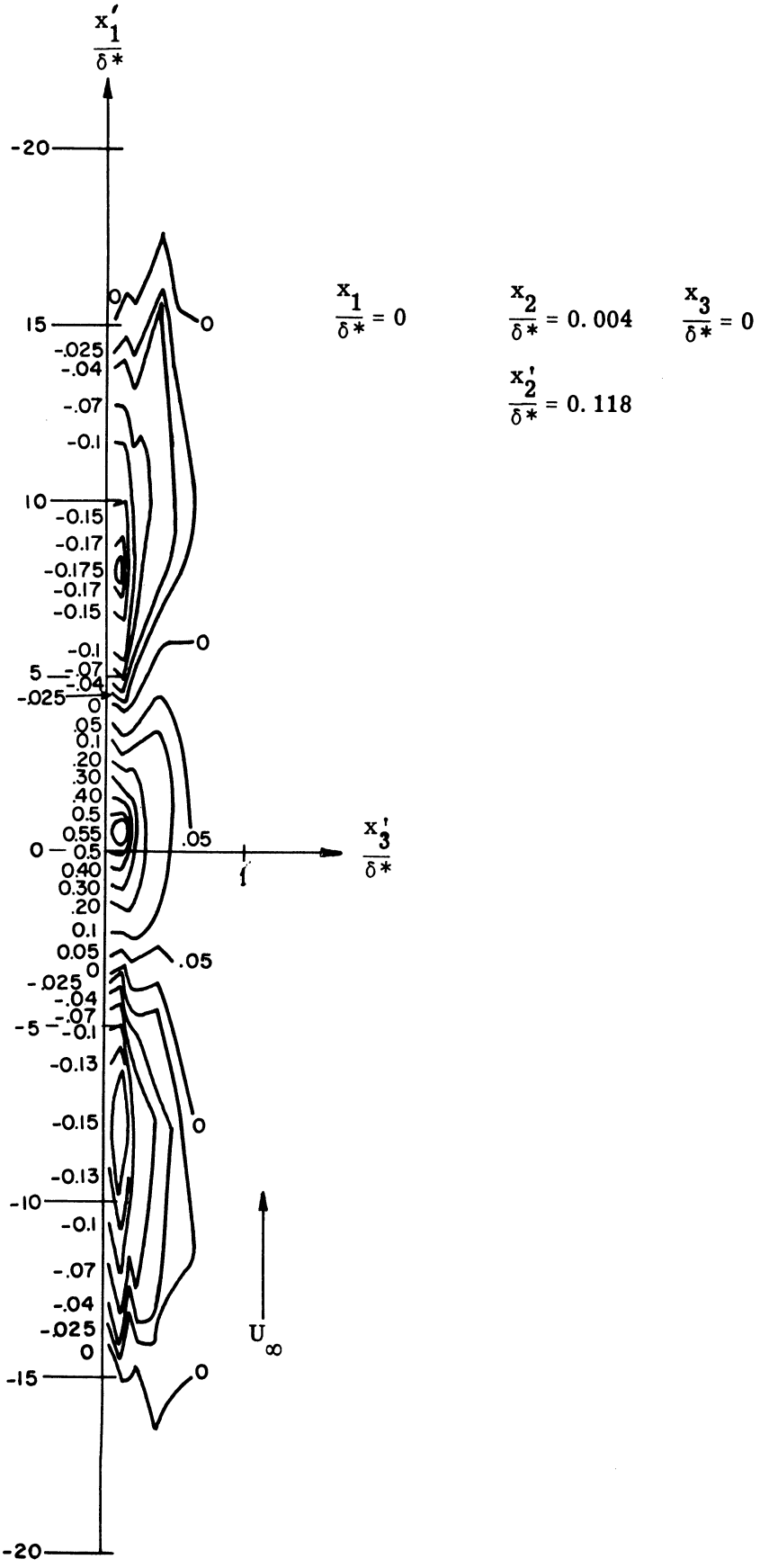

Fig. 40. Correlation contours of constant R_{uu} near the wall.

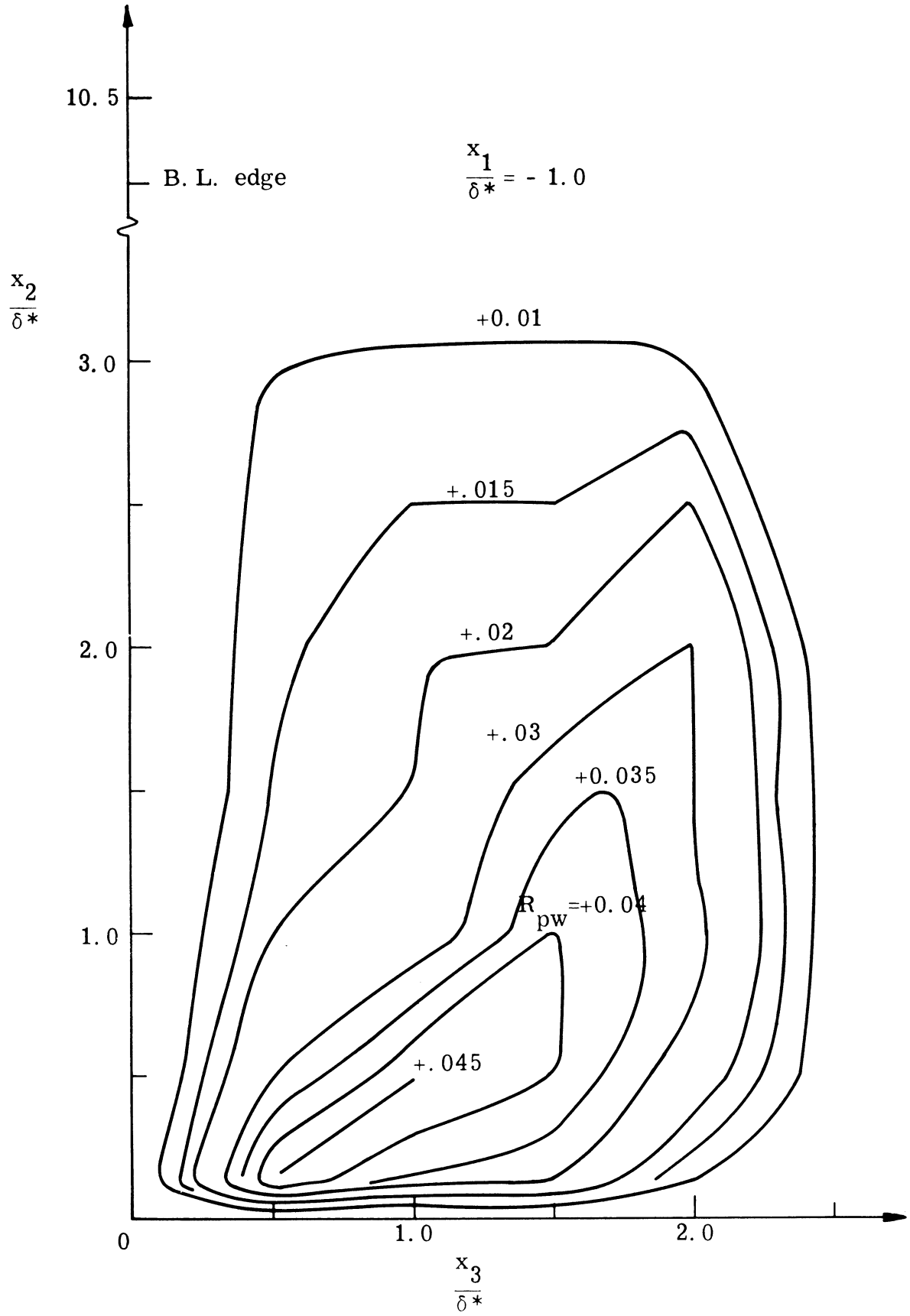

Fig. 41. Correlation contours of constant R_{pw} in the x_2-x_3 plane. Origin of coordinate system at pressure transducer.

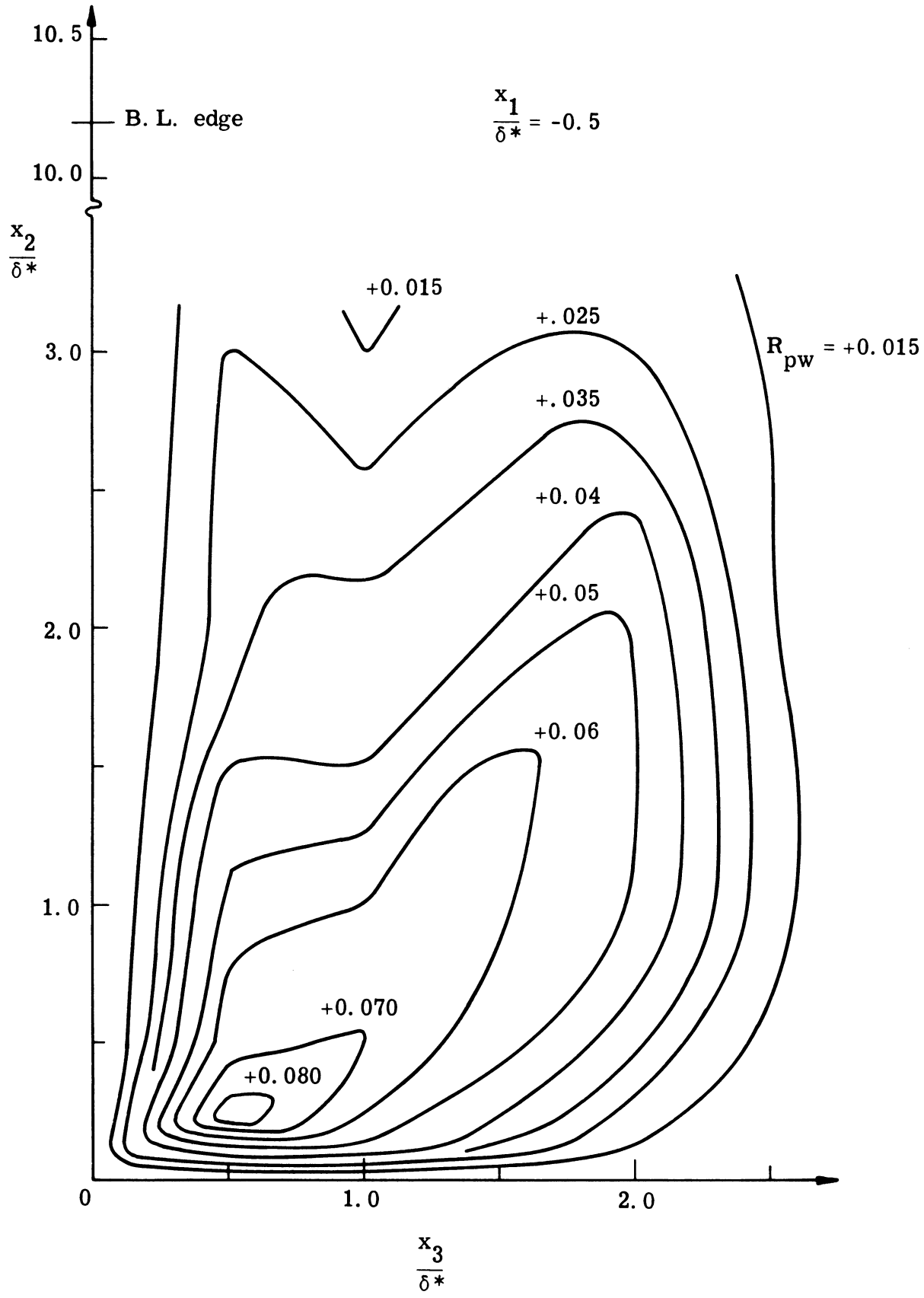

Fig. 42. Correlation contours of constant R_{pw} in the x_2-x_3 plane. Origin of coordinate system at pressure transducer.

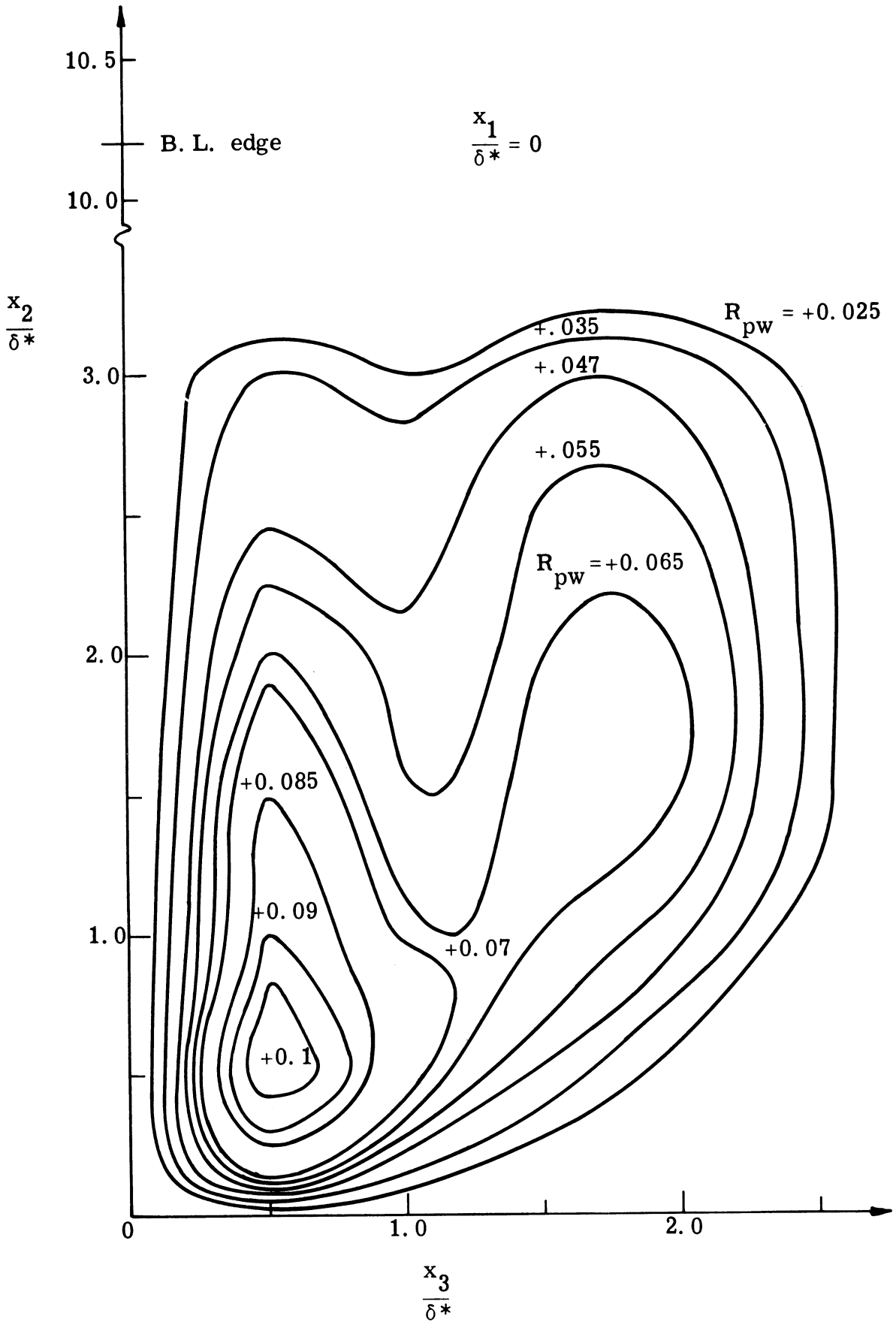

Fig. 43. Correlation contours of constant R_{pw} in the x_2-x_3 plane. Origin of coordinate system at pressure transducer.

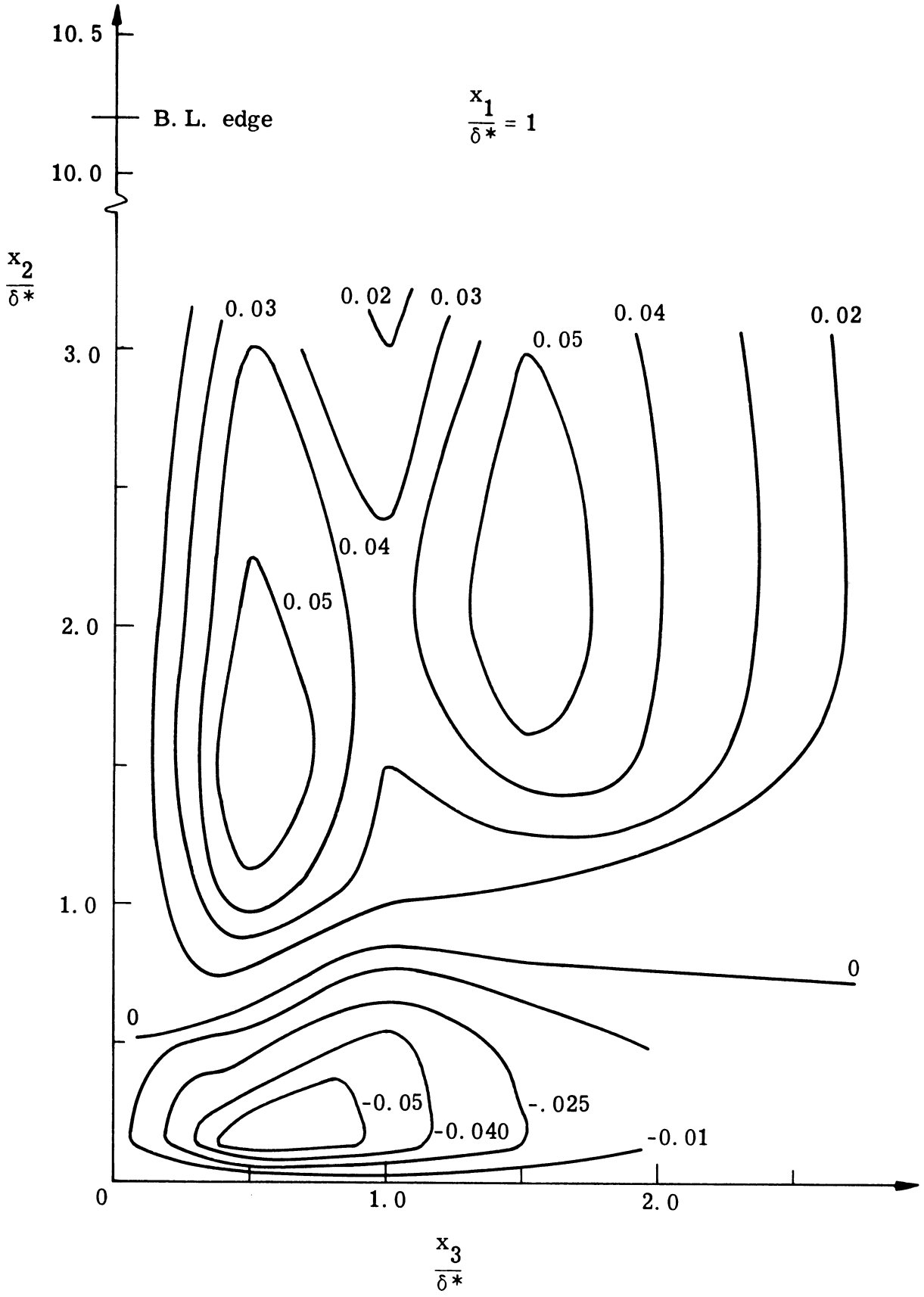

Fig. 44. Correlation contours of constant R_{pw} in the x_2-x_3 plane. Origin of coordinate system at pressure transducer.

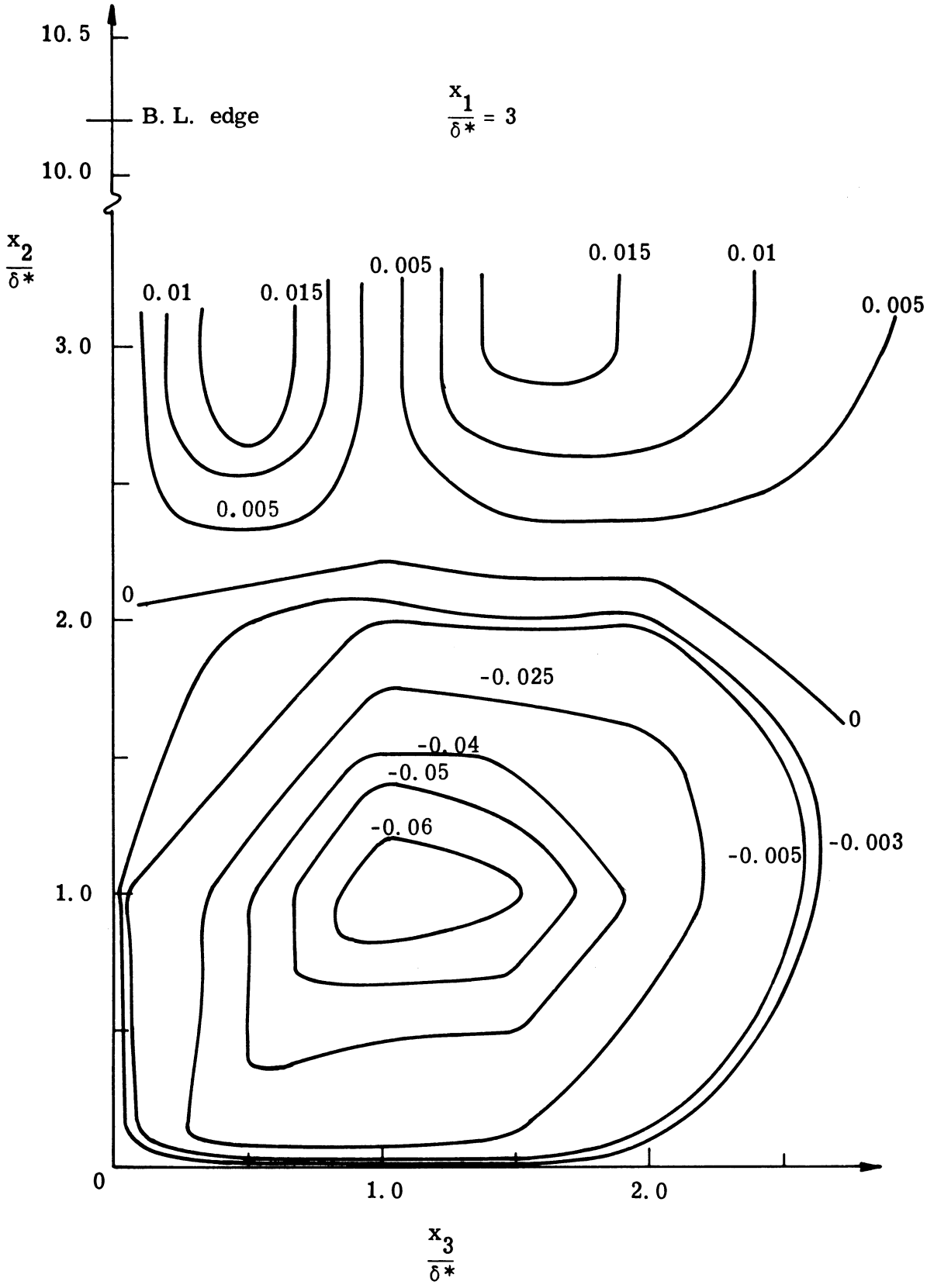

Fig. 45. Correlation contours of constant R_{pw} in the x_2-x_3 plane. Origin of coordinate system at pressure transducer.

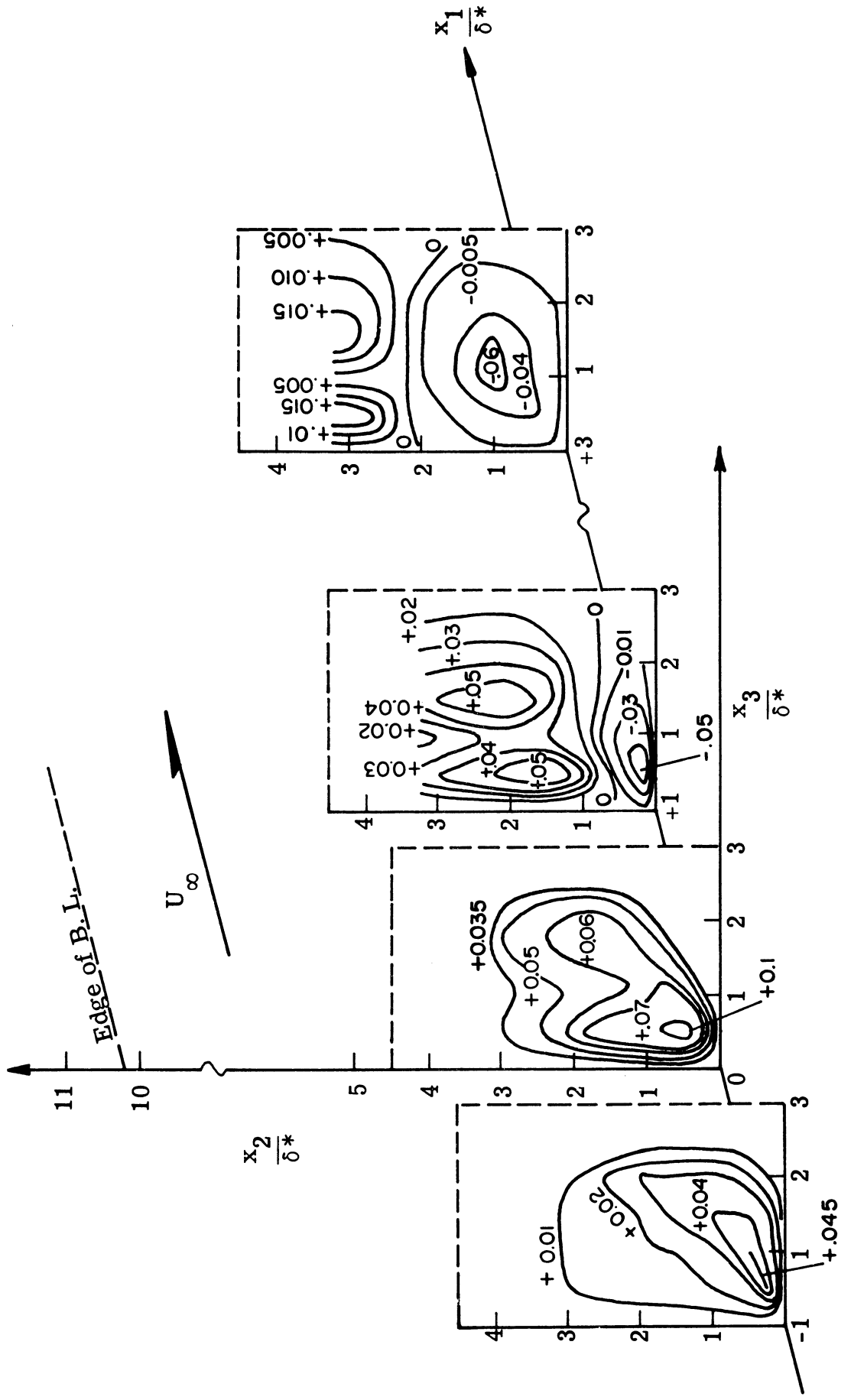

Fig. 46. Three-dimensional diagram of contours of Rpw = Const. (also see Figs. 41-45).

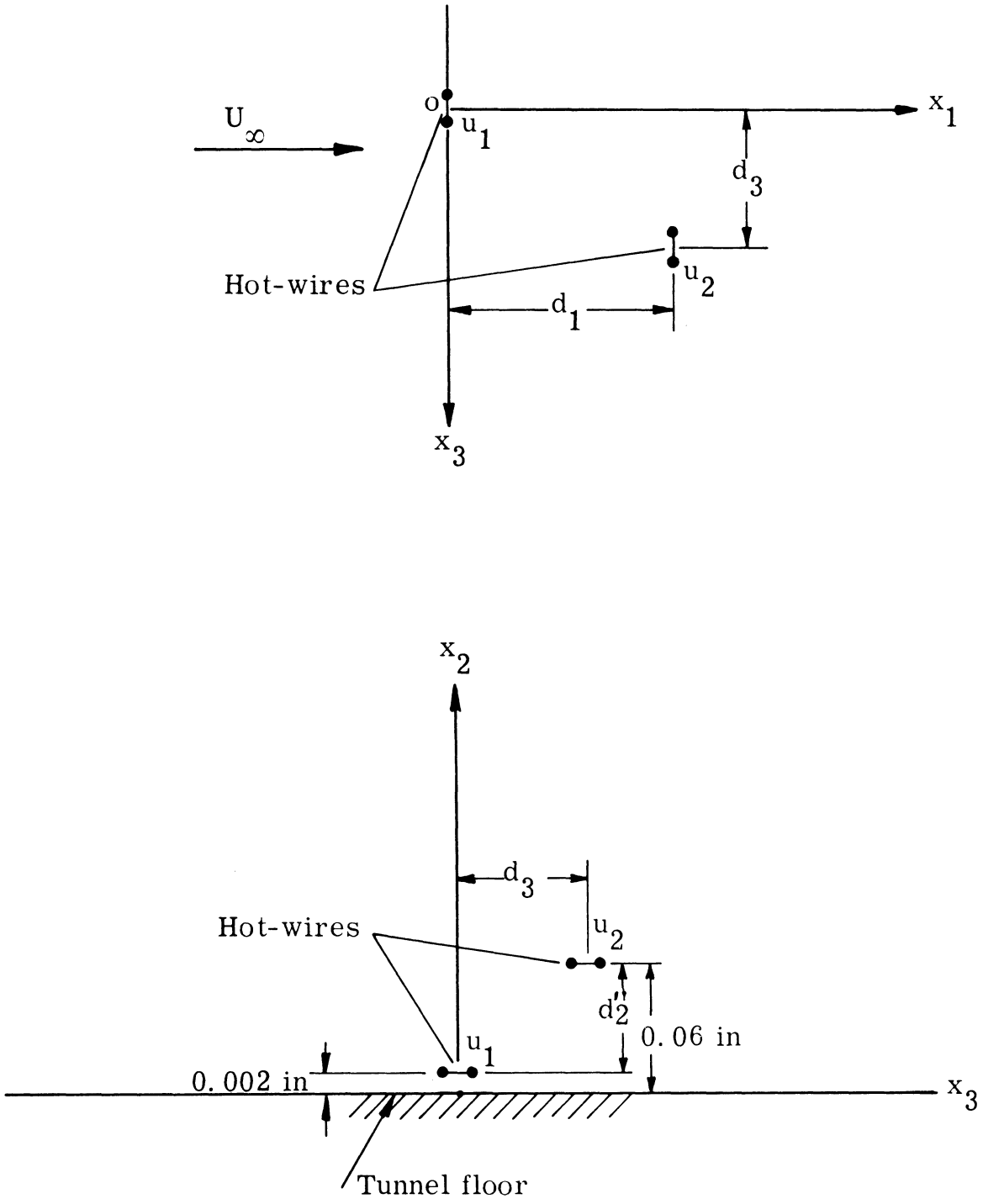

Fig. 47. The location of hot-wires for measurements of the displacement of eddies due to convection and turbulent diffusion near the wall.

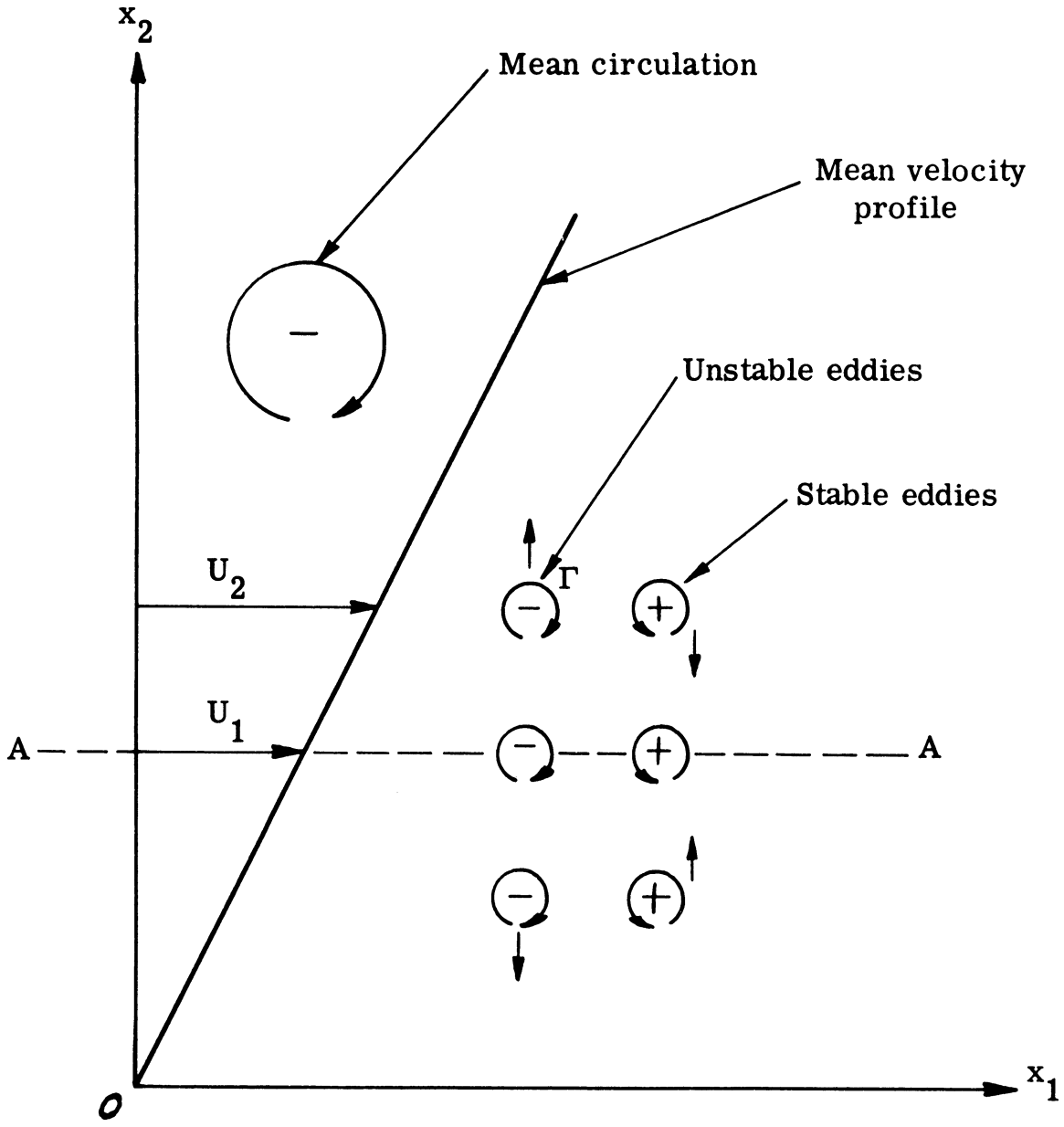

Fig. 48. The behavior of eddies in a shear flow.

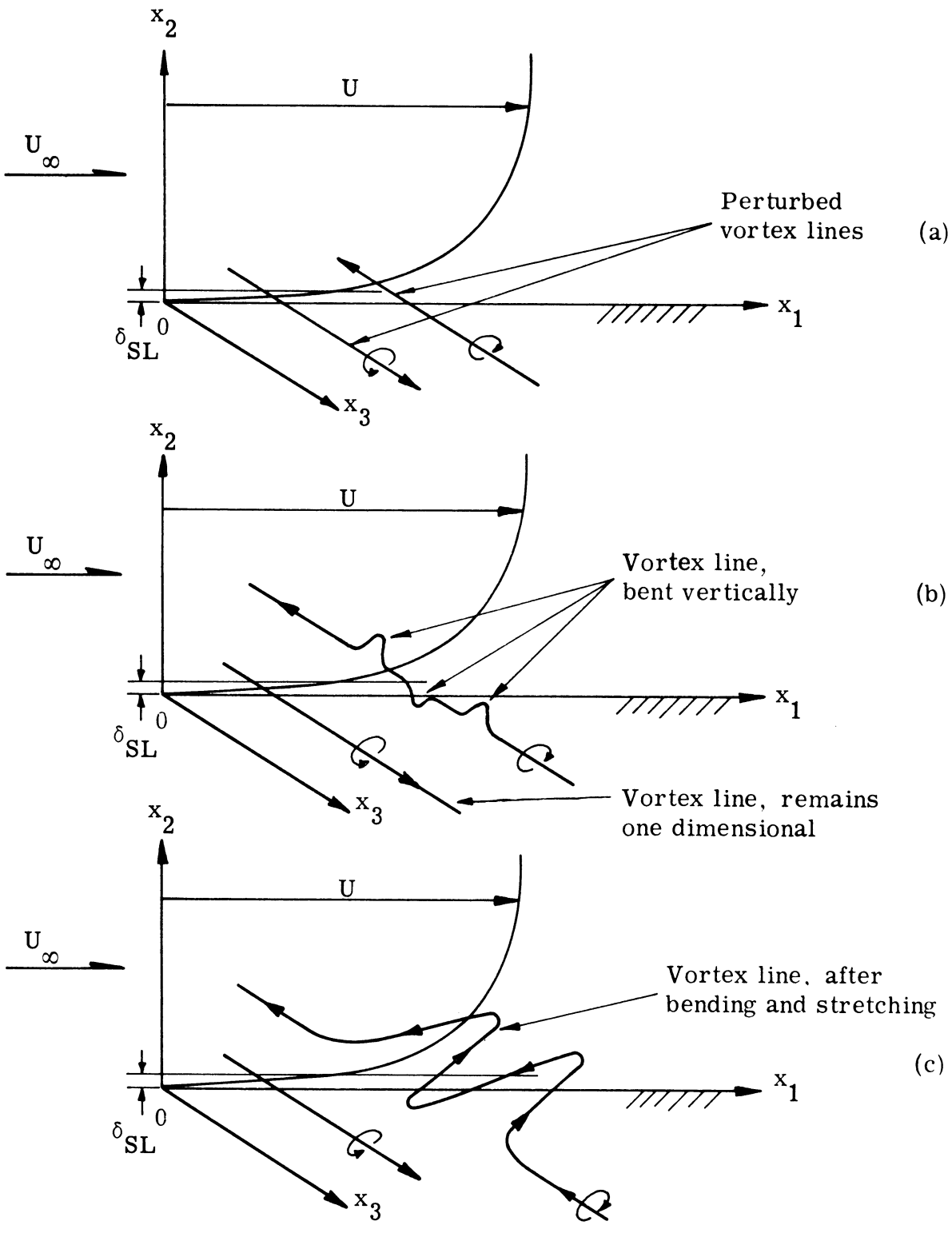

Fig. 49. The development of random vortex lines near the wall.

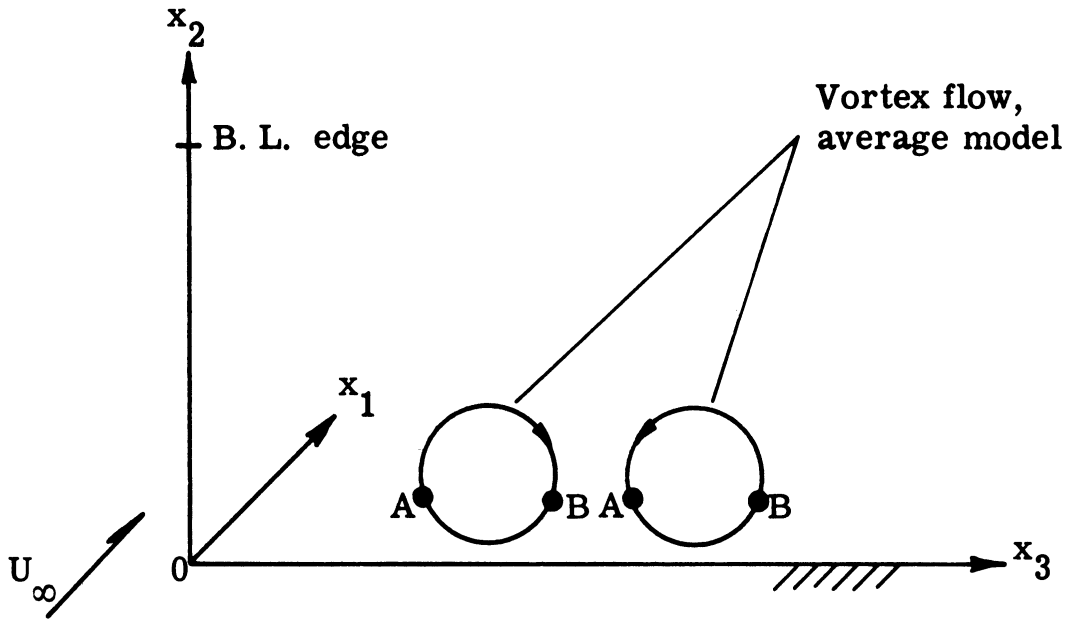

Fig. 50. Random vortex flow in the x_2-x_3 plane near the wall. Points A and B are the locations of hot-wire measuring R_{vv}.

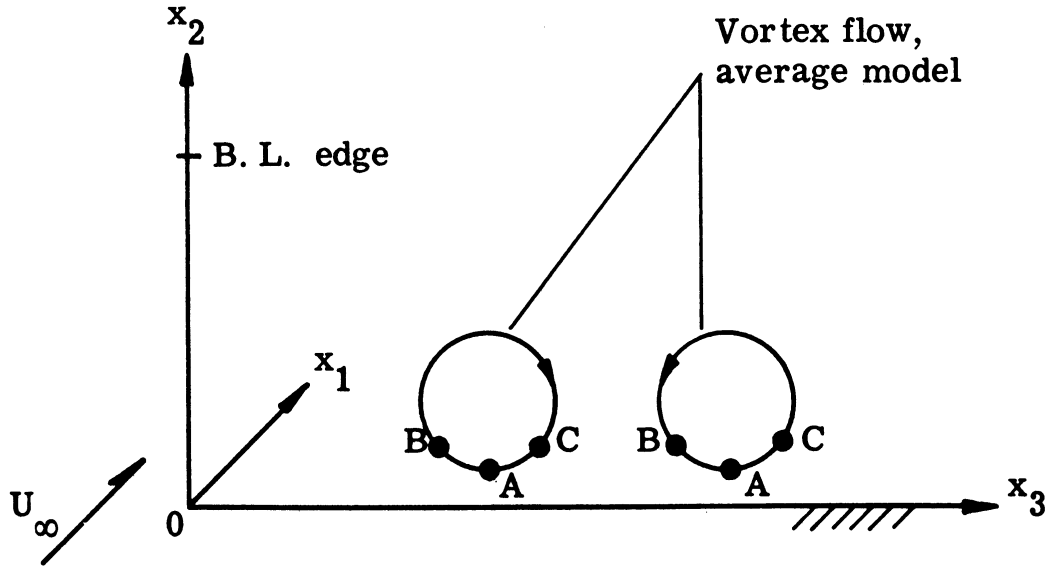

Fig. 51. Random vortex flow in the x_2-x_3 plane near the wall. Points A, B, and C are the locations of hot-wire measuring R_{wv}.

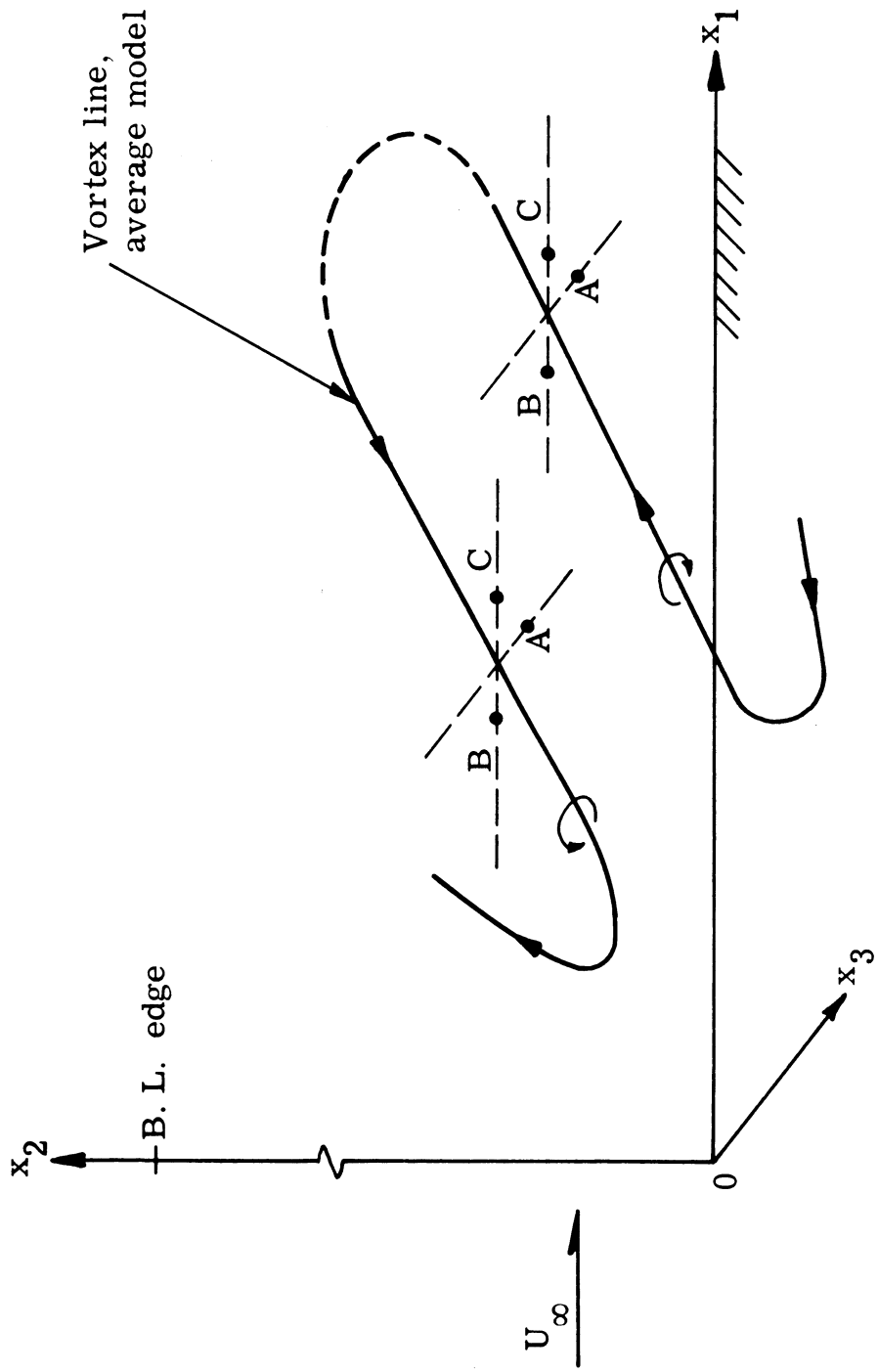

Fig. 52. Random vortex line near the wall. Points A, B, and C are the locations of hot-wire measuring R_{wv}.

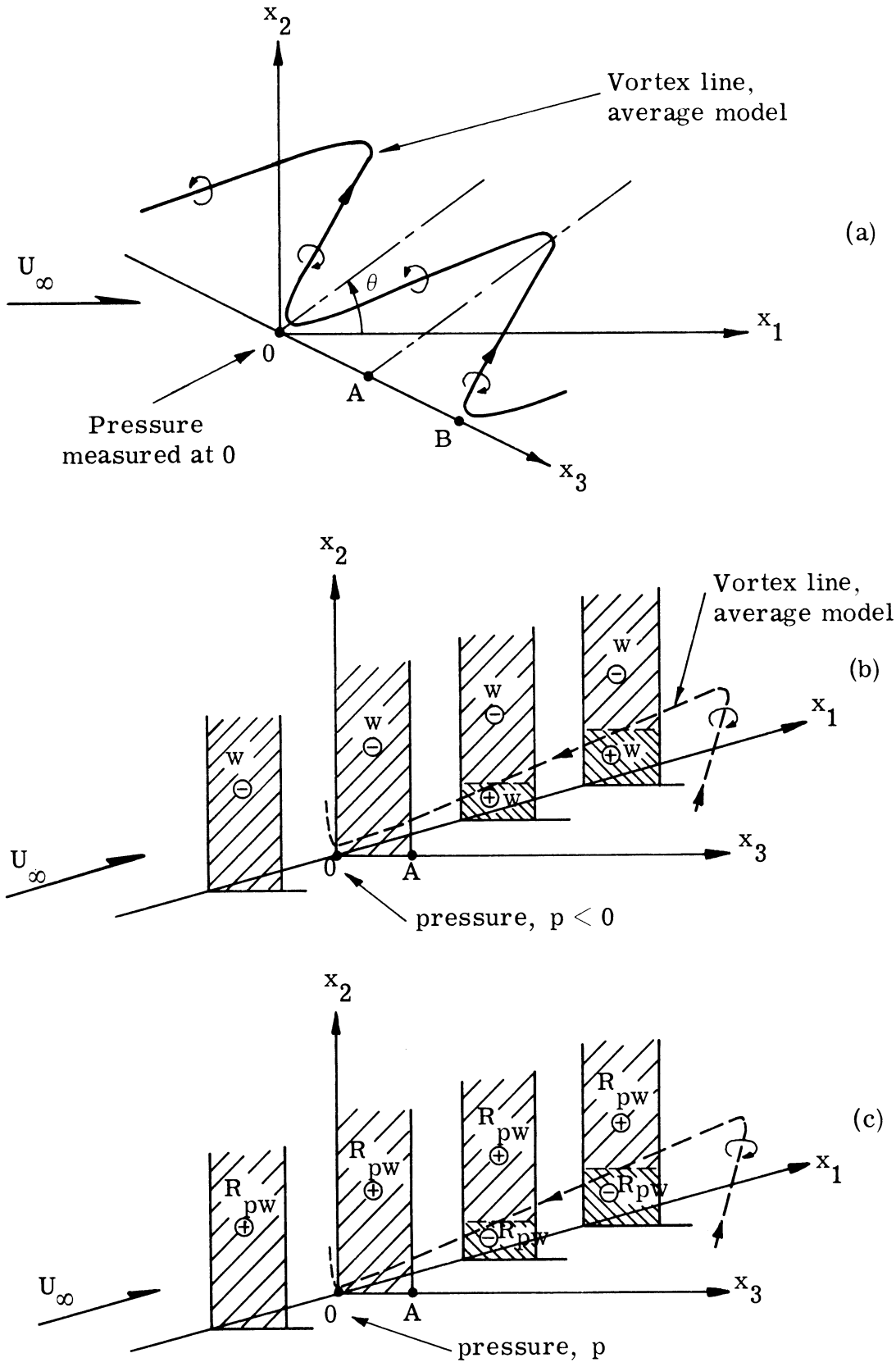

Fig. 53. Structure of a random vortex line near the wall and the explanation of measurements of contours of constant R_{pw} at different x_2-x_3 planes (also see Fig. 46).

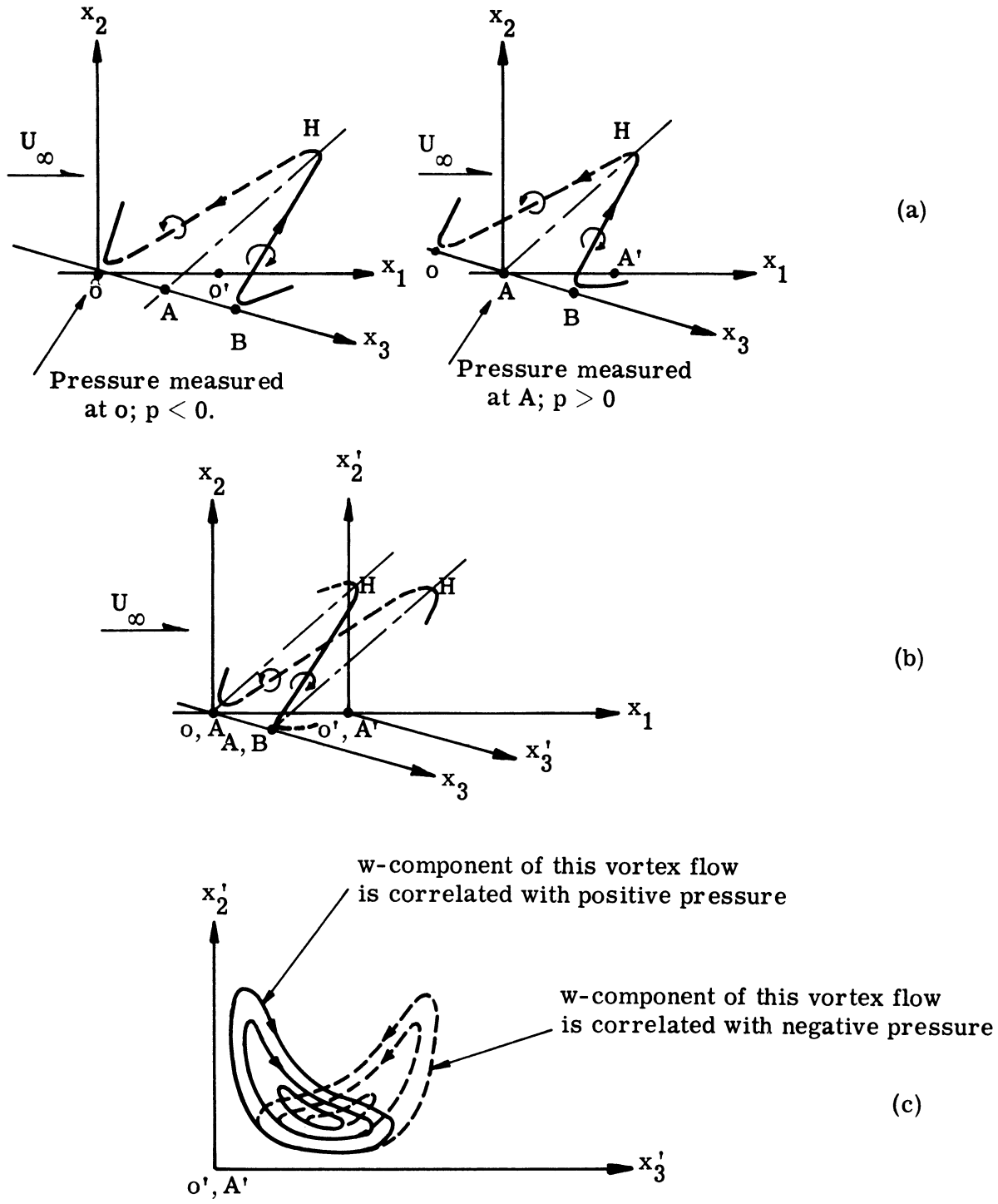

Fig. 54. Explanation of the separation of positive contours of constant R_{pw} in the present measurement (also see Figs. 44-46).

DISTRIBUTION LIST
(One copy unless otherwise noted.)

Chief of Naval Research
Department of the Navy
Washington 25, D. C.
Attn: Code 438 3
Attn: Code 461
Attn: Code 463
Attn: Code 466

Commanding Officer
Office of Naval Research
Branch Office
495 Summer Street
Boston 10, Massachusetts

Commanding Officer
Office of Naval Research
Branch Office
346 Broadway
New York 13, New York

Commanding Officer
Office of Naval Research
Branch Office
1030 East Green Street
Pasadena, California

Commanding Officer
Office of Naval Research
Branch Office
1000 Geary Street
San Francisco 9, California

Commanding Officer 10
Office of Naval Research
Branch Office
Navy No. 100, Fleet Post Office
New York, New York

Director 6
Naval Research Laboratory
Washington 25, D. C.
Attn: Code 2027

Chief, Bureau of Naval Weapons
Department of the Navy
Washington 25, D. C.
Attn: Code RUAW-4
Attn: Code RRRE
Attn: Code RAAD
Attn: Code RAAD-222
Attn: Code DIS-42

Chief, Bureau of Ships
Department of the Navy
Washington 25, D. C.
Attn: Code 310
Attn: Code 312
Attn: Code 335
Attn: Code 420
Attn: Code 421
Attn: Code 440
Attn: Code 442
Attn: Code 449

Chief, Bureau of Yards and Docks
Department of the Navy
Washington 25, D. C.
Attn: Code D-400

Commanding Officer and Director
David Taylor Model Basin
Washington 7, D. C.
Attn: Code 108
Attn: Code 142
Attn: Code 500
Attn: Code 513
Attn: Code 520
Attn: Code 526
Attn: Code 526A
Attn: Code 530
Attn: Code 533
Attn: Code 580
Attn: Code 585
Attn: Code 589
Attn: Code 591
Attn: Code 591A
Attn: Code 700

DISTRIBUTION LIST (Continued)

Commander
U. S. Naval Ordnance Test Station
China Lake, California
Attn: Code 753

Commander
U. S. Naval Ordnance Test Station
Pasadena Annex
3202 E. Foothill Blvd.
Pasadena 8, California
Attn: Code P-508

Commander
Planning Department
Portsmouth Naval Shipyard
Portsmouth, New Hampshire

Commander
Planning Department
Boston Naval Shipyard
Boston 29, Massachusetts

Commander
Planning Department
Pearl Harbor Naval Shipyard
Navy No. 128, Fleet Post Office
San Francisco, California

Commander
Planning Department
San Francisco Naval Shipyard
San Francisco 24, California

Commander
Planning Department
Mare Island Naval Shipyard
Vallejo, California

Commander
Planning Department
New York Naval Shipyard
Brooklyn 1, New York

Commander
Planning Department
Puget Sound Naval Shipyard
Bremerton, Washington

Commander
Planning Department
Philadelphia Naval Shipyard
U. S. Naval Base
Philadelphia 12, Pennsylvania

Commander
Planning Department
Norfolk Naval Shipyard
Portsmouth, Virginia

Commander
Planning Department
Charleston Naval Shipyard
U. S. Naval Base
Charleston, South Carolina

Commander
Planning Department
Long Beach Naval Shipyard
Long Beach 2, California

Commander
Planning Department
U. S. Naval Weapons Laboratory
Dahlgren, Virginia

Commander
U. S. Naval Ordnance Laboratory
White Oak, Maryland

Dr. A. V. Hershey
Computation and Exterior
Ballistics Laboratory
U. S. Naval Weapons Laboratory
Dahlgren, Virginia

DISTRIBUTION LIST (Continued)

Superintendent
U. S. Naval Academy
Annapolis, Maryland
Attn: Library

Superintendent
U. S. Naval Postgraduate School
Monterey, California

Commandant
U. S. Coast Guard
1300 E Street, N. W.
Washington, D. C.

Secretary Ship Structure Committee
U. S. Coast Guard Headquarters
1300 E Street, N. W.
Washington, D. C.

Commander
Military Sea Transportation Service
Department of the Navy
Washington 25, D. C.

U. S. Maritime Administration
GAO Building
441 G Street, N. W.
Washington, D. C.
Attn: Division of Ship Design
Attn: Division of Research

Superintendent
U. S. Merchant Marine Academy
Kings Point, Long Island, New York
Attn: Capt. L. S. McCready (Dept. of Engineering)

Commanding Officer and Director
U. S. Navy Mine Defense Laboratory
Panama City, Florida

Commanding Officer
NROTC and Naval Administrative Unit
Massachusetts Institute of Technology
Cambridge 39, Massachusetts

U. S. Army Transportation Research and Development Command 2
Fort Eustis, Virginia
Attn: Marine Transport Division

Director of Research
National Aeronautics and Space Administration
1512 H Street, N. W.
Washington 25, D. C.

Director
Langley Research Center
Langley Field Virginia
Attn: Mr. J. B. Parkinson 2
Attn: Mr. I. E. Garrick
Attn: Mr. D. J. Marten

Director Engineering Sciences Division
National Science Foundation
1951 Constitution Avenue, N. W.
Washington 25, D. C.

Director
National Bureau of Standards
Washington 25, D. C.
Attn: Fluid Mechanics Division (Dr. G. B. Schubauer)
Attn: Dr. G. H. Keulegan
Attn: Dr. J. M. Franklin

Defense Documentation Center 10
Cameron Station
Alexandria, Virginia 22314

DISTRIBUTION LIST (Continued)

Office of Technical Services
Department of Commerce
Washington 25, D. C.

California Institute of Technology
Pasadena 4, California
Attn: Professor M. S. Plesset
Attn: Professor T. Y. Wu
Attn: Professor A. J. Acosta

University of California
Department of Engineering
Los Angeles 24, California
Attn: Dr. A. Powell

Director
Scripps Institute of Oceanography
University of California
La Jolla, California

Professor M. L. Albertson
Department of Civil Engineering
Colorado A&M College
Fort Collins, Colorado

Professor J. E. Cermak
Department of Civil Engineering
Colorado State University
Fort Collins, Colorado

Professor W. R. Sears
Graduate School of Aeronautical Engr.
Cornell University
Ithaca, New York

State University of Iowa
Iowa Inst. of Hydraulic Research
Iowa City, Iowa
Attn: Dr. H. Rouse
Attn: Dr. L. Landweber

Harvard University
Cambridge 38, Massachusetts
Attn: Professor G. Birkhoff
(Dept. of Mathematics)
Attn: Professor G. F. Carrier
(Dept. of Mathematics)

Massachusetts Institute of Technology
Cambridge 39, Massachusetts
Attn: Department of Naval Architecture and Marine Engineering
Attn: Professor A. T. Ippen

University of Michigan
Ann Arbor, Michigan
Attn: Professor R. B. Couch
(Dept. of Naval Architecture)
Attn: Professor W. W. Willmarth
(Aerospace Engr. Department)
Attn: Professor M. S. Uberoi
(Aerospace Engr. Department)

St. Anthony Falls Hydraulic Lab
University of Minnesota
Minneapolis 14, Minnesota
Attn: Dr. L. G. Straub, Director
Attn: Professor Silberman
Attn: Mr. J. N. Wetzel

Professor J. J. Foody
Engineering Department
New York State University Maritime College
Fort Schulyer, New York

New York University
Institute of Mathematical Sciences
25 Waverly Place
New York 3, New York
Attn: Professor J. Keller
Attn: Professor J. J. Stoker
Attn: Professor R. Kraichnan

The Johns Hopkins University
Department of Mechanical Engineering
Baltimore 18, Maryland
Attn: Professor S. Corrsin
Attn: Professor O. M. Phillips 2

Massachusetts Institue of Technology
Department of Naval Architecture and
Marine Engineering
Cambridge 39, Massachusetts
Attn: Prof. M. A. Abkowitz, Head

Ordnance Research Laboratory
Pennsylvania State University
University Park, Pennsylvania
Attn: Dr. G. F. Wislicenus
Attn: Dr. M. Sevik

Professor R. C. DiPrima
Department of Mathematics
Rensselaer Polytechnic Institute
Troy, New York

Stevens Institute of Technology
Davidson Laboratory
Castle Point Station
Hoboken, New Jersey
Attn: Professor E. V. Lewis
Attn: Mr. D. Savitsky
Attn: Mr. J. P. Breslin
Attn: Mr. C. J. Henry
Attn: Mr. S. Tsakonas

Webb Institue of Naval Architecture
Crescent Beach Road
Glen Cove, New York
Attn: Technical Library

Director
Woods Hole Oceanographic Institute
Woods Hole, Massachusetts

Commander
Air Research and Development Command
Air Force Office of Scientific
Research
14th and Constitution
Washington 25, D. C.
Attn: Mechanics Branch

Commander
Wright Air Development Division
Aircraft Laboratory
Wright-Patterson Air Force Base, Ohio
Attn: Mr. W. Mykytow, Dynamics
Branch

Cornell Aeronautical Laboratory
4455 Genesee Street
Buffalo, New York
Attn: Mr. W. Targoff
Attn: Mr. R. White

Massachusetts Institute of Technology
Fluid Dynamics Research Laboratory
Cambridge 39, Massachusetts
Attn: Professor H. Ashley
Attn: Professor M. Landahl
Attn: Professor J. Dugundji

Hamburgische Schiffbau-Versuchsanstalt
Bramfelder Strasse 164
Hamburg 33, Germany
Attn: Dr. O. Grim
Attn: Dr. H. W. Lerbs

Institut für Schiffbau der
Universität Hamburg
Berliner Tor 21
Hamburg 1, Germany
Attn: Professor G. P. Weinblum,
Director

Max-Planck Institut für Strömungsforschung
Bottingerstrasse 6/8
Gottingen, Germany
Attn: Dr. H. Reichardt

Hydro-og Aerodynamisk Laboratorium
Lyngby, Denmark
Attn: Professor Carl Prohaska

Skipsmodelltanken
Trondheim, Norway
Attn: Professor J. K. Lunde

Versuchsanstalt für Wasserbau und Schiffbau
Schleuseninsel im Tiergarten
Berlin, Germany
Attn: Dr. S. Schuster, Director

Technische Hogeschool
Institut voor Toegepaste Wiskunde
Julianalaan 132
Delft, Netherlands
Attn: Professor R. Timman

Bureau D'Analyse et de Techerche Appliquées
47 Avenue Victor Cresson
Issy les Moulineaux (Seine)
Paris, France
Attn: Professor Siestrunck

Netherlands Ship Model Basin
Wageningen, Netherlands
Attn: Dr. Ir. J. D. van Manen

National Physical Laboratory
Teddington, Middlesex, England
Attn: Dr. F. H. Todd, Superintendent
Ship Division
Attn: Head Aerodynamics Division
Attn: Mr. A. Silverleaf

Head, Aerodynamics Department 2
Royal Aircraft Establishment
Farnborough, Hants, England
Attn: Mr. M. O. W. Wolfe

Boeing Airplane Co.
Seattle Division
Seattle, Washington
Attn: Mr. M. J. Turner

Electric Boat Division
General Dynamics Corporation
Groton, Connecticut
Attn: Mr. Robert McCandliss

General Applied Sciences Labs, Inc.
Merrick and Stewart Avenues
Westbury, Long Island, New York

Gibbs and Cox, Inc.
21 West Street
New York, New York

Grumman Aircraft Engineering Corp.
Bethpage, Long Island, New York
Attn: Mr. E. Baird
Attn: Mr. E. Bower

Grumman Aircraft Engineering Corp.
Dynamic Developments Division
Babylon, New York

Lockheed Aircraft Corporation
Missiles and Space Division
Palo Alto, California
Attn: R. W. Kermeen

Midwest Research Institute
425 Volker Blvd.
Kansas City 10, Missouri
Attn: Mr. Zeydel

DISTRIBUTION LIST (Concluded)

Director, Department of Mechanical
Sciences
Southwest Research Institute
8500 Culebra Road
San Antonio 6, Texas
Attn: Dr. H. N. Abramson
Attn: Mr. G. Ransleben
Attn: Editor, Applied Mechanics
Review

Convair
A Division of General Dynamics
San Diego, California
Attn: Mr. R. H. Oversmith
Attn: Mr. A. D. MacLellan
Attn: Mr. H. T. Brooke

Dynamic Developments, Inc.
15 Berry Hill Road
Oyster Bay, Long Island, New York

Dr. S. F. Hoerner
148 Busteed Drive
Midland Park, New Jersey

Hydronautics, Incorporated
200 Monroe Street
Rockville, Maryland
Attn: Mr. Phillip Eisenberg

Rand Development Corporation
13600 Deise Avenue
Cleveland 10, Ohio
Attn: Dr. A. S. Iberall

U. S. Rubber Company
Research and Development Department
Wayne, New Jersey
Attn: Mr. L. M. White

Technical Research Group, Inc.
2 Aerial Way
Syosset, Long Island, New York
Attn: Mr. Jack Kotik

Unclassified
Security Classification

DOCUMENT CONTROL DATA - R&D

(Security classification of title, body of abstract and indexing annotation must be entered when the overall report is classified)

1. ORIGINATING ACTIVITY (Corporate author)
The University of Michigan
Department of Aerospace Engineering, Aerodynamics Laboratory
Ann Arbor, Michigan

2a. REPORT SECURITY CLASSIFICATION
Unclassified

2b. GROUP

3. REPORT TITLE

AN EXPERIMENTAL STUDY OF THE STRUCTURE OF TURBULENCE NEAR THE WALL THROUGH CORRELATION MEASUREMENTS IN A THICK TURBULENT BOUNDARY LAYER

4. DESCRIPTIVE NOTES (Type of report and inclusive dates)
Technical Report

5. AUTHOR(S) (Last name, first name, initial)
Tu, Bo-Jang
Willmarth, William W.

6. REPORT DATE
March 1966

7a. TOTAL NO. OF PAGES
126

7b. NO. OF REFS
33

8a. CONTRACT OR GRANT NO.
Nonr-1224(30)

b. PROJECT NO.
NR-062-234

c.

d.

9a. ORIGINATOR'S REPORT NUMBER(S)
02920-3-T

9b. OTHER REPORT NO(S) (Any other numbers that may be assigned this report)

10. AVAILABILITY/LIMITATION NOTICES
Qualified requesters may obtain copies from DDC.

11. SUPPLEMENTARY NOTES

12. SPONSORING MILITARY ACTIVITY
Department of the Navy
Office of Naval Research
Washington, D. C.

13. ABSTRACT

An experimental investigation is described in which emphasis is given to revealing the structure of turbulence near the wall in a boundary layer. Measurements made include space-time correlations between the fluctuating wall pressure and the span-wise velocity component w, and between the various velocity components. The velocity correlations include measurements of the space-time correlation of the streamwise component of the fluctuating wall shear stress. Experiments have been conducted in a thick (5 in.) turbulent boundary layer with zero pressure gradient which is produced by natural transition on a smooth surface.

Sufficient data have been obtained to allow us to propose a qualitative model for the structure of turbulence near the wall. The proposed model outlines the sequence of events that result in the production of intense pressure and velocity fluctuations by stretching of the vorticity after it is produced by viscous stresses within and near the edge of the viscous sublayer. The measurements are in qualitative agreement with the model. Here, qualitative agreement means that the size and shape of the contours of constant correlation and the sign of the measured correlations are in agreement with the proposed model for the turbulent structure.

DD FORM 1 JAN 64 1473

Unclassified
Security Classification

14. KEY WORDS	LINK A		LINK B		LINK C	
	ROLE	WT	ROLE	WT	ROLE	WT

INSTRUCTIONS

1. ORIGINATING ACTIVITY: Enter the name and address of the contractor, subcontractor, grantee, Department of Defense activity or other organization *(corporate author)* issuing the report.

2*a*. REPORT SECURITY CLASSIFICATION: Enter the overall security classification of the report. Indicate whether "Restricted Data" is included. Marking is to be in accordance with appropriate security regulations.

2*b*. GROUP: Automatic downgrading is specified in DoD Directive 5200.10 and Armed Forces Industrial Manual. Enter the group number. Also, when applicable, show that optional markings have been used for Group 3 and Group 4 as authorized.

3. REPORT TITLE: Enter the complete report title in all capital letters. Titles in all cases should be unclassified. If a meaningful title cannot be selected without classification, show title classification in all capitals in parenthesis immediately following the title.

4. DESCRIPTIVE NOTES: If appropriate, enter the type of report, e.g., interim, progress, summary, annual, or final. Give the inclusive dates when a specific reporting period is covered.

5. AUTHOR(S): Enter the name(s) of author(s) as shown on or in the report. Enter last name, first name, middle initial. If military, show rank and branch of service. The name of the principal author is an absolute minimum requirement.

6. REPORT DATE: Enter the date of the report as day, month, year; or month, year. If more than one date appears on the report, use date of publication.

7*a*. TOTAL NUMBER OF PAGES: The total page count should follow normal pagination procedures, i.e., enter the number of pages containing information.

7*b*. NUMBER OF REFERENCES: Enter the total number of references cited in the report.

8*a*. CONTRACT OR GRANT NUMBER: If appropriate, enter the applicable number of the contract or grant under which the report was written.

8*b*, 8*c*, & 8*d*. PROJECT NUMBER: Enter the appropriate military department identification, such as project number, subproject number, system numbers, task number, etc.

9*a*. ORIGINATOR'S REPORT NUMBER(S): Enter the official report number by which the document will be identified and controlled by the originating activity. This number must be unique to this report.

9*b*. OTHER REPORT NUMBER(S): If the report has been assigned any other report numbers *(either by the originator or by the sponsor)*, also enter this number(s).

10. AVAILABILITY/LIMITATION NOTICES: Enter any limitations on further dissemination of the report, other than those imposed by security classification, using standard statements such as:

(1) "Qualified requesters may obtain copies of this report from DDC."

(2) "Foreign announcement and dissemination of this report by DDC is not authorized."

(3) "U. S. Government agencies may obtain copies of this report directly from DDC. Other qualified DDC users shall request through _____."

(4) "U. S. military agencies may obtain copies of this report directly from DDC. Other qualified users shall request through _____."

(5) "All distribution of this report is controlled. Qualified DDC users shall request through _____."

If the report has been furnished to the Office of Technical Services, Department of Commerce, for sale to the public, indicate this fact and enter the price, if known.

11. SUPPLEMENTARY NOTES: Use for additional explanatory notes.

12. SPONSORING MILITARY ACTIVITY: Enter the name of the departmental project office or laboratory sponsoring *(paying for)* the research and development. Include address.

13. ABSTRACT: Enter an abstract giving a brief and factual summary of the document indicative of the report, even though it may also appear elsewhere in the body of the technical report. If additional space is required, a continuation sheet shall be attached.

It is highly desirable that the abstract of classified reports be unclassified. Each paragraph of the abstract shall end with an indication of the military security classification of the information in the paragraph, represented as *(TS), (S), (C), or (U)*

There is no limitation on the length of the abstract. However, the suggested length is from 150 to 225 words.

14. KEY WORDS: Key words are technically meaningful terms or short phrases that characterize a report and may be used as index entries for cataloging the report. Key words must be selected so that no security classification is required. Identifiers, such as equipment model designation, trade name, military project code name, geographic location, may be used as key words but will be followed by an indication of technical context. The assignment of links, rules, and weights is optional.